Intelligence Driven Load-pull Measurement Strategies

A thesis submitted to Cardiff University in candidature for the degree of

Doctor of Philosophy

By

Randeep S. Saini, MEng.

Division of Electronic Engineering

School of Engineering

Cardiff University

United Kingdom

DECLARATION

This work has not previously been accepted in substance for any degree and is not concurrently submitted in candidature for any degree.

Signed …… (Candidate)

Date ……

STATEMENT 1

This thesis is being submitted in partial fulfilment of the requirements for the degree of PhD.

Signed …… (Candidate)

Date ……

STATEMENT 2

This thesis is the result of my own independent work/investigation, except where otherwise stated. Other sources are acknowledged by explicit references.

Signed …… (Candidate)

Date ……

STATEMENT 3

I hereby give consent for my thesis, if accepted, to be available for photocopying and for inter-library loan, and for the title and summary to be made available to outside organisations.

Signed …… (Candidate)

Date ……

STATEMENT 4

I hereby give consent for my thesis, if accepted, to be available for photocopying and for inter-library loans after expiry of a bar on access approved by the Graduate Development Committee.

Signed …… (Candidate)

Date ……

Abstract

The objective of this thesis is to provide improved load-pull measurement strategies based on an open-loop active load pull measurement system. A review of the evolution of non-linear measurement systems as well as behavioural model generation approaches has been presented. An intelligence driven active load-pull system has been presented in this thesis, based on deriving local PHD models to aid the prediction of the desired active signal in order to achieve a target reflection coefficient. The algorithm proved to be effective in reducing the number of iterations in an open-loop active load-pull system and thus improving the utilisation efficiency. A non-linear measurement approach suitable for wafer mapping and technology screening applications has also been presented as an application of this new algorithm. In this thesis, it has also been shown how the Cardiff Behavioural model is effective in its ability to interpolate or extrapolate non-linear measurement data and thereby improve the quality of measurement data and speed of measurement systems. This investigation was carried out in two stages; fundamental interpolation testing and harmonic interpolation and extrapolation testing.

Summary

1. Discussed and investigated the inherent problems with active and passive load-pull measurement systems.
2. Discussed the current trends in Non-linear Behavioural modelling.
3. Designed and implemented an algorithm, based on deriving and using local Polyharmonic Distortion models to aid the prediction of the desired load emulation point and thus reduce the number of iterations in an open loop active load-pull system.
4. Developed and demonstrated a non-linear wafer mapping technique based on the above algorithm and the ability to archive non-linear data using the Cardiff Behavioural Model formulations.
5. Investigated the interpolation and extrapolation capabilities of non-linear behavioural models based on load-pull measurements on the fundamental and second harmonic tones.

Acknowledgements

- I would first of all like to thank my parents for providing me this opportunity to reach such a high and distinguished level of education and my wife, for supporting me and keeping me focussed.
- Prof Paul J. Tasker, my supervisor, for his committed effort and support towards my PhD and thesis objectives. I would also like to thank Prof Johannes Benedikt and Dr Jonathan Lees, for providing me a wealth of practical experience and knowledge.
- Dr. Simon Woodington, who guided me through my research and provided a platform for the research objectives presented in my thesis.
- I am also grateful to Dr. Tudor Williams and Mr. Simon Mathias of Mesuro Limited, for providing me the resources and opportunity to develop a software platform for active load-pull measurements.
- Finally, to my friends: James Bell, Rob Smith, Alex Spyro and Ana Pelaez for their support during my PhD.

List of Publications

R. S. Saini, S. Woodington, J. Lees, J. Benedikt, and P. J. Tasker,"An Intelligence driven active load-pull system," in Proc. 75th Microwave Measurements Conf. (ARFTG), pp. 1–4, May 2010.

Saini, R.S.; Bell, J.W.; Canning, T.A.J.; Woodington, S.P.; FitzPatrick, D.; Lees, J.; Benedikt, J.; Tasker, P.J.; , "High speed non-linear device characterization and uniformity investigations at X-band frequencies exploiting behavioral models," Microwave Measurement Conference (ARFTG), 2011 77th ARFTG , vol., no., pp.1-4, 10-10 June 2011

Saini, R.S.; Bell, J.J.; Williams, T.; Lees, J.; Benedikt, J.; Tasker, P.J.; , "Interpolation and extrapolation capabilities of non-linear behavioural models," Microwave Measurement Symposium (ARFTG), 2011 78th ARFTG , vol., no., pp.1-4, 1-2 Dec. 2011

Other Contributions

J. Horn, S. Woodington, R. Saini, J. Benedikt, P. J. Tasker, and D. E. Root; "Harmonic Load-Tuning Predictions from Xparameters," IEEE PA Symposium, San Diego, Sept. 2009

Woodington, S. P.; Saini, R. S.; Willams, D.; Lees, J.; Benedikt, J.; Tasker, P. J.; , "Behavioral model analysis of active harmonic load-pull measurements," Microwave Symposium Digest (MTT), 2010 IEEE MTT-S International, vol., no., pp.1, 23-28 May 2010

FitzPatrick, D.; Saini, R.; Lees, J.; Benedikt, J.; Cripps, S.C.; Tasker, P.J., "A waveform engineering approach to the design of improved efficiency wideband MMIC amplifiers," *Wireless and Microwave Technology Conference (WAMICON), 2011 IEEE 12th Annual* , vol., no., pp.1,6, 18-19 April 2011

Bell, J.J.; Saini, R.; Woodington, S.; Lees, J.; Benedikt, J.; Cripps, S.; Tasker, P.J., "Behavioral model analysis using simultaneous active fundamental load-pull and harmonic source-pull measurements at X-band," *Microwave Symposium Digest (MTT), 2011 IEEE MTT-S International* , vol., no., pp.1,4, 5-10 June 2011

Bell, J.J.W.; Saini, R.; Lees, J.; Benedikt, J.; Cripps, S.; Tasker, P.J.; , "X-band behavioral model analysis using an active harmonic source- pull and load-pull measurement system," Microwave Conference Proceedings (APMC), 2011 Asia-Pacific , vol., no., pp.1430-1433, 5-8 Dec. 2011

Powell, J.R.; Uren, M.J.; Martin, T.; McLachlan, A.; Tasker, P.; Woodington, S.; Bell, J.; Saini, R.; Benedikt, J.; Cripps, S.C.; , "GaAs X-band high efficiency

(>65%) Broadband (>30%) amplifier MMIC based on the Class B to Class J continuum," Microwave Symposium Digest (MTT), 2011 IEEE MTT-S International , vol., no., pp.1-4, 5-10 June 2011

Table of Contents

List of Abbreviations

ADS	Advanced Design System
ALP	Active Load-pull
AM-AM	Amplitude to Amplitude distortion
AM-PM	Amplitude to Phase distortion
AWR	Applied Wave Research
CAD	Computer Aided Design Tool
CBM	Cardiff Behavioural Model
DUT	Device Under Test
FFT	Fast Fourier Transform
F0	Fundamental Tone of a signal
GaAs	Gallium Arsenide
HEMT	High Electron Mobility Transistor
LSNA	Large Signal Network Analyser
MMIC	Monolithic Microwave Integrated Circuit
MTA	Microwave Transition Analyser
MWO	Microwave Office
NVNA	Non-Linear Vector Network Analyser
PA	Power Amplifier

PDK	Process Design Kit
S-parameters	Scattering parameter(s)
SSPA	Solid State Power Amplifier
VNA	Vector Network Analyser
X-parameter	Agilent's Non-linear equivalent of S-parameters

Chapter 1 – Introduction

1.1 Background

Radio Frequency (RF) amplifiers are a key component in communication systems and their design often determines a system's architecture. In the early days of amplifier development, vacuum tubes were used to increase the amplitude of a signal. In 1904 the diode was invented by Sir John Ambrose Fleming and was used as a radio detector and rectifier [1]. In 1905, an RF receiver known as the "Marconi–Fleming Valve Receiver" was designed to incorporate the invention commercially. This invention was a revolutionary idea, and put down the foundations for many further inventions. The next few decades saw an increase in demand for high frequency receivers such as for radar applications including the use of cavity magnetron [2] for radar receivers. Soon after World War II a significant invention took place; named the point-contact transistor [3]. The birth of the transistor was marked by this development in 1947 by Walter House Brattain, John Bardeen and William Bradford Shockley who were working at Bell Laboratories at the time. Their work was driven by the desire to replace vacuum tubes in telephone systems and eventually led to

the development of the first Bipolar Junction Transistor in 1950 [4] and hence Solid State Power Amplifiers (SSPA) started emerging based on using silicon substrates.

There were various advantages of the solid state technology such as reliability, ruggedness, size, characteristics of operation and cost [5]. In the 1960s a significant advancement in this technology boosted amplifier development for power generation, control and amplification. SSPA components became critical factor in reducing the cost and size of communication subsystems due to improvement in the manufacturing process. Using silicon substrates made it possible to integrate both active and passive components on the same substrate, thus the realisation of Integrated Circuits (ICs) as well as Monolithic Microwave Integrated Circuits (MMICs) [6]. The resulting circuits were very compact in size and could operate at reduced supply voltages eventually leading to the development of portable handheld equipment.

Requirements and applications of modern communication systems are therefore very varied in terms of frequency of operation and power. A table of RF frequency allocations from 9 KHz to 275 GHz, as released in 2010 by independent regulator and competition authority for the UK communications industries (OFCOM) is provided in [7]. Implementation of each of these applications entails providing a specific modulation format and output power level. This makes it necessary to provide a unique design solution for each component in a communication system for effective usage in transmitting/receiving technologies.

1.2 The rise in requirements for efficiency

It has been recently reported [8] that there are over 6 billion mobile phone subscribers world-wide. At the present time, this accounts for more than a third of the world's population and the number is still growing.

With the introduction of 3rd and 4th Generation (3G and 4G) mobile networks [9], users are now equipped with more than just a wireless telephone service on their mobile phone. Subscribers globally now have access to Global Positioning System (GPS) applications, internet, email, music and video streaming and many other features which require faster data transfer rates and thus a higher cost to both the subscribers and network operators.

At the same time, there is a demand for "greener" systems, placing a demand on portability of devices as well as improved battery life. Thus the drive for improved power efficiency does not only come from the mobile handset market. Network provider infrastructures such as base stations are also prone to the same cost, efficiency and power requirements. The mobile phone market is just one example of this demand trend. There is a similar constraint on military and aerospace applications whereby reliability, weight and size govern the design of equipment.

When narrowed-down, it is the RF Power Amplifier (RFPA) stage which governs how efficient and portable the communication system is. For example, in the mobile handset industry, power requirements of the low power amplifiers within the handset control how long the battery life is. Maximising the output power as well as the DC-to-RF conversion (also called the efficiency) of the RFPA is therefore paramount in designing such demanding wireless components.

1.3 Tools for high efficiency RFPA design

Traditionally, RFPAs were designed using linear design based on s-parameters [10]. This provided insight into the characteristics of the behaviour of the transistor such as for a two-port device: gain (s21), input match (s11), output match (s22) and stability. In order to capture the desired data for linear design, s-parameter measurements are carried out

under small-signal conditions (no harmonic content) using a Vector Network Analyser (VNA) [11]. The s-parameters can then be imported into Computer Aided Design tools (CAD) and the RFPA designer can then simulate and prototype the PA in a time-efficient manner. Whilst linear amplifier design provides very good RF small-signal gain, the maximum theoretical achievable efficiency in such modes of operation is 50%. The system total efficiency will be further reduced by dealing with the DC energy not converted to RF energy, but dissipated as heat. This is known as the Class-A mode of operation [12].

High efficiency modes of operation of RFPAs are governed by driving the device sufficiently into compression (> 1dB gain compression). The consequence of this is that the device under test (DUT) starts to generate additional spectral products. Efficiency improvements can be noticed when the fundamental output impedance and the impedance at these additional spectral products, most notably at the second and third harmonic frequencies are matched appropriately using load-pull measurements. Such modes include Class-F and Class-J [13]-[14]. S-parameters however fail to represent non-linear behaviour of active devices and thus new measurement techniques are required to design such modes of RFPAs.

1.3.1 Non-linear Vector Network Analysers (NVNAs)

Until the release of specific NVNA hardware, non-linear device instrumentation was largely based on VNA measurements with extended capabilities. An example is power and spectral measurements with an appropriate test set and extended load-pull functionality. While measurement and acquisition of data using a VNA is very rapid, its inability to provide a full non-linear response introduces limitations on design. Using a Class-F RFPA design as an example, the current waveform

is required as a half-wave rectified sinusoid, and the voltage is a square wave [13]. An accurate measurement of magnitude and phase of the fundamental tone as well as the harmonically related tones is thus required. Measurement of magnitude of the spectral components is possible using a spectrum analyser or power meter. However, due to the lack of phase information, the calculation of voltage and current waveforms from standard VNA instrumentation is impossible making the Class-F design example difficult to achieve and impossible to verify.

Non-linear test and measurement instrumentation (NVNA) was therefore developed to provide insight into the time-domain voltage and current waveforms and used in conjunction with source- and load-pull measurement systems to provide control over the shape of these waveforms. As a concept, measurement of time-domain waveforms can be carried out directly at the terminals of the DUT using an oscilloscope (a time domain solution) or via measured frequency components (frequency domain solution). At the present time, both these solutions are commercially available. The Agilent PNA-X [15] for example, provides a NVNA capability with a phase reference unit to provide calibrated time-domain waveforms. The Mesuro MB150 Active Load-pull system features a time-domain solution whereby a Tektronix Digital Sampling Oscilloscope (DSO) is used as the primary receiver [16].

1.3.2 Source- and Load-pull systems

Load-pull is the accurate measurement of key nonlinear performance parameters such as output power, gain, efficiency and linearity as a function of frequency, input drive, temperature and many other factors. Most importantly, these measurements are carried out as function of fundamental load impedance [17]. Commercial load-pull implementations include a calibrate-able test-set, and more recently, an NVNA capable of

measuring time-domain waveforms and an automated mechanism of controlling the desired reflection coefficients. Load-pull systems are classified into two broad categories.

The first, passive load-pull is based on a stepper-motor driven tuning mechanism which contains one or more stubs that can alter the fundamental or harmonic load impedance by controlling the position and length of these stubs [18]. These tuning instruments are widely used in many labs around the world. However they are faced with the challenge of achieving high enough reflection coefficients due to the inherent losses within the tuners.

The second approach is called active load-pull [19]. In this mode, an active signal, provided by a phase-controllable synthesiser is amplified and injected thus addressing the problems of loss and allowing unrestricted coverage of the smith-chart. There are various problems with this technique. Firstly, the active signal requires an amplifier that has a large enough gain and thus the load-pull signal to achieve the desired impedance. Independent synthesisers are also required for each controllable harmonic. The cost of amplifiers as well as synthesisers however increases with frequency and it thus becomes an expensive implementation. Secondly, if an open-loop [19] mechanism is used for active load-pull, the measurement system becomes iterative, increasing the time taken for device measurement. This is because in the open-loop mode, there is no prior knowledge of the reflected waves and thus the system has to iterate via a mathematical algorithm or otherwise to achieve the desired reflection coefficient.

One of the objectives of the work presented in this thesis is therefore to research and develop strategies for faster active load-pull measurements using the open-loop architecture and thus improve the measurement system utilisation efficiency.

1.3.3 Non-linear behavioural models

While non-linear measurement instrumentation provides the desired functionality in collecting the required measurement data for high efficiency design, it is of paramount importance to provide such data in the CAD environment. The two main CAD tools in use at the present time are Agilent's Advanced Design System (ADS) [20] and Applied Wave Research's (AWR) Microwave Office [21].

The data collected from the aforementioned measurement systems is typically represented as a black-box behavioural model. More recently, behavioural modelling development has focussed on frequency-domain concepts with a fundamental motivation to define a non-linear formulation that is an equivalent of linear s-parameter formulations [22]. Another consequence of this desire is that the model definitions have been derived in the travelling wave domain. Current trends in non-linear behavioural modelling include:

i) Volterra Input Output (VIOMAP) [23]
ii) Poly Harmonic Distortion Modelling (PHD) [24]
iii) S-functions [25]
iv) X-parameters™ [26]
v) Cardiff Behavioural Model [27]

It has to be noted that the approaches named above have similar formulations for example; they all include phase conjugated mixing products. The underlying concepts have been proven to describe behaviour of the DUT to map load-pull contours over the entire smith chart [28].

Non-linear measurement service providers and instrument manufacturers often provide their own mechanism for providing a suitable

model in CAD. Most notably, for example, is X-parameters™ developed by Agilent Technologies. This is a black-box non-linear behavioural model which, according to Agilent, is the "non-linear equivalent of s-parameters" [26]. X-parameters were released as a measurement option with Agilent's new generation PNA-X and a passive load-pull tuning system developed by Maury Microwave. This provided a turn-key solution to extracting a non-linear device model for use in CAD [29].

X-parameters, like S-functions and the Cardiff Behavioural, all have a common "root", the Poly Harmonic Distortion (PHD) modelling concept [24]. In theory, these models describe a generalised transfer function relating an input signal at a given port to the observed output signal at all ports. These transfer functions are captured using both the incident and reflecting travelling waves to and from a port under a given drive level. This therefore makes them reduce to s-parameters under linear excitation conditions as described by Baylis et al. in [22].

Measurement based models such as these however suffer from various deficiencies as pointed out by Heimlich et al. in [30]. The measurement density and discrete parameterisation required to capture a full non-linear model under various stimuli e.g. frequency, input power, temperature, input and output bias creates an explosion in model file size. Another factor, mainly seen in X-parameter and S-function extraction, is the accuracy of harmonic predictions. A harmonic model in these implementations is based on measurements carried out using "tickle tone" signals. These are small signal tones approximately 20dBc below the fundamental excitation used to derive harmonic cross products at each fundamental load-pull point. Using such a model, the measurement data is then extrapolated within the simulator to predict performance all around the smith chart.

One of the objectives of the work presented in this thesis is therefore to investigate and provide evidence on the accuracy of fundamental interpolation and harmonic extrapolation and interpolation.

1.4 Objectives and structure of the thesis

The objective of this thesis is to provide improved load-pull measurement strategies based on an open-loop active load pull measurement system.

The first strategy is to develop an improved load-pull convergence algorithm, based on deriving local PHD models to aid the prediction of the desired active signal in order to achieve a target reflection coefficient. With the aid of this algorithm, measurement system utilisation efficiency will be greatly improved allowing the user to carry out faster load-pull sweep plans. An investigation into numerical concepts was used to define the problem area followed by a discussion on the load-pull error model. A new strategy was then designed and proved to be effective in reducing the number of iterations and thus improving the utilisation efficiency from a typical value of < 30% up-to 90%. The work was demonstrated by carrying out load-pull measurements on 0.5W Gallium Arsenide (GaAs) devices as an example of load-pull characterisation. The load-pull measurement system used was developed in Cardiff University and based on a time-domain measurement capability provided for by a 4-channel Tektronix Digital Sampling oscilloscope as the primary receiver.

Applications of the improved load-pull measurement system described above were the subject of the next strategy whereby a non-linear wafer mapping process was used as an example of high speed device characterisation using an active load-pull system. Using the Cardiff Behavioural modelling formulations, it was shown that non-linear data collected from the wafer mapping process can be readily archived and thus

made available in CAD with the same elegance as S-parameter data was for small-signal measurements.

The final objective is to investigate the fundamental and harmonic accuracy of a measurement based behavioural model.

Using the data and conclusions of this investigation, recommendations for the size of load-pull data grids and extent to which harmonic extrapolation can be carried out will determine the recommended strategy for performing fundamental and harmonic load-pull measurements. This is a critical question when faced with the challenge of reducing measurement time due to iterations in active load-pull or lack of impedance coverage when using passive load-pull.

1.5 Chapter Synopsis

Chapter 2 is a literature review, aimed to discuss the evolution of microwave measurement systems from linear RF measurements to the non-linear RF measurement domain. It includes a historical account of measurement architectures, eventually leading to automated source- and load-pull measurement systems. A detailed discussion of passive and active load-pull architectures provides an insight into the advantages and short comings of each technique. By the end of this chapter, the reader is introduced to the automated open-loop active load-pull measurement system architecture – the focus of this thesis.

Chapter 3 aims to review various non-linear behavioural model generation approaches available today. Starting with a comparison of behavioural models to compact and physical models, the chapter explores various advantages of using this approach. The theory behind the PHD model is also described and shown how most modern frequency domain behavioural modelling implementations follow this theory. A discussion of model extraction using commercially available hardware is also discussed

along with its drawbacks. The reader is then familiarised with the Cardiff Behavioural Model formulations. Various examples of model coefficient extraction are used to explain the concept and show the accuracy of the model predictions in both fundamental and harmonic load-pull.

Chapter 4 describes how an application of the PHD model can add intelligence to an open loop active load-pull system. A discussion of the load-pull error model in open loop active load-pull measurement systems was used to examine the iterative nature of such a system. This was followed by demonstrations of the existing numerical techniques and their associated problems. As a solution to the problem, a new approach was introduced which utilised the X-parameter formulations for carrying out load-pull predictions. A locally derived X-parameter model was thus shown to be capable of adding intelligence to an open loop active load-pull system. This approach enabled a significant improvement in the system's ability to provide the desired load emulation capability.

Chapter 5 investigates a non-linear measurement approach suitable for wafer mapping and technology screening applications. It is shown how rapid characterisation and uniformity investigations of non-linear devices are possible through the use of an intelligence driven, open-loop active load-pull measurement system which uses localised behavioural models to improve speed of device characterisation and thus measurement system utilisation efficiency.

Chapter 6 describes how the Cardiff Behavioural model is effective in its ability to interpolate or extrapolate non-linear measurement data and thereby improve the quality and speed of measurement systems. The analysis included testing the interpolation capability of a fundamental-only model. This was followed by using measurement data to examine the extrapolation and interpolation capabilities of a second harmonic model.

Chapter 7 is a conclusions and future work section. It aims to summarise the main findings of the work presented in this thesis and explore possible future trends that can benefit from this work.

References

[1] Brittain, J.E. "Electrical Engineering Hall of Fame: John A. Fleming", Proceedings of the IEEE, Volume 95, Issue 1, 2005 pp. 313-315.

[2] Osepchuk, J.M.; , "The magnetron and the microwave oven: A unique and lasting relationship," Origins and Evolution of the Cavity Magnetron (CAVMAG), 2010 International Conference on the , vol., no., pp.46-51, 19-20 April 2010

[3] Arns, R.G.; , "The other transistor: early history of the metal-oxide semiconductor field-effect transistor," Engineering Science and Education Journal, vol.7, no.5, pp.233-240, Oct 1998

[4] Ernest Braun and Stuart Macdonald, "Revolution in miniature", Cambridge University Press, Cambridge and New York, 2nd ed. 1982

[5] Franco Sechi, Marina Bujatti, "Solid-State Microwave High-Power amplifiers," Artech House, 1ed 2009.

[6] Steve Marsh, "Practical MMIC Design, "Artech House, 2006

[7] Online: http://stakeholders.ofcom.org.uk/binaries/spectrum/spectrum-policy-area/spectrum-management/ukfat2010.pdf [Accessed 15-Dec-2012]

[8] Online: http://www.unmultimedia.org/radio/english/2012/10/itusix-billion-mobile-phone-subscribers-worldwide-and-still-growing/ [Accessed 15-Dec-2012]

[9] Online: http://www.bbc.co.uk/news/technology-19543041 [Accessed 15-Dec-2012]

[10] David Pozar, "Microwave Engineering", third edition, John Wiley & Sons, 2005. pp 174-175.

[11] Agilent Technologies, "Agilent Network Analyzer Basics", accessed the Application note available at www.agilent.com on 12 July 2011.

[12] Steve C. Cripps, "RF Power Amplifiers for Wireless Communications," Artech House, 2ed 2006, pp 18-19

[13] P. Wright, A. Sheikh, C. Roff, P. J. Tasker, and J. Benedikt, "Highly efficient operation modes in GaN power transistors delivering upwards of 81% efficiency and 12W output power," in IEEE MTT-S Int. Microwave Symp. Dig., June 15–20, 2008, pp. 1147–1150.

[14] P. Wright, J. Lee, P. J. Tasker, J. Benedikt, and S. C. Cripps, "An efficient, linear, broadband class-J-mode PA realised using RF waveform engineering," in IEEE MTT-S Int. Microwave Symp. Dig., June 2009, pp. 653–656.

[15] Agilent Technologies, Data sheet; "Agilent 2-port and 4-port network analyser," available online: http://cp.literature.agilent.com/litweb/pdf/N5242-90007.pdf [Accessed: 15-Dec-2012]

[16] Online: http://mesuro.com/ [Accessed: 15-Dec-2012]

[17] Tasker, P.J.; , "Practical waveform engineering," Microwave Magazine, IEEE , vol.10, no.7, pp.65-76, Dec. 2009

[18] Tsironis, C.; Jurenas, A.; Liu, C.; , "Highly accurate harmonic tuners for load pull testing," Microwave Conference, 2001. APMC 2001. 2001 Asia-Pacific , vol.3, no., pp.1311-1314 vol.3, 2001

[19] J. Benedikt, R. Gaddi, P.J. Tasker and M. Goss "High-Power Time-Domain Measurement System with Active Harmonic Load-Pull for High-Efficiency Base-Station Amplifier Design" IEEE Transactions on Microwave Theory and Techniques, Vol. 48,No.12, pp.2617-2624, December 2000

[20] Agilent Technologies;, "Advanced Design System brochure", Available online: http://cp.literature.agilent.com/litweb/pdf/5988-3326EN.pdf [Accessed: 15-Dec-2012]

[21] Applied Wave Research (AWR);, "Microwave Office Brochure," Available online: http://www.awrcorp.com/sites/default/files/content/attachments/MWO-Brochure.pdf [Accessed: 15-Dec-2012]

[22] Baylis, C.; Marks, R.J.; Martin, J.; Miller, H.; Moldovan, M.; , "Going Nonlinear," Microwave Magazine, IEEE , vol.12, no.2, pp.55-64, April 2011

[23] F. Verbeyst and M. Vanden Bossche, "VIOMAP, the S-parameter equivalent for weakly nonlinear RF and microwave devices," in IEEE MTT-S Int. Microwave Symp. Dig., May 1994, vol. 3, pp. 1369–1372.

[24] J. Verspecht and D. E. Root, "Polyharmonic distortion modeling," IEEE Microwave Mag., vol. 7, no. 3, pp. 44–57, June 2006.

[25] M. Myslinski, F. Verbeyst, M. V. Bossche, and D. Schreurs, "S-functions behavioral model order reduction based on narrowband modulated large-signal network analyzer measurements," in Proc. 75th Microwave Measurements Conf. (ARFTG), May 2010, pp. 1–6.

[26] D. Root, J. Horn, L. Betts, C. Gillease, and J. Verspecht, "X-parameters: The new paradigm for measurement, modeling, and design of nonlinear RF and microwave components," Microwave Eng. Eur., vol. 51, no. 12, pp.16–21, Dec. 2008

[27] Tasker, P.J.; Benedikt, J.; , "Waveform Inspired Models and the Harmonic Balance Emulator," Microwave Magazine, IEEE , vol.12, no.2, pp.38-54, April 2011

[28] Woodington, S. P.; Saini, R. S.; Willams, D.; Lees, J.; Benedikt, J.; Tasker, P. J.; , "Behavioral model analysis of active harmonic load-

pull measurements," Microwave Symposium Digest (MTT), 2010 IEEE MTT-S International, vol., no., pp.1, 23-28 May 2010

[29] Simpson, G.; Horn, J.; Gunyan, D.; Root, D.E.; , "Load-pull + NVNA = enhanced X-parameters for PA designs with high mismatch and technology-independent large-signal device models," ARFTG Microwave Measurement Symposium, 2008 72nd, vol., no., pp.88-91, Dec. 2008

[30] Heimlich, M.; , "Get on the Same Nonlinear Page," Microwave Magazine, IEEE , vol.12, no.2, pp.32-37, April 2011

Chapter 2 – Evolution and Current Trends of Non-linear Measurement Systems

Design and modelling of microwave devices and circuits requires accurate device measurement and characterisation. In this chapter, the evolution of microwave measurement systems will be discussed from linear RF measurements through to the non-linear RF measurement domain. This literature review will discuss the different measurement architectures and the advantages and disadvantages of each of the measurement techniques, paying particular attention to design of high performance components for modern wireless systems.

At low frequencies, the voltage (at a terminal) can be directly measured using a high impedance probe and the current (through a node) can be measured via a series low-impedance probe. These measurements therefore allow the computation of admittance and impedance parameters. In microwave components, the electrical behaviour (phase) of the voltage or current changes significantly over the physical extent of the component as a result of the dimensions of the phase velocity being coupled to the physical dimensions and material

construction of the component being measured. This characteristic of microwave components created a practical measurement problem.

Measurement of travelling incident- and reflected waves to and from a port respectively provided a solution to this problem and thus allowed the maintenance of a constant impedance environment (Z0 = 50Ω) across the required bandwidth. These ideas led to the scattering matrix [10] representation, for an *n*-port network, which provides a complete description of the network. A scattering parameter (s-parameter) thus provides us with a complex number that is a ratio of the incident (a_n) and reflected (b_n) travelling wave from a port, *n*. This elegance accounts for both magnitude and phase information and can now be used to compute impedance and admittance parameters.

2.1 Small Signal (S-parameter) measurements

Since the adoption of S-parameters in the microwave industry, a significant improvement in the design cycle was seen. This is because they created the ability to directly describe the four main characteristics of any passive *n*-port device i.e. transmission (s_{21}), output match (s_{22}), isolation (s_{12}) and input match (s_{11}) for a two port device.

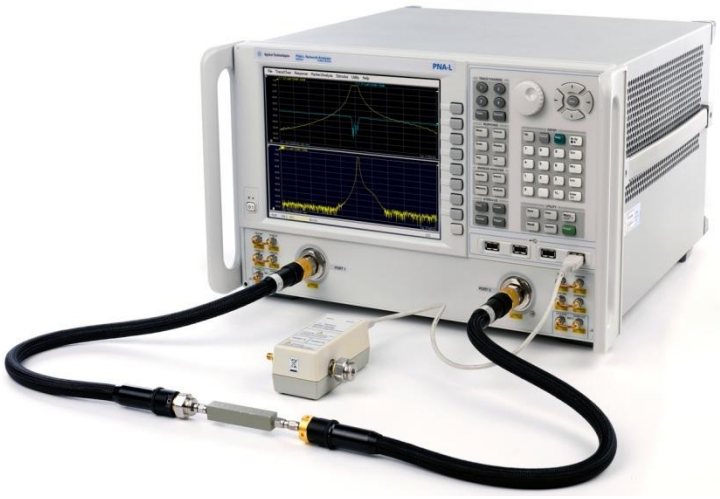

Figure 2-1: Photograph of the Agilent PNA-L series Network Analyser

The S-parameters of passive and active networks can be measured directly with a calibrated Vector Network Analyser (VNA). Presently, there are many VNAs available in the market e.g. Agilent PNA series [2] (photograph shown in Figure 2-1), Rohde & Schwarz ZVA series, etc. This is typically a two- or a four- port instrument which can measure the incident and reflected travelling waves from the Device-Under-Test (DUT). A simplified block diagram of a two-port analyser [10] is shown in Figure 2-2. In this architecture, a source is required for injecting the incident wave into the DUT at the required frequency or at a range of frequencies (sweep mode). In most modern network analysers today, this component is a synthesized source, integrated into the analyser to achieve good frequency resolution as well as stability. The next component in the block diagram is a signal separation module, commonly termed as a test set. A typical network analyser test set contains a combination of directional couplers and bridges, which provide a range of signal separation options. Firstly, a low insertion loss directional coupler is used to extract a portion of the incident signal, e.g. a_1 to provide a reference for calculating ratios.

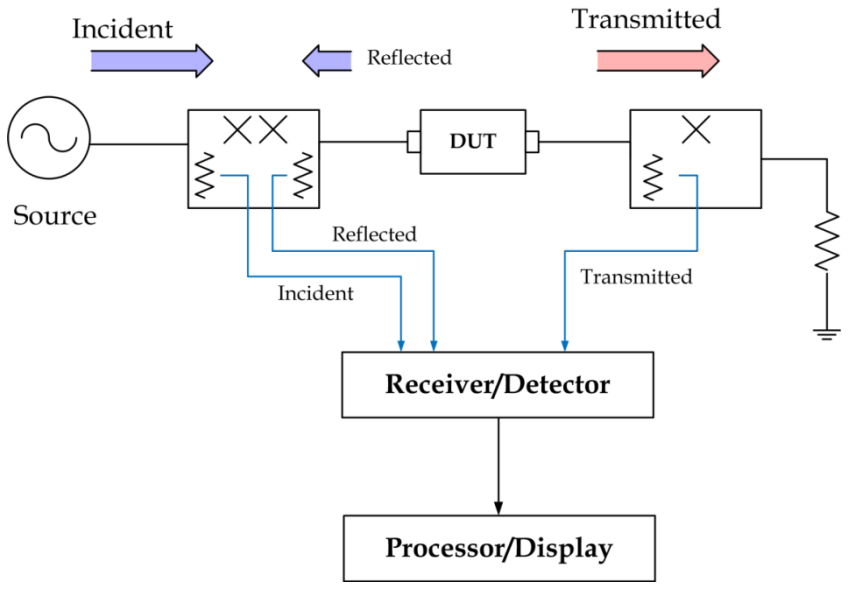

Figure 2-2: Simplified block diagram of a Vector Network Analyser (VNA)

A second function of the test set is to separate the incident and reflected signals to and from- the DUT. A bridge is used instead of a coupler to carry out this operation. This is due to the fact that a truly broad-band coupler is difficult to realise and the capability to measure signals down to DC is therefore restricted. The receiver module can either utilize a diode-detector to convert the RF signal to a proportional DC level or utilize a Local Oscillator (LO) to mix the RF down to a lower Intermediate Frequency (IF). Locking the LO to the RF or IF signal provides a tuning mechanism to reference the RF signal present at the reference port. In modern VNAs, an analogue-to-digital (ADC) converter is used to extract magnitude and phase information from the IF signal in this tuned-receiver approach.

The VNA determines s_{11} and s_{21} by measuring the magnitude and phase of the incident, reflected and transmitted voltage signals when the output is terminated into a perfect reference impedance (Z_0); thus guaranteeing that a_2 is zero. This is shown in (2-1) and (2-2).

$$s_{11} = b_1 / a_1 \Big| a_2 = 0 \qquad (2\text{-}1) \qquad s_{21} = b_2 / a_1 \Big| a_2 = 0 \qquad (2\text{-}2)$$

Likewise, injecting the signal at port 2 and thereby terminating port 1 in a perfect load ensures that a_1 is zero thus makes measurements of s_{22} and s_{12} can be made possible as shown in (2-3) and (2-4).

$$s_{22} = b_2 / a_2 \Big| a_1 = 0 \qquad (2\text{-}3) \qquad s_{12} = b_1 / a_2 \Big| a_1 = 0 \qquad (2\text{-}4)$$

The ability to measure, model and then simulate using s-parameters of a DUT therefore provides us with virtually all the information we need to carry out linear design. They are also independent of the measurement system and the data generated is repeatable and reliable. Therefore, for linear circuits, s-parameters provide an essentially complete behavioural model of the DUT. The circuit can be replaced by an s-parameter simulation block for use in Computer Aided Design (CAD) and hence the behaviour of microwave systems can be evaluated at a higher level of abstraction.

These small signal parameters however fail to represent non-linear behaviour (under large signal excitations). W.H. Leighton et al. and R.J Chaffin et al. presented papers on the design of RF amplifiers with "Large Signal" s-parameters in 1973 [4]-[5]. The papers concluded that s-parameters gave insight into the operation of devices under large signal conditions however the measured s-parameters were found to be drive and bias dependent thus making them difficult to use as a representation for large signal device behaviour. They are therefore only defined for systems behaving linearly to small signal excitations around a static operating point e.g. response measured only at a frequency and power level under which it is excited. Under large signal excitations [6], however, active devices generate harmonics, inter-modulation distortion and cause spectral re-growth.

2.2 Evolution of Non-linear measurement systems

Traditionally, a combination of a network analyser and a spectrum analyser was used to measure the most important non-linear properties of active devices, most commonly, power amplifiers. These properties include gain vs. frequency ($|S_{21}|$), harmonic inter-modulation distortion (if using a modulated carrier signal), harmonic and fundamental

magnitude measurements, linearity measurements, etc. Power sweeps and gain compression/expansion measurements can be carried out within the network analyser, whereby the input power is swept and a trace of $|S_{21}|$ shows compressive behaviour as shown in Figure 2-3. Depending on the size of device, an external amplifier may be required to provide a large enough drive for attaining device compression. Spectrum analysers are usually single-receiver units, which also contain tuneable local oscillators in their receivers.

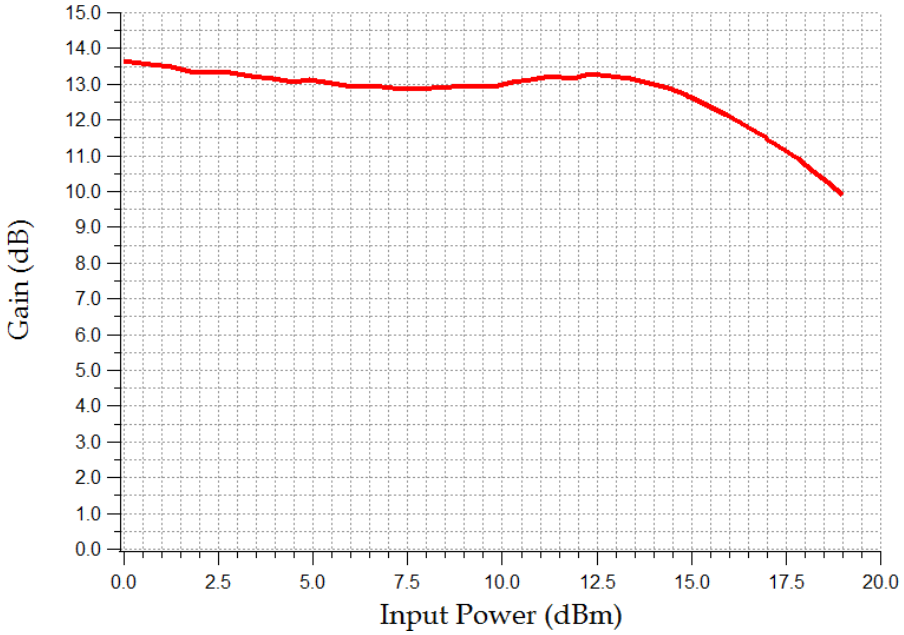

Figure 2-3: Gain Compression (|S21|)

The receiver component however handles a wider range of IF bandwidths covering a larger dynamic range and thus offers a different measurement application when compared to a network analyser. To make a measurement, the analyser simply tunes the LO to each frequency bin and makes a power-in-band measurement on the resulting signal. It can therefore be used to measure amplitudes of the fundamental and harmonic signals, as shown in Figure 2-4 as well as inter-modulation distortion and spurious emissions.

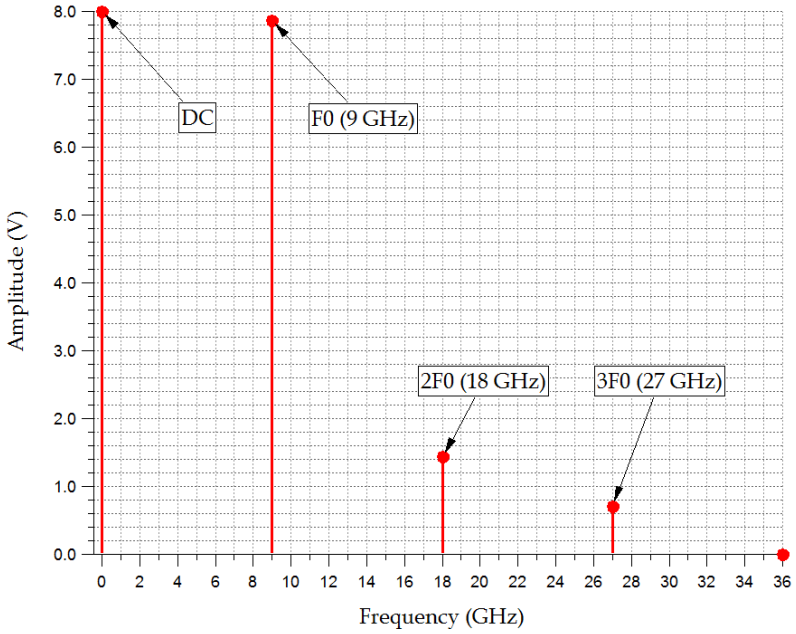

Figure 2-4: Spectral content of the signal at the output of a non-linear DUT

Due to the unavailability of phase measurements, its use is limited to magnitude-only and thus limiting non-linear characterization whereby the calculation of voltage and current waveforms is a proven technique for providing information for high efficiency PA design [7]-[22].

In the late 1980's Sipila et. al. [23] demonstrated a calibrated waveform-based non-linear measurement system based on the Tektronix DSO oscilloscope. Prior to this work, even though high speed sampling oscilloscopes existed for a long time, the errors caused by frequency response of measurement systems as well as mismatches and multiple reflections made it difficult to perform voltage and current waveform measurements at microwave frequencies. These measurements provided both magnitude and phase information of the fundamental and harmonic components by carrying out a Fast Fourier Transform (FFT) on measured time-domain data. This was followed by reconstruction of the time-domain waveforms after error-correction by an inverse FFT function.

An alternative to this approach was implemented by Lott [24], also in the late 1980's. In this approach, a VNA was used to measure the individual spectral components in sequence while using a phase

generator[1] to maintain a coherent phase reference. This procedure resulted in better sensitivity than the sampling scope approach due to the smaller noise bandwidth and it did not suffer from trigger-jitter problems.

Non-linear measurements systems saw an accelerated development phase [25]-[31] between 1990-2000 with the introduction of the Hewlett Packard Microwave Transition Analyser (MTA or HP 71500 Series). This instrument was a dual channel sampling oscilloscope with a dynamic range of 60 dB and was able to operate over a large bandwidth, compared to oscilloscopes at the time (up to 50 GHz). The presence of an internal trigger relaxed the requirement for providing an external trigger and thus simplifying measurement circuitry as well as improving robustness of the measurement system. The MTA was also able to emulate traditional VNA functionality in its "frequency sweep" mode, ideal for calibration of the measurement system. This combination of a calibrate-able test-set, synthesizer and receiver unit capable of non-linear measurements has since been termed "Non-linear Vector Network Analyser" (NVNA).

Figure 2-5 depicts one such setup based on [28] whereby an on-wafer NVNA was developed, based on the MTA for characterisation of large signal behaviour of transistors. This system allowed measurements of the input reflection and transmission coefficients of the non-linear DUT as a function of power and frequency. The acquired measurement data was also used to re-assemble harmonically-rich input and output voltage waveforms. Addition of a high frequency amplifier (2GHz to

[1] The phase generator device was one that had a much faster switching time than the typical DUT. At the time, the reference circuit was a GaAs beam lead diode (Marconi DC 1346), connected in parallel to a 50 ohm micro strip line.

26.5 GHz) in the test setup provided sufficient power for transistors to be driven into saturation.

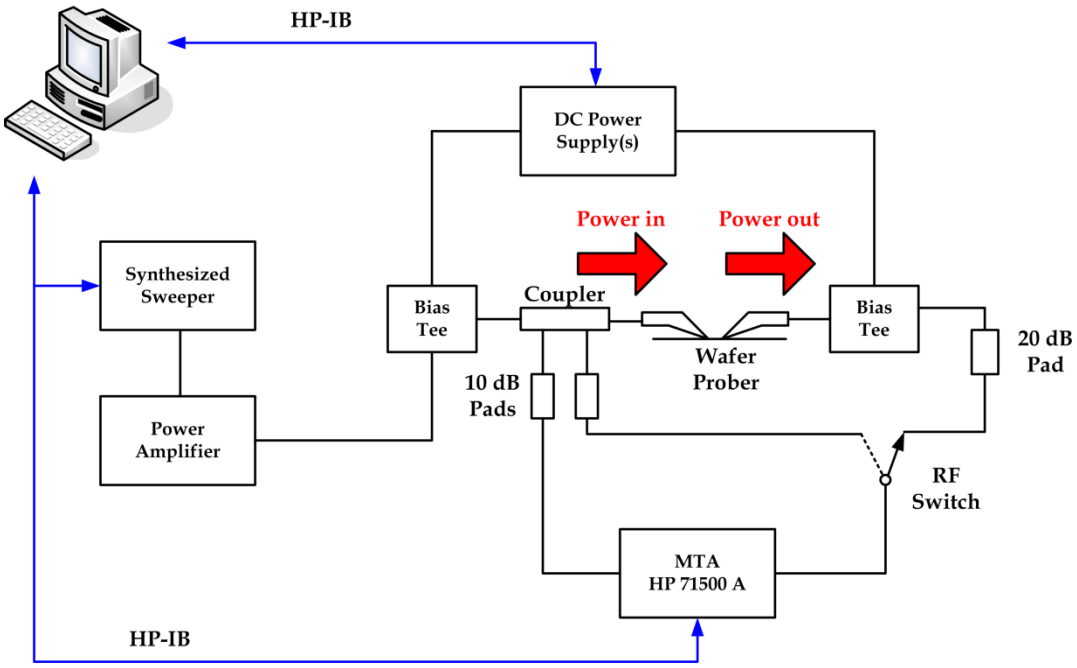

Figure 2-5: Block diagram of a high frequency NVNA system based on the MTA

In order to measure both the incident and reflected travelling waves, a set of couplers was used at the input in combination with a 50 GHz coaxial switch. The attenuation provided by 10 dB pads provided protection to the receiver ports. Note that this was a forward-only system hence both $a_1(f)$ and $b_1(f)$ travelling waves were measured at port 1. At port 2, only the reflected wave, $b_2(f)$ was measured.

2.2.1 Calibrating a 2-port NVNA

A flow graph of an error model for a full two-port NVNA is shown in Figure 2-6 as described in [30]. In this flow, a description of the relationship between the Fourier coefficients i.e. $a_0(f)$, $b_0(f)$, $a_3(f)$, $b_3(f)$ of measured time-varying voltage travelling waveforms to the Fourier coefficients i.e. $a_1(f)$, $b_1(f)$, $a_2(f)$, $b_2(f)$ of actual time-varying normalized voltage travelling waveforms is shown. These transforms are given in

equations (2-5) to (2-8) assuming all the travelling waves are expressed as Fourier coefficients thus ignoring post-fix *(f)*. The calibration process can be divided into two distinct stages [27] and [30]. Firstly, a vector calibration routine; very similar to a VNA calibration is required to provide the complex error terms ε_{00}, ε_{11}, ε_{22} and ε_{33} as well as complex products $\varepsilon_{10}\varepsilon_{01}$, $\varepsilon_{10}\varepsilon_{32}$ and $\varepsilon_{23}/\varepsilon_{10}$.

Figure 2-6: Flow graph showing an eight term error model

$$b_1 = (b_0 - \varepsilon_{00}.a_0)/\varepsilon_{01} \quad (2\text{-}5)$$

$$a_1 = ((\varepsilon_{01}.\varepsilon_{10} - \varepsilon_{00}.\varepsilon_{11}).a_0 + \varepsilon_{11}.b_0)/\varepsilon_{01} \quad (2\text{-}6)$$

$$b_2 = (b_3 - \varepsilon_{33}.a_3)/\varepsilon_{32} \quad (2\text{-}7)$$

$$a_2 = ((\varepsilon_{32}.\varepsilon_{23} - \varepsilon_{33}.\varepsilon_{22}).a_3 + \varepsilon_{22}.b_3)/\varepsilon_{32} \quad (2\text{-}8)$$

The limitation inherent with the standard VNA calibration procedure is that it operates on s-parameters, which are defined as travelling wave ratios. As a consequence, only relative measurements are calibrated, and the absolute power associated with incoming and outgoing waves remains undetermined meaning that the absolute values of ε_{10} ε_{01}, ε_{32} and ε_{23} cannot be determined. This restriction therefore needed to be eliminated for non-linear measurements.

Therefore, an absolute calibration stage was required and used to determine one of the missing coefficients, ε_{23} or $\varepsilon_{10;}$ providing access to all

error terms i.e. ε_{00}, ε_{10}, ε_{11}, ε_{01}, ε_{32}, ε_{23}, ε_{22}, ε_{33}. As an example, the magnitude of ε_{10} was determined by performing a comparison of the magnitude read by one of the receiver channels at Port 1 with a calibrated power meter attached to Port 1. Various implementations to date have provided the phase of ε_{10}. Using either a calibrated phase meter [32] or a calibrated phase source [33], a phase comparison measurement can be carried out. In the first approach, using a Tektronix DSA sampling oscilloscope, this was done by directly attaching one of the receiver channels directly to Port 1 and making a comparison phase measurement. In the second approach, a harmonic phase reference generator was attached to Port 1 instead of the receiver channel. Following the correction described above, accurate time-varying voltage and current waveforms were measured at the DUT's input and output terminals.

The NVNA system described above addressed the need for rapid and accurate data thus enabling evaluation of a transistor, its performance and suitability in an application. However, there are certain limitations that prevented a full non-linear characterisation with this setup. Unlike S-parameters, the non-linear DUT cannot always be referenced to a 50Ω impedance. While the waveforms contained non-linear data, a single measured waveform could not be used to compute, via linear algebra or otherwise, waveforms into another arbitrary terminal impedance. This imposed serious restrictions for CAD designers. A lot of research has gone into the non-linear modelling of RF waveform data for use in CAD however the non-linear equivalent of s-parameters is still being sought [34]. Designers have therefore relied on the accurate measurements of key nonlinear performance parameters such as output power, gain, efficiency and linearity as a function of frequency, input drive, temperature and many other factors. Most importantly, they carry out these measurements as function of

fundamental load impedance. These measurements are termed as *Load-pull*.

2.3 Load-pull Measurements

Load-pull is a black-box measurement technique whose main aim is to find optimum performance of an active device via measuring performance into a set of fundamental and harmonic impedances. Performance can be measured in terms of the direct measurement of key non-linear parameters such as output power, gain, efficiency and linearity. The impedance presented to the DUT can be stored in many formats e.g. Z_L (consisting of R + jX), voltage standing ratio (VSWR) and reflection coefficient (Γ_L). Considering a two port device, Γ_L is given by a_2/b_2, i.e. the ratio between the forward and reverse travelling waves. A harmonic load pull system is one in which a harmonic of the fundamental test tone can be simultaneously varied with the fundamental impedance termination. The generalised formula is given by (2-6) whereby *h*-harmonic index and *p*-port index.

$$\Gamma_{p,h} = a_{p,h} / b_{p,h} \qquad (2\text{-}6)$$

An example dataset of a load pull experiment is shown in Figure 2-7 whereby a set of fundamental load-pull impedance points were used to plot the output power contours of a Gallium Arsenide (GaAs) device. Load-pull contours such as this can therefore aid the designer in finding optimum operating points for a device and thus developing the most effective matching circuits.

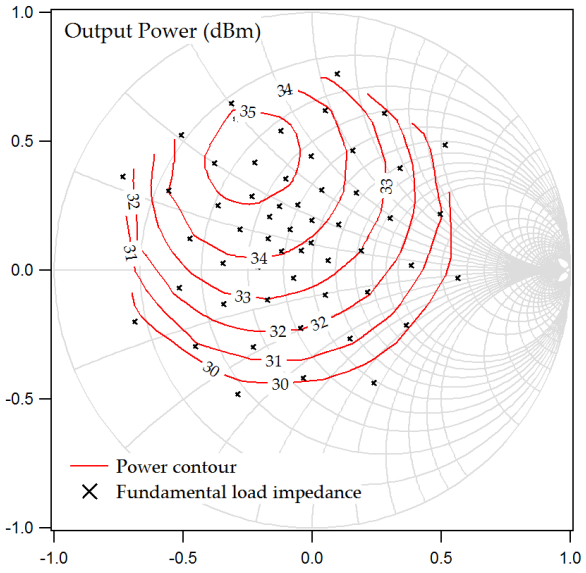

Figure 2-7: Load pull contours

Load pull can be deployed via a sequence of systematic measurements or using a trial and error approach. However, the variation of input drive and quiescent current can be regarded as modifying the current waveform and tuning the load impedances can be regarded as modifying the voltage waveform. It therefore provides an excellent platform for waveform engineering especially if designers are required to meet the increasing demands on system requirements whereby theoretically derived optimum waveforms can now be practically implemented using harmonic load and source[2] pull systems.

2.3.1 Passive Load pull

In its simplest terms, variable load impedance can be achieved by incorporating a stub tuner impedance transformer between the DUT and a 50-ohm matched termination. This provides a way of manipulating the output reflection coefficient (Γ_L) as shown in Figure 2-8.

[2] Source pull is the process of varying the impedance seen by the input of a DUT to other than 50 ohms in order to measure performance parameters.

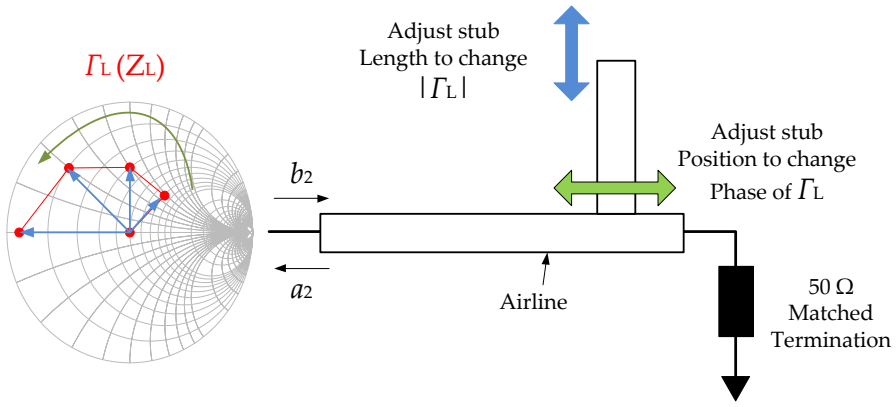

Figure 2-8: Principle of Variable load impedance

The magnitude and phase of the output reflection coefficient can be controlled using this mechanism by altering the length of the stub and the position of the stub respectively.

Modern versions of this technique have included development of stepper-motor-driven, precisely engineered tuners [35]-[36].

Fundamental load pull tuning is achieved via a single tuning stub or a combination of stubs with regard only to the fundamental frequency impedance. Harmonic control is achieved via a combination of two, three or more stub tuners [36]. This is shown in Figure 2-9; two sets of two stubs (resonator circuits) are used.

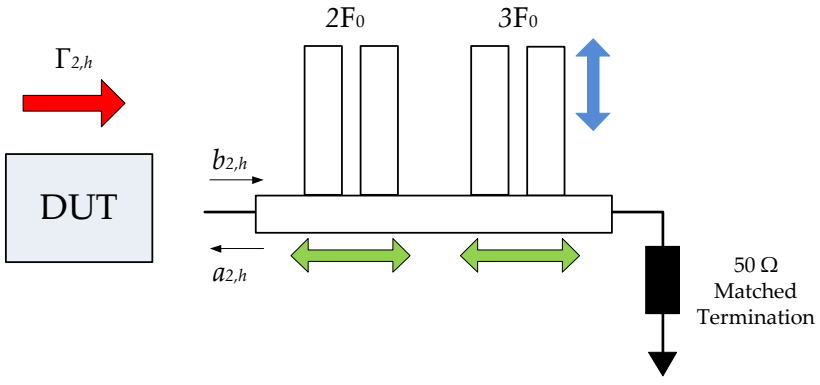

Figure 2-9: Harmonic load pull tuner principle

The above tuner uses the principle of sliding resonator circuits in parallel to a very low loss transmission line. In combination with robust software

algorithms, computation and synthesis of arbitrary harmonic impedances is therefore possible.

Tsironis et. al. [18] and De Groote et. al. [39] demonstrated a load pull measurement system using Focus™ MPT tuners. These systems allowed the characterization of complex and strongly nonlinear behaviour of microwave transistors, including hot IV curves, saturation plots and load pull contours all under controlled conditions of the 2nd and 3rd harmonic impedances. Both these systems utilized a Large Signal Network Analyser (LSNA) as a receiver unit. Based on the above two references, Figure 2-10 is a schematic of a typical passive tuner-based load pull system. In this setup, two passive tuners have been used. The first is a single-slug input tuner, used to adjust the fundamental source impedance, thus providing a mechanism to provide optimum power delivery to the DUT and therefore maximise gain from the device.

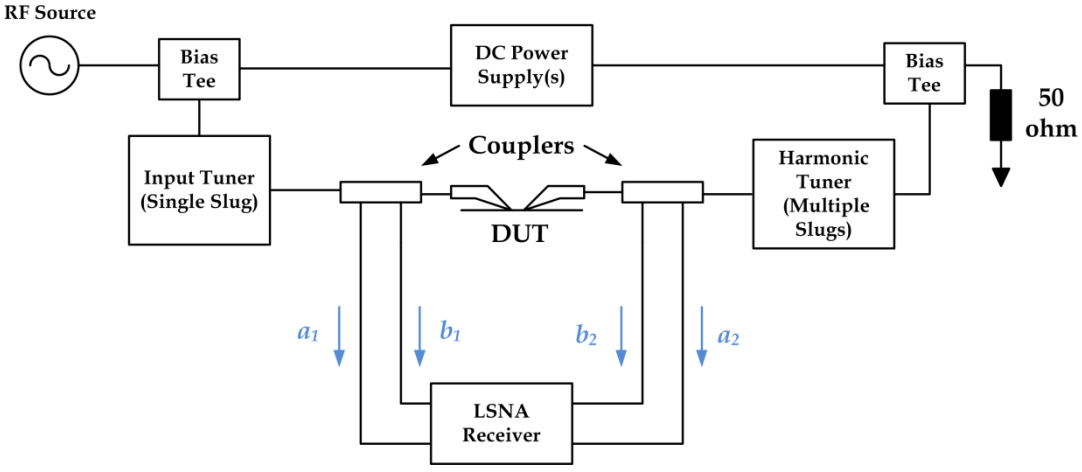

Figure 2-10: Harmonic Load pull demonstrated using passive tuners

On the output side, a multiple stub tuner has been used. This tuner provides control of- and ability to- read and display the fundamental, second and third harmonic impedances independently thus providing the designer with a very effective load pull measurement system.

Since a_2 will always be lower than b_2 in a passive mechanical tuner setup, mainly due to the reflection limitations from the loss in the tuner and losses through the couplers, the maximum achievable value of Γ_L is usually less than 1.0. This setup is therefore limiting especially for harmonic tuning which require an ideal reflection coefficient of $\Gamma_L = 1$.

2.3.2 Active Load pull

This is an alternative to passive load pull techniques, whereby the means of synthesizing the magnitude and phase of the injected signal, a_2 has been replaced by a phase-synchronized signal source. Active load pull systems can be classed into two broad categories:

i. Closed Loop Systems and Envelope Systems
ii. Open Loop Systems

Closed Loop Systems

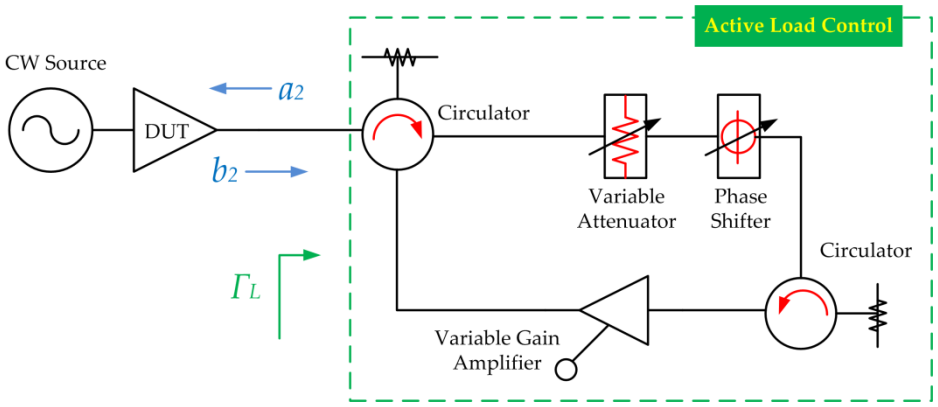

Figure 2-11: Closed-loop Active load-pull setup

The active closed loop system was first realized by Bava et al. [40] in the early 1980's. In this approach (Figure 2-11), the transmitted signal, b_2, is appropriately phase shifted and then attenuated or amplified. It is then

fed back at the DUT output port as the injected new signal, a_2, to achieve the desired load reflection coefficient. As this system uses b_2 to emulate the load, any change in the DUT characteristics or operating conditions is immediately sensed in the injected signal, a_2.

There are several advantages of this technique over traditional mechanical load pull tuners. Firstly, it virtually takes a fraction of the time to change an impedance position, when compared to the movement of a mechanical stub in a passive tuner. Secondly, there is access to a drive-level independent emulation of load impedances. There are some major drawbacks in this architecture though. If the variable gain amplifier in the load pull loop is broad band in nature, there is a strong possibility of RF device oscillations. This problem is further compounded by leakages in the various passive components. In order to reduce these oscillations, significant filtering is implemented in the closed-loop solution. The extra filtering therefore makes the approach a narrow band one as well as increasing implementation costs.

Active Envelope Load-pull Systems (AELP)

The Active Envelope Load-pull system (AELP) further builds and improves the closed loop technique. Tudor Williams et al. [41] first suggested this high speed technique in which the transmitted signal b_2 is down-converted using a quadrature demodulator thus providing a mechanism to "close the loop" at base band frequencies. This is achieved by using external control signals, X and Y as shown in Figure 2-12.

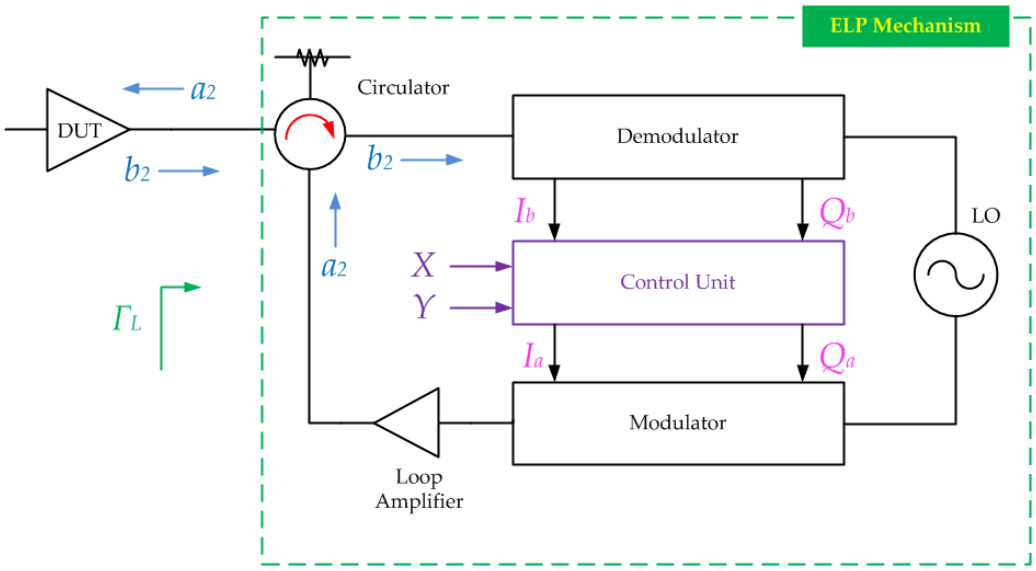

Figure 2-12: Envelope Load-pull Architecture

The modified base band signals are then up-converted by a quadrature modulator and fed back to the DUT output port to emulate the desired load reflection coefficient. This system therefore overcomes oscillation problems inherent at RF frequencies. Improvements to the technique and provision of more robust and realisable calibration routines saw the realisation of the *heterodyne* mode of operation of the AELP system, by Hashmi et al [42].

The biggest draw-back of the AELP technique, however, was that a calibration loop was required before load-pull measurements could be carried out on a device. This calibration loop required multiple measurements, to be able to map the control settings against the desired reflection coefficients used for device characterization for high efficiency design.

Open Loop Active Load-pull

The open loop architecture was originally introduced in the late 70s by Takayama et al. [43]. In this technique (Figure 2-13), both the input and the output of the DUT were driven using external signals; separated at

the source by a power splitter and then amplified at the fundamental frequency.

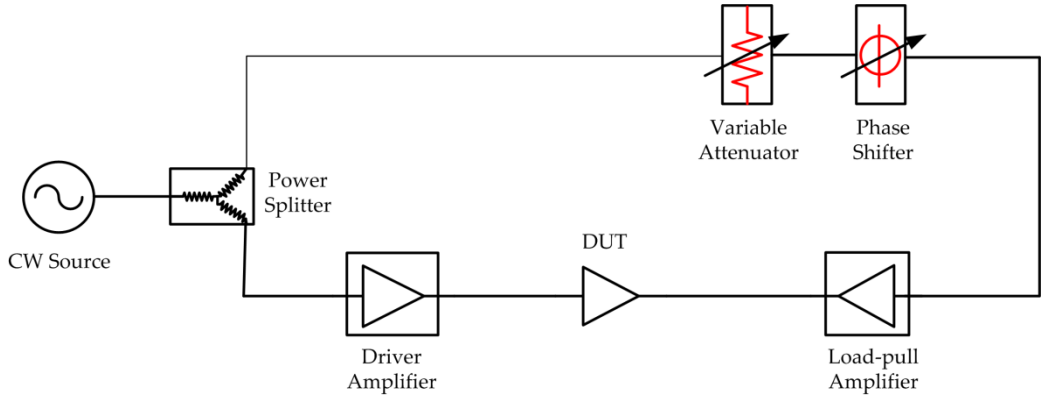

Figure 2-13: Open loop architecture

The variation in the reflection coefficient of the device was achieved manually using a mechanical phase shifter and a variable attenuator. A natural progression of this system was demonstrated [44] by including control and measurement of second and third harmonics thus providing the means of designing amplifiers in Class-F and Class-B modes of operation. Note that the aforementioned open loop systems utilized power meter measurements at the fundamental and harmonic tones to provide a mechanism for collecting load pull data and a six port reflectometer to provide output load impedance readings.

Benedikt et al. [45] presented a measurement system that combined a vector corrected waveform measurement with active harmonic load-pull thus aiding real-time experimental waveform engineering of devices operating up to a 30W power level, between 0.5 - 12.5 GHz. The system was based on the MTA, with a similar structure to the system described in Figure 2-5. Using the setup, time domain voltage and current data for the first 5 harmonic components could be obtained. However, a limitation in the architecture of this system was that manual tuning of the load impedances of fundamental and harmonic components was required as the input power level was toggled during a power sweep.

2.4 Automated Active Source pull and Load pull Measurement systems

2.4.1 Architecture of the system

David Williams et al. [46] demonstrated a fully automated calibrate-able load and source-pull open loop active load pull system, also based on the HP MTA. An external test set was developed in this system, containing two broadband directional couplers, with additional attenuation for power scaling in the measurements.

A matrix of high frequency coaxial switches also allowed the two channels of the MTA to operate as a four-channel receiver measuring all four incident and reflected waveforms. Channel 1 based on the direction of switch 'A' was used to measure the forward travelling waves, a_1 and a_2. Channel 2, with the aid of switch B was used to measure the reverse travelling waves, b_1 and b_2. DC Bias to the DUT was provided via a set of Bias-Tees and measured using a programmable DC power supply (HP 6629A dual-channel supply).

Active load pull power for the fundamental and harmonic tones was provided via independent phase-synchronized electronic signal generators (ESGs). These were phase-locked to a common 10MHz signal and the MTA via a cascaded phase reference link. Custom written software provided a means to automate the entire process from calibration to load pull control and waveform measurement. A schematic of the system architecture is shown Figure 2-14.

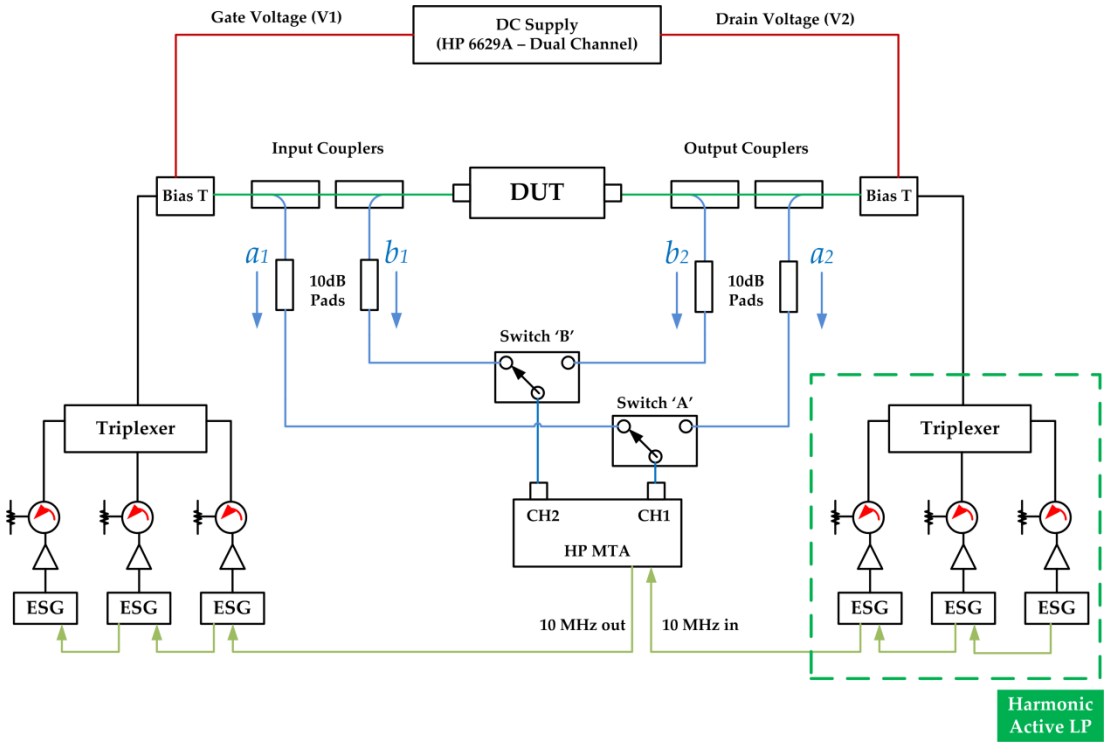

Figure 2-14: Architecture an automated open loop source/load pull system.

With this system, it was therefore possible to carry out a full non-linear characterization on a DUT whilst automatically changing variables such as fundamental and harmonic impedances, gate and drain bias, input power and frequency. In order to attain target load emulation point, a numerical technique was used to calculate the desired active signal from the ESG for each harmonic being load-pulled. Numerical convergence was a major problem in the iteration process; oscillations by the numerical algorithms slowed down and even prevented the final solution from being obtained. Efforts to reduce these oscillations involved using numerical damping or weighting functions to restrict the signal generator variables. This however had a significant effect on the convergence speed and the system was very iterative in nature, especially when a full characterisation required load-pull control of fundamental and harmonic components.

One of the objectives of the work presented in this thesis is therefore to improve this convergence loop by investigating various numerical and device behavioural model approaches. Numerical and behavioural concepts will be discussed and explored in detail in subsequent chapters.

2.5 Summary

This chapter aimed to discuss the evolution of microwave measurement systems from linear RF measurements to the non-linear RF measurement domain. A historical account of measurement architectures included the development of Vector Network Analysers (VNAs) typically useful for measurement of small signal S-parameters. Due to the short comings of S-parameters in the non-linear domain of operation, it was shown that various measurement systems had to be developed to provide designers with accurate non-linear data leading to the introduction of Non-linear Network Analysers (NVNAs). As discussed, this step also required a revamp of the calibration techniques to account for absolute power and phase measurements.

Over the past 3 decades, many commercially available solutions have been developed with a proven track record for collecting calibrated non-linear data and thus aiding PA and component designers in achieving their design goals. This chapter also introduced the concept of "Load-pull" and "Source-pull" which gives access to the direct measurement of key non-linear parameters such as output power, linearity, and drain efficiency as a function of the load or source impedance. For high efficiency design e.g. Class-F, Class-F^{-1} it is required to tune more than one harmonically related frequency e.g. second and third harmonic impedances need to be tuned to high reflects such as an open circuit or a short circuit.

It was shown that manufacturers of NVNAs often provide load- or source-pull tuning mechanisms that allow designers collect non-linear data in almost any arbitrary impedance albeit at the fundamental or harmonic frequencies. Such tuning systems include passive load pull, active systems including closed-loop and open-loop and finally hybrid

systems. Passive tuners are mechanically controlled and thus losses within the tuner inevitably mean that the maximum achievable reflection coefficient will always be less than 1.0. This characteristic limits their use for high efficiency design whereby it is vital to collect data at high reflects for harmonically related frequencies or for device technologies where by the optimum impedance of operation is very low e.g. LDMOS[3].

Active load-pull systems are guided by electronically controlled signal generators, typically one for each harmonic required. These systems offer unrestricted coverage of the smith chart at both fundamental and harmonic frequencies and are only limited by the cost and size of the load pull or source pull amplifiers. Various types of active load pull techniques were discussed including open loop and closed loop techniques. Despite the speed of closed loop techniques, it was discussed that if the variable gain amplifier in the load pull loop is broad band in nature, there is a strong possibility of creating device oscillations.

Open-loop systems are the focus of the work presented in this thesis. They offer unrestricted coverage of the smith chart and unlike closed loop systems, are less prone to device oscillations. An automation summary of an open loop system was discussed in this thesis and it was shown that the major setback in this technique is the number of iterations required for a load pull loop to converge for the fundamental and harmonic impedances. One of the objectives of the work presented in this thesis is therefore to improve this convergence loop by investigating various numerical and device behavioural model approaches. Numerical and behavioural concepts will be discussed and explored in detail in subsequent chapters.

[3] LDMOS (laterally diffused metal oxide semiconductor) transistors are used in RF power amplifiers

References

[1] David Pozar, "Microwave Engineering", third edition, John Wiley & Sons, 2005. pp 174-175.

[2] Online: http://cp.literature.agilent.com/litweb/pdf/N5235-90004.pdf
[Accessed 06-12-2012]

[3] Agilent Technologies, "Agilent Network Analyzer Basics", Accessed the Application note available at www.agilent.com on 12 July 2011.

[4] William. H. Leighton, Roger J. Chaffin, John G. Webb "RF Amplifier Design with Large Signal S-Parameters" IEEE Transactions on Microwave Theory and Techniques Vol MTT-21, No.12, December 1973.

[5] R. J. Chaffin and W.H. Leighton, "Large-Signal S-Parameter Characterization of UHF Power Transistors," MTT 1973.

[6] S.A. Maas "Nonlinear Microwave Circuits Second Edition" Artech House Microwave Library 2003, ISBN 1-58053-484-8

[7] David E. Root and John Wood, "Fundamentals of Non Linear Behavioral Modeling for RF and Microwave Design", Artech House, 2005, ISBN: 1-58053-775-8. pp 20-36

[8] F. H. Raab, "Class-F power amplifiers with maximally flat waveforms," IEEE Transactions on Microwave Theory and Techniques, Volume 45, pp. 2007-2012, November 1997.

[9] P. Colantonio, F. Giannini, G. Leuzzi, E. Limiti, "High Efficiency Low-Voltage Power Amplifier Design by Second Harmonic Manipulation," International Journal of RF and Microwave Computer-Aided Engineering, Volume 10, Issue 1, January 2000, pp. 19-32.

[10] F. H. Raab, "Maximum efficiency and output of class-F power amplifiers," IEEE Transactions on Microwave Theory and Techniques, Volume 49, Issue 6, pp. 1162-1166, Jun 2001.

[11] F. H. Raab, "Class-E, class-C, and class-F power amplifiers based upon a finite number of harmonics," IEEE Transactions on Microwave Theory and Techniques, Volume 49, Issue 8, pp. 1462-1468, August 2001.

[12] P. Colantonio, F. Giannini, G. Leuzzi, E. Limiti, "Theoretical facet and experimental results of harmonic tuned PAs," International Journal of RF and Microwave Computer-Aided Engineering, Volume 13, Issue 6, pp. 459-472, 2003.

[13] Y. Y. Woo, Y. Yang and B. Kim, "Analysis and Experiments for High-Efficiency Class-F and Inverse Class-F Power Amplifiers," IEEE Transactions on Microwave Theory and Techniques, Volume 54, Issue 5, pp. 1969-1974, May 2006.

[14] C. J. Wei, P. DiCarlo, Y. A. Tkachenko, R. McMorrow, D. Bartle, "Analysis and Experimental Waveform Study on Inverse Class Class-F Mode of Microwave Power FETs," 2000 IEEE MTT-S International Microwave Symposium Digest, pp. 525-528, June 2000.

[15] P. Colantonio, F. Giannini, E. Limiti, "HF Class F design guidelines," 15th International Conference on Microwaves, Radar and Wireless Communications, MIKON-2004, Volume 1, pp. 27-37, 17-19 May 2004.

[16] M. C. Curras-Francos et al. "Experimental Demonstration and CAD Investigation of Class B HFET Transistor Operation at Microwave Frequencies," Proceedings of the 28th IEEE European Microwave Conference Amsterdam, 1998, pp. 1386-1388.

[17] P. Colantonio, F. Giannini, E. Limiti, A. Ticconi, "Class F design criteria validation through non linear load pull simulation," IEEE Workshop on Integrated Nonlinear Microwave and Millimeter-Wave Circuits, January 2006, pp. 30-33.

[18] C. Roff, J. Benedikt, and P. J. Tasker, "Design Approach for Realization of Very High Efficiency Power amplifiers," in IEEE MTT-S Int. Microwave Symp. Dig., June 3–8, 2007, pp. 143–146.

[19] Sheikh, C. Roff, J. Benedikt, P. J. Tasker, B. Noori, P. Aaen, and J. Wood, "Systematic waveform engineering enabling high efficiency modes of operation in Si LDMOS at both L-band and S-band frequencies," in IEEE MTT-S Int. Microwave Symp. Dig., June 15–20, 2008, pp. 1143–1146.

[20] P. Wright, A. Sheikh, C. Roff, P. J. Tasker, and J. Benedikt, "Highly efficient operation modes in GaN power transistors delivering upwards of 81% efficiency and 12W output power," in IEEE MTT-S Int. Microwave Symp. Dig., June 15–20, 2008, pp. 1147–1150.

[21] P. Wright, J. Lee, P. J. Tasker, J. Benedikt, and S. C. Cripps, "An efficient, linear, broadband class-J-mode PA realised using RF waveform engineering," in IEEE MTT-S Int. Microwave Symp. Dig., June 2009, pp. 653–656.

[22] S. C. Cripps, P. J. Tasker, A. L. Clarke, J. Lees, and J. Benedikt, "A New General Formulation for High Efficiency R.F. Amplifiers," IEEE Microwave Wireless Compon. Lett., Oct. 2009.

[23] M. Sipilä, K. Lethinen, and V. Porra, "High-frequency periodic time-domain waveform measurement system," IEEE Trans. Microwave Theory Tech., vol. 36, no. 10, pp.1397–1405, Oct. 1988.

[24] L. Urs, "Measurement of magnitude and phase of harmonics generated in nonlinear microwave two-ports," IEEE Trans. Microwave Theory Tech., vol. 37, no. 10, pp.1506–1511, Oct. 1989.

[25] G. Kompa, and F. van Raay, "Error-corrected large signal waveform measurement system combining network analyser and sampling oscilloscope capabilities," IEEE Trans. Microwave Theory Tech., vol. 38, no. 4, pp. 358–365, Apr. 1990.

[26] F. van Raay and G. Kompa, "A new on-wafer large-signal waveform measurement system with 40 GHz harmonic bandwidth," in 1992 IEEE MTT-S Int. Microwave Symp. Dig., June 1992, vol. 3, pp.1435–1438.

[27] T. van den Broeck and J. Verspecht, "Calibrated vectorial nonlinear-network analyzers," in 1994 IEEE MTT-S Int. Microwave Symp.Dig., San Diego, USA, June 1994, pp. 1069–1072.

[28] M. Demmler, P. J. Tasker, and M. Schlechtweg, "A vector corrected high power on-wafer measurement system with a frequency range for the high harmonics up to 40 GHz," in Proc. 24th European Microwave Conf., Cannes, France, Sept. 1994, pp: 1367–1372.

[29] Ch. Clark et al., "Time-domain envelope measurement technique with application to wideband power amplifier modelling," IEEE Trans. Microwave Theory Tech., vol. 46, no. 12, pp. 2531–2540, Dec. 1998.

[30] J. Benedikt, R. Gaddi, P. J. Tasker, and M. Goss, "High-power time-domain measurement system with active harmonic loadpull for high-efficiency base-station amplifier design," IEEE Trans. Microwave Theory Tech., vol. 48, no. 12, pp. 2617–2624, Dec. 2000.

[31] D. J. Williams, J. Leckey, and P. J. Tasker, "Envelope domain analysis of measured time domain voltage and current waveforms

provide for improved understanding of factors effecting linearity," in 2003 IEEE MTT-S Int. Microwave Symp. Dig., June 2003, vol. 2, pp.1411–1414.

[32] D. Williams, P. Hale, K. A. Remley, "The sampling oscilloscope as a microwave instrument," IEEE Microwave Mag., vol. 8, no. 4, pp. 59–68, Aug. 2007.

[33] J. A. Jargon, D. C. DeGroot, and D. F. Vecchia, "Repeatability study of commercial harmonic phase standards measured by a nonlinear vector network analyzer," in Proc. 62nd ARFTG Microwave Measurements Conf., Fall 2003, Dec. 4–5, pp. 243–258

[34] Baylis, C.; Marks, R.J.; Martin, J.; Miller, H.; Moldovan, M.; , "Going Nonlinear," Microwave Magazine, IEEE , vol.12, no.2, pp.55-64, April 2011

[35] Online: http://www.maurymw.com [Accessed: 15-Dec-2012]

[36] Online: http://www.focusmicrowaves.com [Accessed: 15-Dec-2012]

[37] Tsironis, C.; Jurenas, A.; Liu, C.; , "Highly accurate harmonic tuners for load pull testing," Microwave Conference, 2001. APMC 2001. 2001 Asia-Pacific , vol.3, no., pp.1311-1314 vol.3, 2001

[38] Roff, C.; Graham, J.; Sirois, J.; Noori, B.; , "A new technique for decreasing the characterization time of passive load-pull tuners to maximize measurement throughput," ARFTG Microwave Measurement Symposium, 2008 72nd , vol., no., pp.92-96, 9-12 Dec. 2008

[39] De Groote et al., "On-wafer time domain load-pull optimization of transistor load cycle with the new multi-harmonic MPT tuner," ARFTG Conference, 2007 69th , vol., no., pp.1-6, June 2007

[40] Bava, G. P.; Pisani, U.; Pozzolo, V.; "Active Load Technique for Load-Pull Characterization at Microwave Frequencies," Electronic Letters, Volume 18, Issue 4, February 18 1982, pages: 178-180.

[41] Williams, T.; Benedikt, J; Tasker, P; "Application of a Novel Active Envelope Load pull Architecture in Large Signal Device Characterization, " 35th European Microwave Conference, October 2005

[42] Hashmi, M.S.; Clarke, A.L.; Woodington, S.P.; Lees, J.; Benedikt, J.; Tasker, P.J.; , "Electronic multi-harmonic load-pull system for experimentally driven power amplifier design optimization," Microwave Symposium Digest, 2009. MTT '09. IEEE MTT-S International , vol., no., pp.1549-1552, 7-12 June 2009

[43] Yoichiro Takayama "A New Load-Pull Characterisation Method for Microwave Power Transistors" IEEE MTT-S International Microwave Symposium Digest 1976 pp. 218-220

[44] F.M. Ghannouchi, F. Beauregard, A.B. Kouki "Large-Signal Stability and Spectrum Characterisation of Medium Power HBT Using Active Load-Pull Techniques" IEEE Microwave and Guided Wave Letters, Vol. 4, No.6, pp.191-193, June 1994

[45] J. Benedikt, R. Gaddi, P.J. Tasker and M. Goss "High-Power Time-Domain Measurement System with Active Harmonic Load-Pull for High-Efficiency Base-Station Amplifier Design" IEEE Transactions on Microwave Theory and Techniques, Vol. 48,No.12, pp.2617-2624, December 2000

[46] D.J. Williams, P.J. Tasker, "An Automated Active Source and Load Pull Measurement System", Proceedings of 6th IEEE High Frequency Postgraduate Colloquium, Cardiff, UK, September 9th-10th 2001. pp. 7-12.

Chapter 3 - Non-linear Behavioural Modelling

3.1 Introduction

The complexity of modern microwave and wireless systems prohibits their complete simulation from the level of a single transistor. This is due to the fact that very large volumes of equations need to be solved for the devices that may include multiple of transistors; Simulations of this nature are time consuming and very computationally expensive to achieve and can be inaccurate. In comparison to a SPICE[4] simulator, the algorithms used by modern simulators such as harmonic balance [2] are far more computationally efficient yet they are still faced with convergence issues when solving transistor model equations. Over the last 3 decades, various solutions to such problems have been suggested and have since been development strategies for transistor and component modelling techniques.

[4] SPICE: Simulation Program with Integrated Circuit Emphasis [1] is a general-purpose, open source analog electronic circuit simulator. This program is used in integrated circuit and board-level design to check the integrity of circuit designs and to predict circuit behaviour.

Transistor models can hence be divided into three broad categories namely; physical, compact and behavioural models. A summary of the qualities of each technique is portrayed in Figure 3-15. Data was extracted from [3].

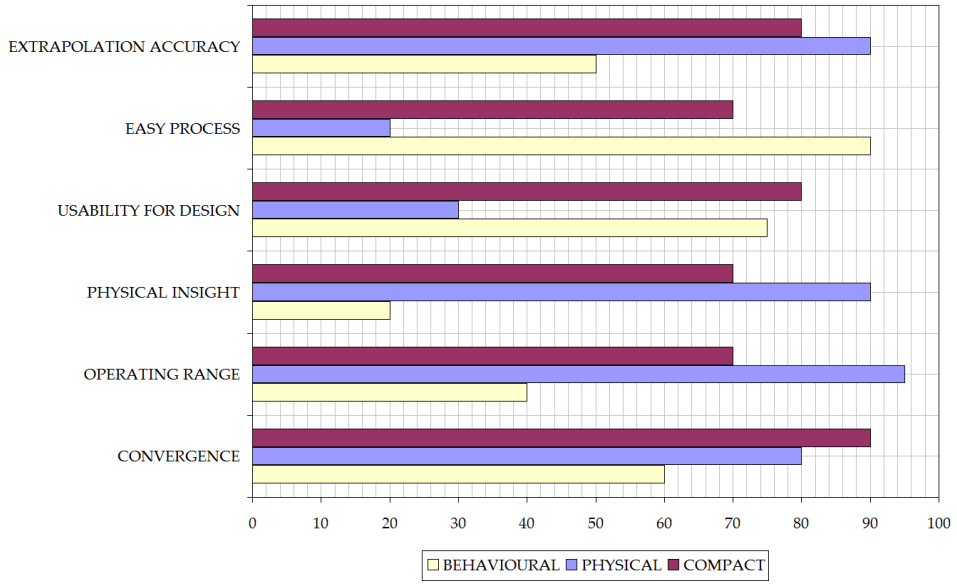

Figure 3-15: Comparison of modelling techniques

A physical model [4] is one which is based on the physics of the device technology and is thus dedicated to the device itself rather than the overall circuit. Complex model equations, rather than actual measurements, are used to derive these models leading to time consuming simulations. The main advantage of this kind of model is that it has the largest operating range compared to alternative techniques. A manufacturer's intellectual property (IP) may also be compromised with such a model as it offers the users full transparency into the physical device technology.

Compact transistor modelling [5] is an alternative solution to the above. It is based on measurements of IV and S-parameters to extract a reduced set of device parameters. Once extracted, predictions can be verified via load pull characterisation. While this technique is ideal for die-level applications, packaged-transistor models need to include a die-level

model, bonding model and package model. This increases the overall measurement and characterisation time and also the time taken to extract or compile the model.

A third solution is to replace the complex transistor circuitry or packaged die, which may contain a number of non-linear functional blocks, with a simplified but accurate behavioural model [5]. Such a model enables the complete simulation of the DUT at a higher level of abstraction while still representing the effect of non-linear blocks on the overall system performance. In general, responses of a component to various controlled stimuli are observed and captured into model coefficients. In its simplest form, behavioural model generation can be regarded as multi-dimensional curve fitting, however, practical implementations of such mathematical concepts lead to a much broader science.

This chapter aims to review the advantages and disadvantages of using behavioural models, discuss the significant developments in this field and highlight the benefits or short comings of each behavioural modelling strategy.

3.2 Advantages of Behavioural Models

There are various advantages of using behavioural models in component design, manufacturing and testing scenarios. Firstly, these models can be used to capture and describe phenomena where the underlying physical processes are not known or too difficult to capture completely.

Manufacturers can also provide behavioural models of their technology as a way of protecting the IP associated with their devices or products. It is practically impossible to reverse engineer, from a set of behavioural model coefficients, the component or set of components being used.

Such models, since they are based on actual measurements, can aid in achieving potential "first-pass design success". This is because the model can be used in simulations to provide direct feedback of microwave circuit or system performance and hence provide an evaluation of the system performance from within the CAD environment. This can save on prototyping costs by reducing the amount of prototyping cycles whilst developing a product.

Behavioural models can be generated via linear and non-linear measurements or by circuit simulations. Depending on the final capabilities required in the model; advanced measurement systems may be required to capture the full dynamical response of the transistor or Integrated Circuit (IC). For example, AM-AM compression can be captured over a frequency range by conducting power sweep measurements at each frequency. Addition of vector error correction provides a mechanism of extracting AM-PM behaviour from the DUT. In the simulator-based approach, a detailed physical or compact model is used as a DUT in a virtual instrumentation environment. This DUT is then excited with the relevant stimuli and the results processed as if they were real data to generate a behavioural model.

The RF community is not alien to behavioural models. S-parameters, which have been in existence since the 1940's, provide a complete behavioural model of a component and can replace complex circuits or components thus allowing simulations at a higher level of abstraction. The non-linear circuit design challenge however makes it difficult to apply methods of such linear analysis as described in the previous chapter.

A great deal of progress has however been made to enable designers access the advantages of non-linear measurements and model generation. Part of the development effort was driven by several instrument manufacturers who sighted the need to "go beyond s-parameters" [7].

The result was an accelerated development of a new generation of Network analysers with non-linear measurement capabilities, for example the Large Signal Network Analyser (LSNA) [8], developed by Agilent Technologies. Development of a mathematical concept to use such instrumentation was also required, resulting in the evolution of the Poly-Harmonic Distortion modelling technique [9]-[10]. In order to provide a smoother transition to these non-linear models, the mathematical descriptions of them have been developed using the travelling wave theory i.e. relying upon calibrated and phase-corrected port quantities: *a*-, *b*- or *v*-, *i*- waveforms in the frequency domain.

3.3 Poly-Harmonic Distortion Modelling (PHD)

PHD modelling is a black-box frequency domain modelling technique, described in Jan Verschpect's famous IEEE Microwave magazine article "Poly-Harmonic Distortion Modelling" [9]. The article formalised an approach that identified a model from the responses of a DUT stimulated by a set of harmonically related discrete tones, where the fundamental tone is dominant and the harmonically related tones are relatively small. The measurement instrumentation (an LSNA at the time) and model generation strategy was to develop a natural extension to S-parameters for non-linear characterisation. Under lower drive conditions (linear region of operation) therefore, the PHD model could be simplified to S-parameters.

It was originally intended for the modelling of microwave amplifiers with narrow band input signals. The constraint of being "narrow band" was not placed on the amplifier itself, rather on the input stimulus. Practically, the consequence of the above was that measurements required for PHD model generation for design of a broadband amplifier dictated that the extraction tones required to stimulate the DUT needed to be at multiple carrier frequencies.

3.3.1 Theory of the PHD Modelling framework

Unlike physical models, the normalized voltage waves (*a*- and *b*-) have been chosen for most behavioural models instead of RF current and voltage (*i*- and *v*-) due to the fact that most modern measurement systems and NVNA instrumentation natively operate in this domain. Equations (3-1) and (3-2) show the mathematical relationship between these waves.

$$A_p(t) = \frac{V_p(t) + Z_0 I_p(t)}{2} \tag{3-1}$$

$$B_p(t) = \frac{V_p(t) - Z_0 I_p(t)}{2} \tag{3-2}$$

$$B_{p,n} = B_p(nF) = F(B_p(t)) \tag{3-3}$$

Measured and stored data tables in this domain therefore consist of Fourier components, $B_{p,n}$ of $B_p(t)$ as shown in (3-3) indexed as a function of the stimulus $A_p(t)$ whose Fourier components are $A_{p,n}$. These travelling waves can therefore exist at any arbitrary frequency where by *n* denotes the frequency index of the excitation signal and *p* denotes the port number. It is however more useful, for high efficiency amplifier design, to describe the incident and reflected waves as a fundamental tone (F0) with indexes for harmonics e.g. 0:-DC, 1:-F0, 2:-2*F0, 3:-3*F0 etc. For a non-linear two port device, this fundamental and harmonic travelling wave concept is illustrated in Figure 3-16, where by *h* denotes the index of the harmonic excitation.

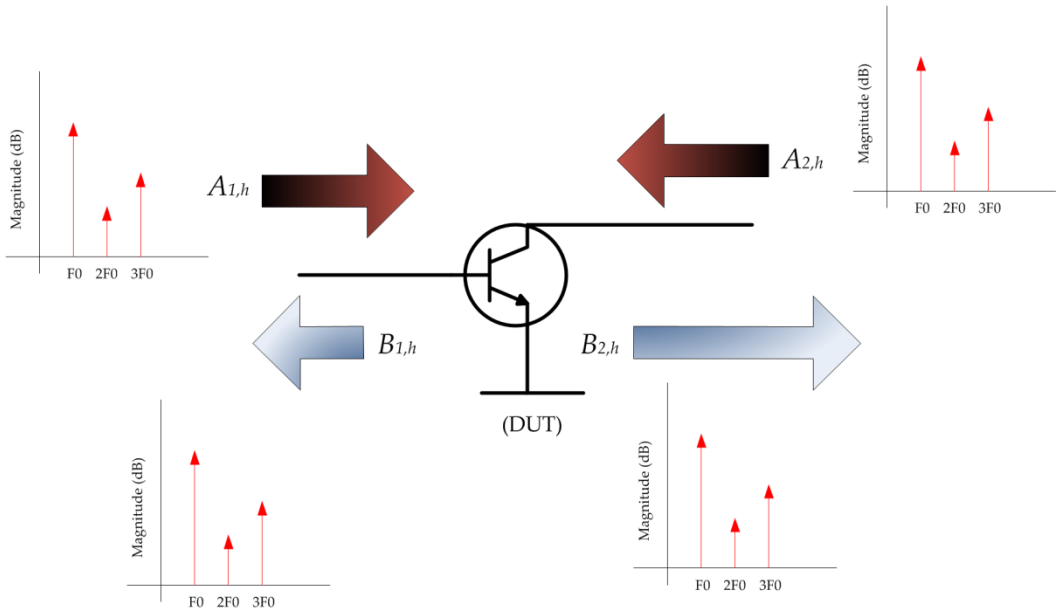

Figure 3-16: Travelling waves with harmonic content

The general PHD model equation was therefore formulated as follows:

- For a given DUT, it is required to determine a set of multivariate complex functions given by $F_{p,h}(.)$ that correlate all the relevant input spectral components $A_{p,h}$ with the output spectral components $B_{p,h}$
- The indices p and h denote the signal port numbers and harmonic indices respectively. Index p ranges from one to the maximum number of ports. Index h ranges from 0 (DC) to the maximum harmonic component ($n*F0$) being captured, n.
- For a two-port system, this function can be generalised (3-4).

$$B_{p,h} = F_{p,h}\left(A_{11}, A_{12}, A_{13}, \ldots A_{2,1}, A_{2,2}, A_{2,3}, \ldots\right) \qquad (3\text{-}4)$$

According to Verschpect's article [9], experiments that were carried out illustrated that the functions $F_{p,h}$ were time invariant. Thus applying a time delay (a linear phase shift in frequency domain) at the input stimuli $A_{p,h}$ resulted in an equivalent time shift on the scattered $B_{p,h}$ waves. Incorporating phase into the generalised non-linear equation therefore yielded (3-5).

$$B_{p,h}e^{jh\theta} = F_{p,h}\left(A_{1,1}e^{j\theta}, A_{1,2}e^{j2\theta}, A_{1,3}e^{j3\theta}, \ldots A_{2,1}e^{j\theta}, A_{2,2}e^{j2\theta}, A_{2,3}e^{j2\theta}, \ldots\right)$$

(3-5)

The equation was then further reduced in complexity by introducing a phase normalisation concept. For power transistor applications, the incident travelling wave at port 1 for the fundamental harmonic (A_{11}) was identified as the dominant large signal component and all the other travelling waves were then phase normalised to this incident wave. This yielded the function shown in (3-6) and (3-7); introducing the phasor, P.

$$P = \angle A_{11}$$

(3-6)

$$B_{p,h} = F_{p,h}\left(\left|A_{1,1}\right|, A_{1,2}P^{-2}, A_{1,3}P^{-3}, \ldots A_{2,1}P^{-1}, A_{2,2}P^{-2}, A_{2,3}P^{-3}, \ldots\right)P^{+h}$$

(3-7)

The first argument of the function $F_{p,h}$ is a magnitude-only term describing the magnitude of the input signal, A_{11}. For power amplifier applications, all other components are relatively small and thus can be described by applying the Harmonic Superposition principle as shown in Figure 3-17.

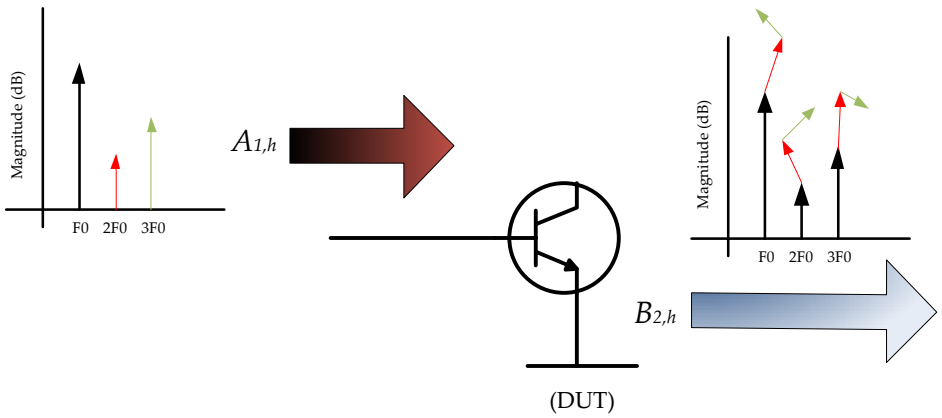

Figure 3-17: Harmonic Superposition Principle

To illustrate this concept, only the presence of the input signal, $A_{1,h}$ is used and the response of the DUT, $B_{2,h}$ is considered. In the first case, (as indicated by black arrows in both the input and output spectra) only the fundamental component ($A_{1,1}$) has been injected at the input of the DUT. As expected, this produces significant harmonic content at the output at 2F0 and 3F0 frequencies.

In the second case, $A_{1,1}$ was held constant and a second input signal ($A_{1,2}$) was injected. The deviation in the output spectrum can now be seen as indicated by the red arrows. Similarly, green arrows denote a deviation for an $A_{1,3}$ signal. The harmonic superposition principle states that the overall deviation of the output spectrum B_2 is the superposition of all individual deviations. This was a very important finding for practical power amplifier design cases and was experimentally verified [11]. It proved to hold for very nonlinear classes of operation such as class-C and class-F. Applying the above theory and linearization, the equation (3-7) can therefore be linearized to yield (3-8).

$$B_{p,h} = \sum_{qn} S_{pq,nh}\left(|A_{11}|\right) P^{+h-n} A_{qn} + \sum_{qn} T_{pq,nh}\left(|A_{11}|\right) P^{+h+n} conj(A_{q,n})$$

(3-8)

The phase-normalised $B_{p,h}$ waves are written as a linear combination of the phase-normalised $A_{q,n}$ waves, the input quantities and their conjugates. The additional subscripts q and n in (3-8) describe the port and harmonic index of the associated input component A. The functions S and T, which have both amplitude and a phase, are the actual scattering functions in this formulation.

They are general nonlinear functions of A_{11} however independent of the components for which the superposition holds. They are thus a natural extension of S-parameters. An example application of the formulation is

shown in (3-9). This is a simple case of the response of a DUT, B_{21} depending only on A_{11} and A_{21}.

$$B_{2,1} = S_{21,11}(|A_{11}|)A_{11} + S_{22,11}(|A_{11}|)A_{21} + T_{22,11}(|A_{11}|)P^2 conj(A_{21})$$

(3-9)

The above equation has various promising applications. Most importantly, its ability to predict fundamental and harmonic load pull behaviour. In this case, the prediction of $B_{2,h}$ is used as a function of the load conditions at the output, both for fundamental and the harmonics. Details of these experiments will be discussed in subsequent sections.

3.3.2 Applications

At the present time, there are various applications and model generation approaches that are derived from the original PHD model equations. Probably the most widely used adaptation is X-parameters™ [5]. Other applications include S-functions and Cardiff Behavioural models. These applications are discussed below.

3.4 X-parameters and S-functions

With the release of a new generation PNA-X [12], featuring a turn-key non-linear vector network analyser solution (NVNA), Agilent also provided its customers with the option to generate non-linear behavioural models at the click of a button. The original PHD modelling framework was restructured and terminologies simplified, thus providing a more commercially viable framework known as X-parameters™ [26]. The updated equation set is shown in (3-10). In the equation, function $X^{(F)}$ provides the large signal response of the DUT to a single large-amplitude tone at a given

[5] X-parameters™ are a registered trademark of Agilent Technologies, Inc.

fundamental frequency, assuming a perfect match at all ports, at all harmonics. The functions $X^{(S)}$ and $X^{(T)}$ correspond to the $S_{pq,nh}$ and $T_{pq,nh}$ respectively from the original PHD modelling framework equations. Simply put, they represent a non-analytic mapping of complex incident phasors at port q and harmonic n into the complex output phasors at port p and harmonic h.

$$B_{p,h} \Big/ P^h = X^{(F)}_{p,h}\left(|A_{11}|, V_{1,0}, V_{2,0}\right) + \sum_{q,n} X^{(S)}_{p,h}\left(|A_{11}|, V_{1,0}, V_{2,0}\right) A_{q,n} P^{-h_s} + \sum_{q,n} X^{(T)}_{p,h}\left(|A_{11}|, V_{1,0}, V_{2,0}\right) A_{q,n} * P^n$$

Whereby $P = e^{j\alpha(A_{11})}$

(3-10)

A commercial reformulation was also released by NMDG [14] and VNA manufacturer, Rohde and Schwarz, this version called S-functions [15], shown in (3-11).

$$\begin{aligned} B = {} & H\left(A_1(f_0), A_2(f_0), V_{dc}\right) \\ & + S_k\left(A_1(f_0), A_2(f_0), V_{dc}\right) A(kf_0) \\ & + S_{kc} S_k\left(A_1(f_0), A_2(f_0), V_{dc}\right) A(kf_0)^* \end{aligned}$$

(3-11)

As the formulations of both X-parameters and S-functions are exceedingly similar, the X-parameter approach will be discussed as an example of extraction and application of the PHD modelling framework.

3.4.1 Extracting X-parameters

An excellent summary of two techniques to measure X-parameters has been provided in [19]. Both the on-frequency and off-frequency techniques can be used to extract each of the three X-parameters for an input port q and harmonic combination n to an output port p and harmonic

combination h and has thus been adopted by various instrumentation solutions. Note that both magnitude and phase measurements of the output signals is necessary to provide accurate extraction. A generalised summary of the procedure is outlined below.

1. All non-input ports and harmonics are terminated in reference impedance (Z_0). A large signal tone is then applied at port 1 (A_{11}).
2. A measurement of the magnitude and phase of all the scattered signals at all ports and for all observable harmonics is then taken; resulting in a matrix of the response signal $B_{p,h}$. Phase correction between harmonics is then necessary to extract the matrix $X_{p,h}^{(F)}$.
3. For each combination of input port q and harmonic n and output port p and harmonic h; in addition to step 1) above:
    - Apply a perturbation consisting of incident signals $A_{q,n}$ and $A_{q,n}$ * synchronised in phase with A_{11} to each port q and harmonic n. Note that more than one measurement is required to make the response of the DUT distinguishable from the effect of the perturbation signal.
    - As an example, two $A_{q,n}$ incident signals, one with 0 phase and another at 90 degrees can thus be used. The device response can then be mathematically decomposed into terms resulting from individual inputs. An additional benefit of using more measurements is that measurement noise can be reduced by measuring several phases and then least-squares [17] fit used to determine the exact solution.
    - Magnitude and phase measurements at port p and harmonic h can then be used to compute $X_{p,h}^{(S)}{}_{q,n}$ and $X_{p,h}^{(T)}{}_{q,n}$.

3.4.2 Load dependent X-parameter measurements with an Agilent PNA-X using a passive tuner

The extraction procedure explained above assumes fixed impedance, by default this is the characteristic impedance of the Network analyser, and therefore has a limited operation range. Simpson et al. [29] introduced a method of extracting X-parameters over large areas of the smith chart, making them usable for characterising high power amplifiers and devices which have optimal performance at high mismatch.

Measurement Setup

In order to make the large-signal measurements necessary for X-parameter extraction, an NVNA was configured using a 4-port Agilent PNA-X network analyser (N5242A).

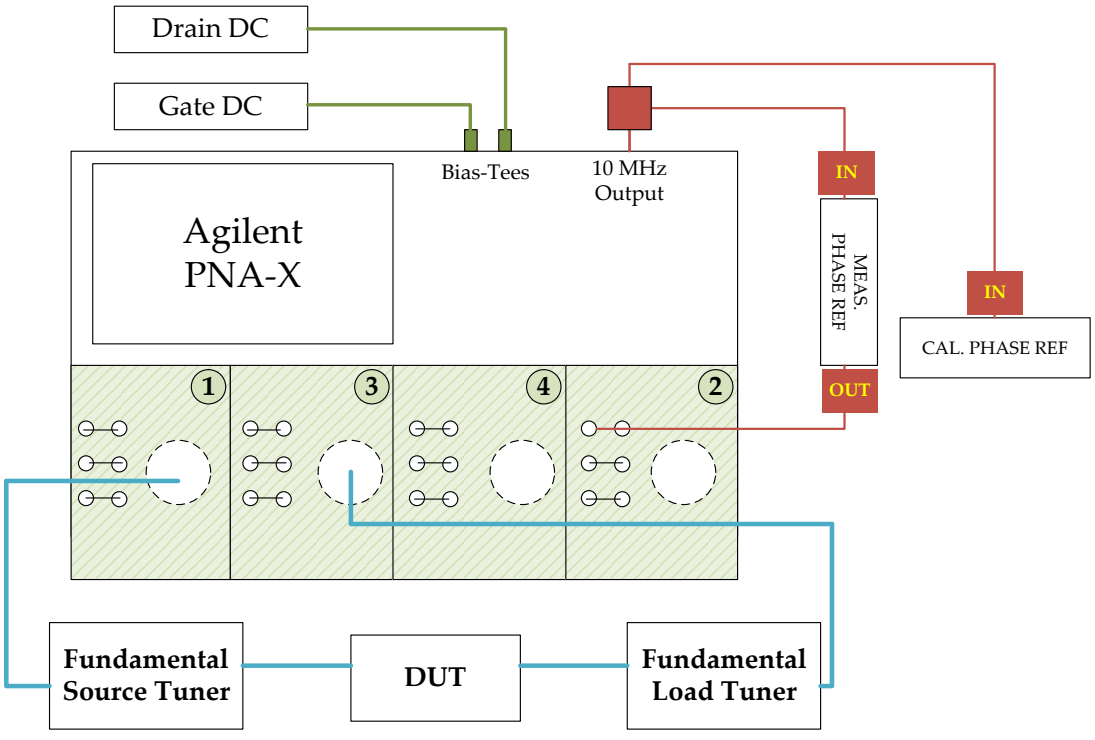

Figure 3-18: Agilent PNA-X hardware setup to measure load dependent X-parameters

By combining the PNA-X with an external phase reference generator and appropriate instrument control and data processing software; high dynamic range, fully calibrated large-signal measurements were made possible. A schematic of the measurement setup is shown in Figure 3-18. Since X-parameter measurements require multiple simultaneous input tones at harmonically related frequencies and multiple ports, a built-in second source, switching capabilities and combiners were designed to offer phase-coherent extraction functionality.

The automated technique emulated functionality of a conventional passive load pull system, developed by Maury Microwaves [29], where by the user was able to select a fundamental load impedance range to start with. A sweep plan of bias, power and frequency was then overlaid followed by a measurement of X-parameters at each fundamental load pull point in the plan. The data file produced after this measurement was compatible with Agilent's ADS™ CAD tool for non-linear simulations and design.

Limitations of Load-dependent X-parameters

The elegance of using load-dependent X-parameters is hampered by the following limitations:

i. An X-parameter model of port p and harmonic h is derived at each fundamental load impedance point in the sweep plan of the passive tuning process. For a two-port 5 harmonic model, this yields a dataset with 210 coefficients. Coupled with external independent variables such as bias, frequency and fundamental drive, the model file size becomes very large [19] (typically > 1GB for a full device characterisation). Although simulator speed in Agilent ADS is not affected, difficulties are caused during data transfer and file storage.

ii. Extracting a load-dependent model with a passive tuner is limited by the maximum achievable gamma by the tuner's mechanical system and the fixture used to mount the DUT. This is due to the internal losses in the tuner as discussed in Chapter 2.

iii. Harmonic X-parameter extraction is carried out using incident waves, A_{qn} at port q and harmonic n. This extraction, unlike fundamental tuning, is carried out with A_{qn} and A_{qn} * perturbations close to the reference impedance of the network analyser (usually close to 50 ohms). The accuracy of the model for high efficiency design (e.g. class-F, class-J) may therefore be compromised as harmonic impedances at precise impedances positions are required for design of these modes. Achieving these design objectives would therefore require harmonic X-parameter extrapolation from 50 ohms to very low/high impedances within the simulator. A thorough analysis of this observation is provided in subsequent chapters of this thesis.

iv. Measurements required for X-parameter extraction provide no further "live" information about the device performance and thus prior to model extraction, a load pull characterisation of the DUT is also required in order to focus the impedance sweeps in the right region of operation, determine the compression points and bias levels. This reduces the overall measurement system utilisation efficiency.

3.5 Cardiff DWLUT model

The Cardiff Direct Wave Look-Up Table model (DWLUT model) is a table-based model which captures the behaviour of a DUT using the extrinsic measured voltage and current waveforms directly [20]-[21]. Figure 3-19 illustrates this approach, defined by the functions (3-12) to (3-13).

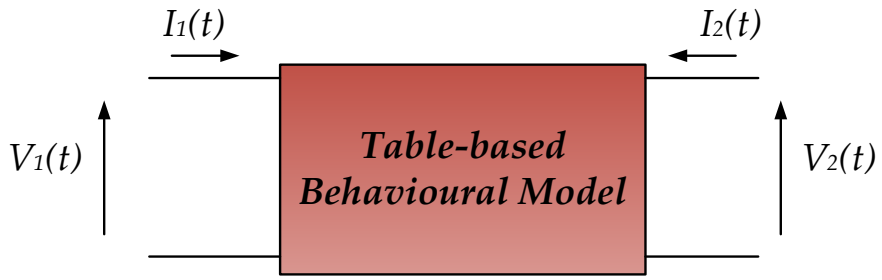

Figure 3-19: Table based behavioural model

The description of current *I(t)* at a port *p* is given by (3-12) where by the number of harmonics is denoted by the index *h.*

$$I_p(t) = I_{p,DC} + \sum_{h=1}^{h} Y_{p,1}(hf_0) V_p^h(t) \qquad (3\text{-}12)$$

Whereby

$$V_p(t) = |V_p| e^{j\theta} e^{j\omega t}$$

The currents and voltages of a two-port network are therefore related using a concept of Y parameters (3-13).

$$Y_{p,h}(hf_0) = \frac{I_p(nf_0)}{V_p^h(f_0)} = F_1(|V_1|, \Gamma_{LOAD}, V_{1DC}, V_{2DC}) \qquad (3\text{-}13)$$

From (3-12), the Y parameters at each harmonic (h) are defined as a function of magnitude of the stimulus voltage (V_1), complex load impedance (Γ_{LOAD}) and the chosen bias point (V_{1DC}, V_{2DC}).

Voltage and current waveforms, originally obtained from the calibrated time-domain measurement system, developed in Cardiff University which is described in Chapter 2, are compressed into their respective Fourier coefficients thus providing an elegant way of calculating, directly, the Y parameters for the input and output ports of the DUT.

Note that the nature of the above equation set meant that a multi-dimensional table extraction was required as the load impedance grid was re-measured for each independent variable (fundamental frequency, bias and input stimulus). This approach provided an elegant link between measurement data and CAD design, providing the users with an accurate archive of the device characterisation measurements they have undertaken including strongly non-linear measurements such as those in class-F device characterisation [22].

In their truest sense, however, these were not behavioural models as their only aim was to make non-linear data available in CAD. The biggest drawback of this approach was that it could only predict the measurements on which it was based. Similar to load-dependent X-parameters, the DWLUT model also required measurement data to be placed on a regular grid. This was however due to the limitations of the data look-up within CAD tools. Thus, the model required more iterations from an active load pull system or an effective data processing technique to place converged load points onto a regular grid. This greatly increased the overall measurement time for device characterisation.

3.6 Cardiff Behavioural Model Formulations

The Cardiff Behavioural Model formulations is a polynomial based modelling approach, also a descendant of the original PHD model formulations. It was first introduced by Qi et al. [21] and Woodington et al. [23], based around measurements on an open-loop active load pull system developed in Cardiff University (described in Chapter 2). Initially, this model was used to capture behaviour of fundamental load pull (3-14).

$$b_{2,1} = P_1.g\left(v_{1,0}, |a_{1,1}|, v_{2,0}, |a_{2,1}|, Q_1/P_1\right)$$

$$\text{Where } P_1 = \angle a_{1,1} = \frac{a_{1.1}}{|a_{1,1}|} \quad \text{and} \quad Q_1 = \angle a_{2,1} = \frac{a_{2.1}}{|a_{2,1}|}$$

(3-14)

The above equation highlights the polar form of $a_{2,1}$ and thus yields two load pull indexing terms, $|a_{2,1}|$ and Q_1/P_1. Since Q_1/P_1 is a periodic function, the measured behaviour of $b_{2,1}$ must also be periodic. With this finding, the phase vector indexing was eliminated from the generalised mathematical formulation for giving the description in (3-15) and thus (3-16). In (3-16), the necessary mixing order w can be determined mathematically by either carrying out a least-squares fit or by Fourier transforming a structured measurement sequence. Experimental verification was carried out by Woodington et al. [23]; by using the latter approach.

$$K_{p,h,m} = g\left(v_{1,0}, |a_{1,1}|, v_{2,0}, |a_{2,1}|\right) \qquad (3\text{-}15)$$

$$b_{p,h} = P_1^h.\left(\sum_{m=-(w-1)/2}^{m=+(w+1)/2} K_{p,h,m}\left(Q_1/P_1\right)^m\right) \qquad (3\text{-}16)$$

3.6.1 Measurement and validation procedure for F0 model extraction

In order to validate this approach as well as determining the necessary order (w) thus coefficient count, an incident signal $a_{2,1}$ was injected, with a fixed magnitude while stepping through values of its phase ($\angle a_{2,1}$) in regular steps through 360º. Experimentally, such measurements were achieved by varying the phase of the constant amplitude signal (a_s) produced by the fundamental signal generator. A passive tuning network (e.g. phase shifter and variable attenuator) was also used in the fundamental loop to centre the measurements about reference impedance (Z_L), such as the optimum of the device (Γ_{opt}) instead of the characteristic impedance of the system (Z_0). This setup is shown in Figure 3-20. A GaAs[6] 8x2x30um 0.5W HBT device was placed under test for this experiment.

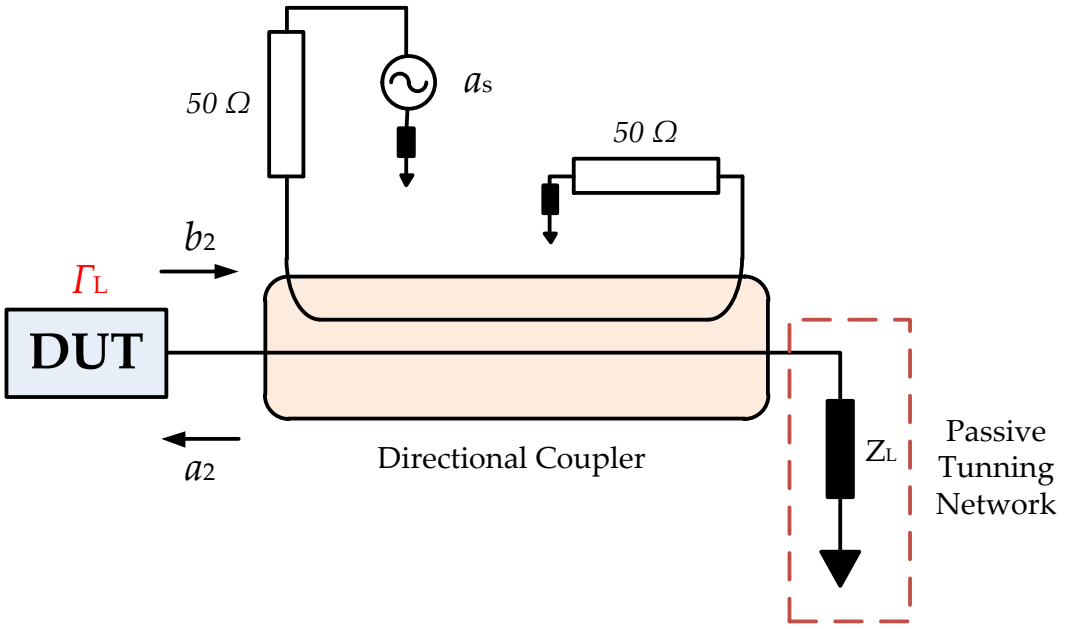

Figure 3-20: Generating the required load pull data by integrating an active source with a passive load pull network

[6] Gallium Arsenide

The resulting sinusoidal periodic variation of $a_{2,1}$, normalised to Z_L produces the closed-loop circles shown in Figure 3-21-(i). Note that this stimulus is identical to that originally used by Verschpect et. al. for the PHD Model extraction as described in [9]. In Figure 3-21-(ii), it can be seen that the response signal $b_{2,1}$ is a periodic function with respect to the phasor Q_1/P_1. Unlike the excitation signal $a_{2,1}$, this response was not circular, thus higher order phase terms were required to model the behaviour i.e. $w>1$.

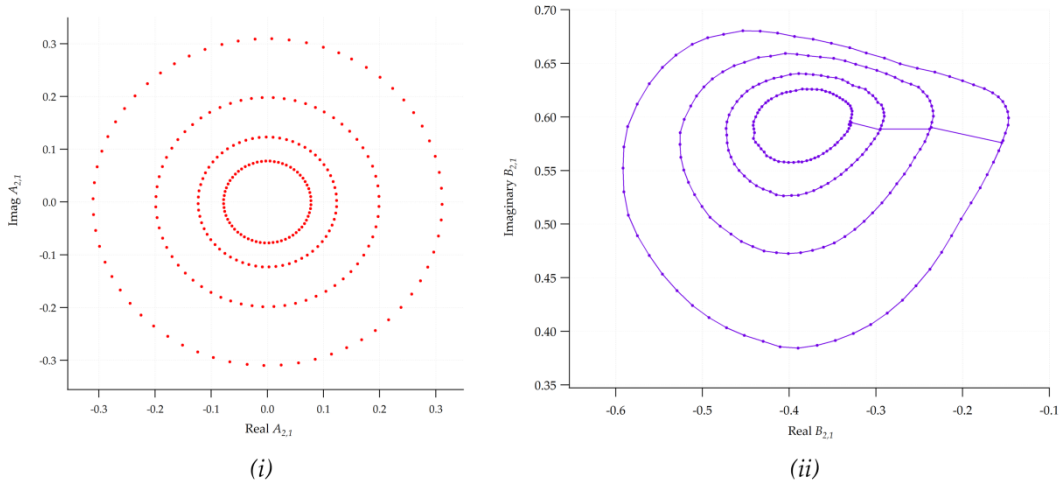

Figure 3-21: (i) Stimulus $A_{2,1}$. (ii) Experimental response of $B_{2,1}$ to stimulus $A_{2,1}$

Validation procedure

In order to validate the modelled data results, two mixing order values were chosen (w=3 and w=5). Predicted load-pull loci from each set were then compared with the measured response as shown in Figure 3-22. Figure 3-23 compares the output power load-pull contours computed from both the measured response and the modelled performance of $b_{2,1}$. The predicted power was within 0.1dB when compared to measured results[7].

[7] All data shown above was collected experiments carried out in [23]

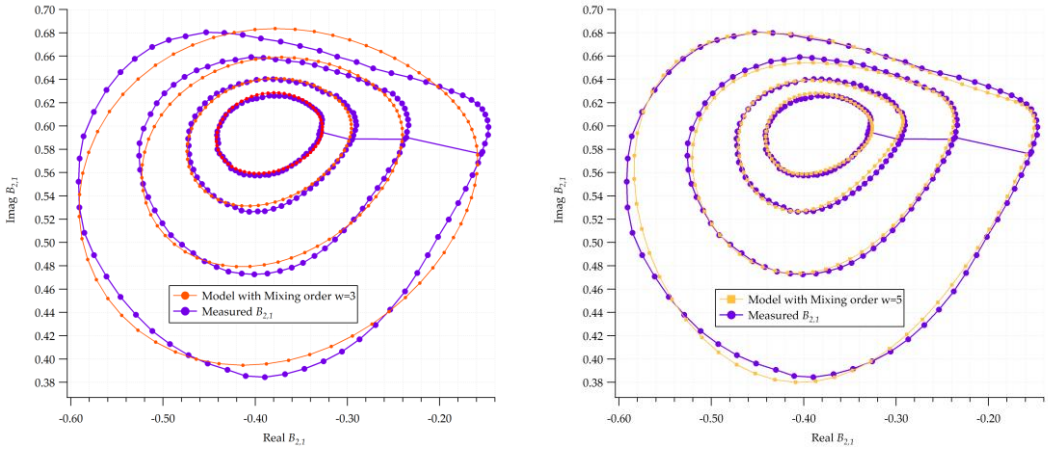

Figure 3-22: Comparison of the quality of different order, w, of models compared to experimental response. (i) Model complexity with w=3. (ii) Model with complexity w=5

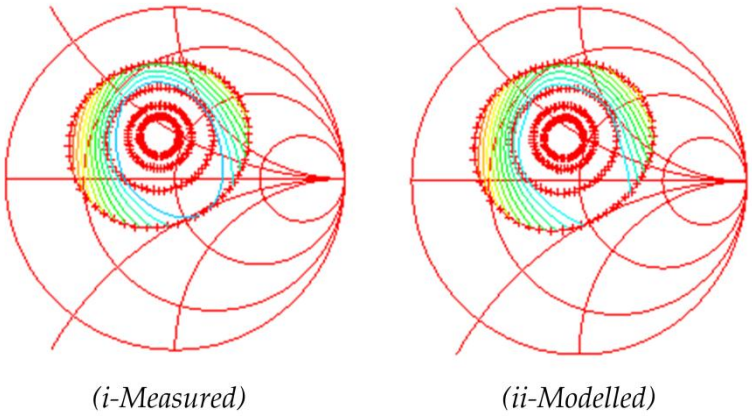

Figure 3-23: Comparison of i) measured and ii) modelled power contours

The above results indicate that it is only necessary to consider a low value of mixing order complexity w i.e. between five and seven to have an equivalent behavioural formulation that can generate the measured behaviour accurately. This allows for a significant compression of measured data while staying in control of accuracy.

As $|a_{2,1}|$ approaches zero, the load variations are confined to an area around the reference impedance and thus the higher order phase terms tend to collapse to 0. As such "local" models can be considered in these regions typically needing no more than model complexity of three model

coefficients (original $S_{22,11}$ and $T_{22,11}$ PHD model coefficients). These local models will be explored for their contribution to development of an intelligence driven active load pull system in later chapters of this thesis.

The model discussed so far describes how changes to fundamental load impedance affects harmonically related frequencies. Any changes to terminations at frequencies other than the fundamental are therefore unaccounted for- leading to degradation in accuracy of the model if they are changed. It is therefore important to extend this model generation capability to account for harmonic perturbations.

3.6.2 Harmonic Load pull and Source pull

The work described above was extended to account harmonic behaviour by Woodington et al. [24] and Bell et al. [25]. The generalised description, in the traveling wave domain for *r* harmonics was described as shown in (3-18).

$$b_{p,h} = P_1^h . g\left(v_{1,0}, |a_{1,1}|, v_{2,0}, |a_{2,1}|, Q_1/P_1 \ldots, |a_{2,r}|, Q_r/P_1^r, \ldots \right)$$

$$\text{Where } P_1 = \angle a_{1,1} = \frac{a_{1.1}}{|a_{1,1}|} \quad \text{and} \quad Q_r = \angle a_{2,r} = \frac{a_{2.r}}{|a_{2,r}|}$$

(3-18)

It was shown that each harmonic phase vector Q_1/P_1^r influences an *n*-dimensional periodic function contributing to the overall harmonic behaviour of $b_{n,h}$. The resulting equation is shown in (3-19). The coefficients in this equation are only functions of the stimuli magnitudes and are independent of their phases. Note that the phase difference between the two signals at the output is accounted for by cross-product terms in the equation.

$$b_{p,h} = P_1^h \cdot \sum_m \sum_r \left(K_{p,h,m,r} \left(Q_1 / P_1 \right)^m \left(Q_r / P_1^r \right)^r \right)$$

(3-19)

It was shown in both [24] (based on 2nd harmonic load pull) and [25] (based on 2nd harmonic source pull) that capturing the cross-product terms leads to a very accurate extraction and thus comparison between measured and modelled behaviour is greatly improved. The number of coefficients however increases as more harmonics are added into the overall behavioural model for the device.

3.6.3 Example: Generation of an output fundamental and second harmonic behavioural model

This example was presented in [24] where by results were taken for a 10x75μm GaAs HEMT device, operating at 9GHz. The open loop active load pull system developed in Cardiff University, described in Chapter 2, was used to carry out fundamental and harmonic load pull measurements on this device. A measurement strategy was developed, which involved the following steps:

i. Using a phase controllable signal generator, spin the second harmonic phase ($\angle a_{2,2}$) around 360 degrees in 18 degree steps whilst holding the fundamental phase vector constant.
ii. Repeat (i) as the fundamental phase vector itself is spun around 360 degrees, with points distributed every 18 degrees.
iii. Finally, capture datasets using (i) and (ii) with varying amplitudes of fundamental and second harmonic stimuli at port 2 ($|a_{2,1}|, |a_{2,2}|$).

The resulting dataset was renormalized to the measured system impedances and the input fundamental phase, $\angle A_{1,1}$, was removed. The measured data, described by its output impedances is shown in Figure 3-24.

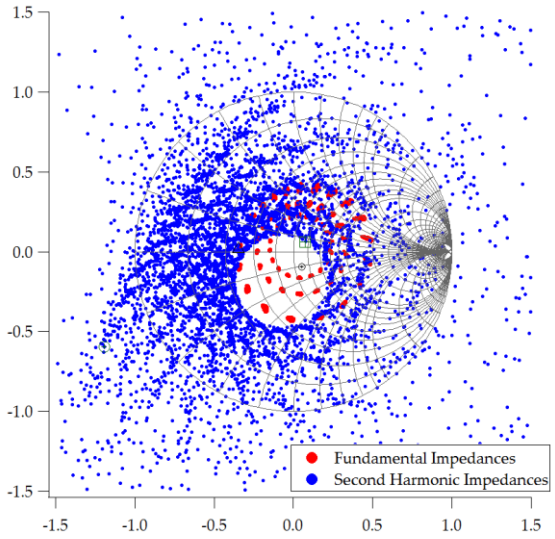

Figure 3-24: Measured fundamental and second harmonic impedances

Model Extraction and Validation

A subset of the original measurement data was used to illustrate the complexity of the coefficient set required in generating an accurate enough model for the dataset above.

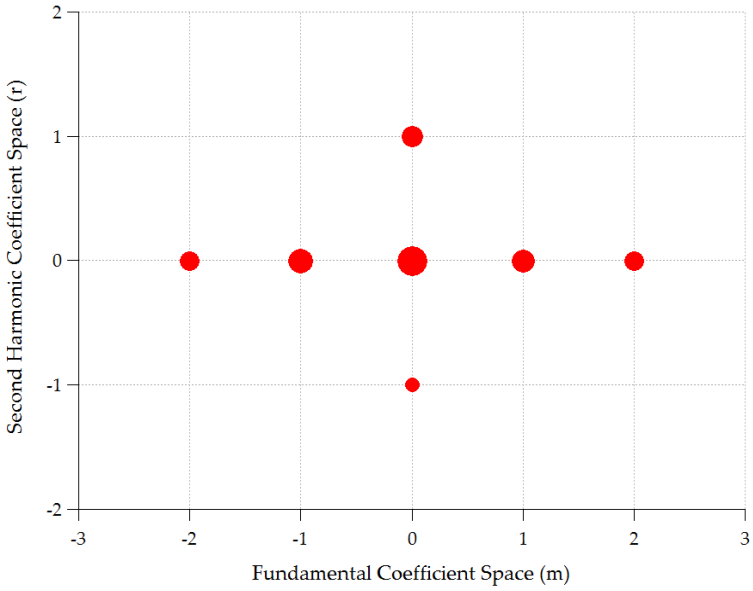

Figure 3-25: Coefficients used in model extraction.

Two distinct model coefficient-sets were therefore used. In the first case, with 7 model coefficients in the fundamental space and 3 coefficients in the second harmonic space, was used to generate a model for this subset (Figure 3-25). The size of the point is indicative of the magnitude of the coefficient. Modelled results from this extraction process were then overlaid onto the original measurement data. The prediction of the behaviour of the reflected wave (b_2) was then used to quantify the accuracy of the approach.

The resulting model (Figure 3-26) indicates that although most of the form of the perturbation is reproduced by the model (typically due to mixing of the fundamental output phase $\angle a_{2,1}$ and the input stimuli signal $a_{1,1}$), it is unable to model the interaction caused by mixing of the injected second harmonic signal $a_{2,2}$ and the injected fundamental signal $a_{2,1}$.

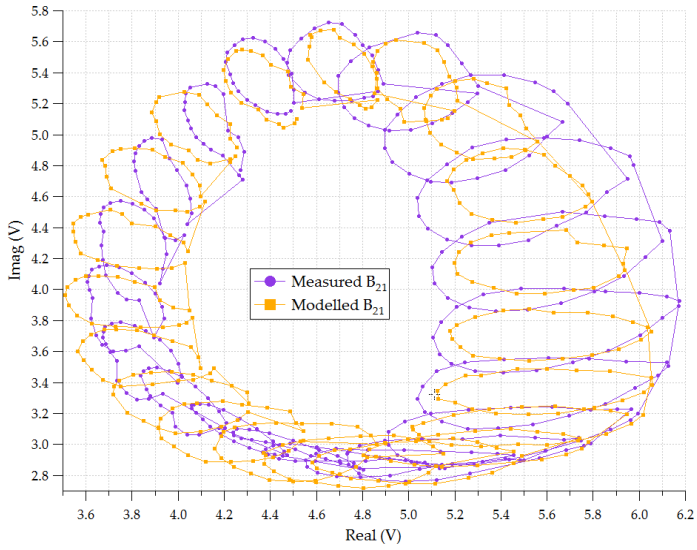

% Errors in prediction

Wave	*Max* %	*Avg* %
B_{21}	5.2	1.7
B_{22}	16.3	5.6
B_{23}	64.0	25.5
B_{12}	12.4	4.1
B_{23}	18.6	6.3

Figure 3-26: Comparison of measured and modelled B_{21}

In the second case, a model strategy was used which contained an optimum number of coefficients including cross product terms (Figure 3-27). This allowed the model to properly track changes in the second harmonic's perturbation around all phases of the fundamental wave $b_{2,1}$.

A comparison of measured and modelled versions (shown in Figure 3-28) of the wave $b_{2,1}$ showed excellent agreement with an average error of 0.14%.

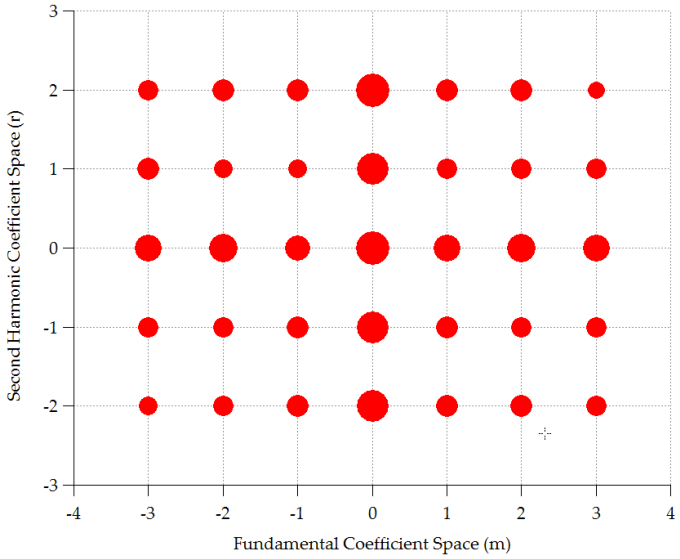

Figure 3-27: Coefficient set used in extraction while accounting for cross product terms

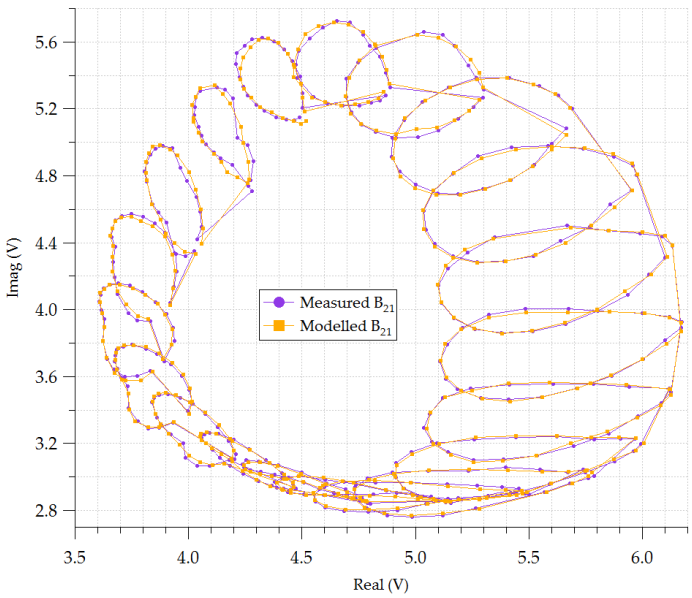

% Errors in prediction

Wave	*Max %*	*Avg %*
B_{21}	0.93	0.14
B_{22}	3.5	0.47
B_{23}	9.5	1.6
B_{12}	4.1	0.5
B_{23}	5.2	0.6

Figure 3-28: Comparison of measured and modelled B_{21}

The modelling coefficient set was then applied onto the entire dataset and the resulting prediction of the measured load pull points is shown in Figure 3-29.

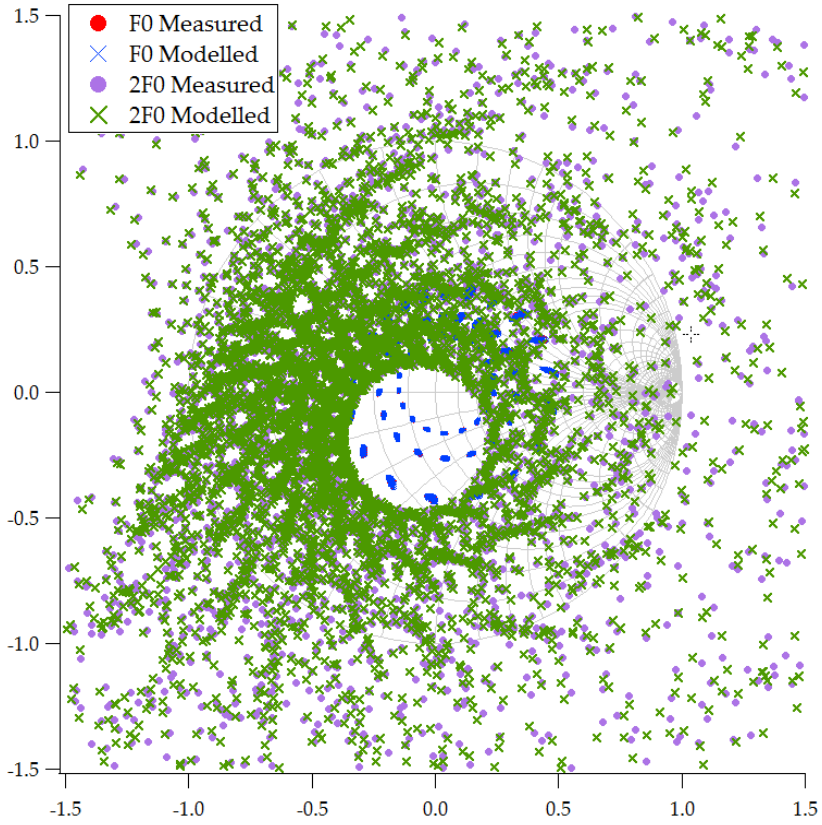

Figure 3-29: Model coefficients applied on the entire measurement set

This mixing-based behavioural model therefore showed a capability of taking into account the changes of load impedance at the fundamental as well as the second harmonic frequencies. Determining the correct coefficient set which includes the necessary cross product terms is however vital to get sufficient accuracy from the modelled data.

3.7 Summary

This chapter discussed various non-linear behavioural model generation approaches available today. Starting with a comparison of behavioural models to compact and physical models, the review discussed various advantages of using this approach. The theory behind the PHD model was described and shown how most modern frequency domain behavioural modelling implementations follow this theory.

Commercially available hardware such as the Agilent PNA-X series network analyser can be used to generate load-dependent X-parameters™ of a device under test. A discussion of this model generation and measurement strategy was described along with its drawbacks.

The Cardiff Direct Wave Lookup Table (DWLUT) model was described as a table based behavioural model, however it was shown that this kind of model is only useful for making non-linear data available in CAD. The biggest drawback of this approach was that it was only good at predicting the measurements on which it was based. In the same way as load-dependent X-parameters™, the DWLUT model requires measurement data to be placed on a regular grid. This requires more iteration from an active load pull system and thus greatly increases the overall measurement time needed for device characterisation.

The introduction of the Cardiff Behavioural Model formulations showed that measurement data was no longer required to be placed on a regular grid. Model coefficients could thus be extracted via techniques such as Least Means Squares (LMS). Various examples of the extraction were discussed in this chapter such as models for: fundamental-only load pull and fundamental and second harmonic load pull behaviour. For harmonic model generation, it was shown that mixing-based behavioural modelling takes into account the changes of load impedance at the fundamental as

well as the second harmonic frequencies. Determining the correct coefficient set which includes the necessary cross product terms is however vital to get sufficient accuracy from the modelled data.

The work presented in this thesis will make use of the Cardiff Behavioural model formulations and the PHD model to explore the interpolation and extrapolation capabilities of such a fundamental and a harmonic model of a non-linear device.

References

[1] Nagel, Laurence W., "SPICE2: A Computer Program to Simulate Semiconductor Circuits", Memorandum No. ERL-M520, University of California, Berkeley, May 1975.

[2] Maas, Stephen A. (2003). "Nonlinear microwave and RF circuits", Artech House. ISBN 1-58053-484-8.

[3] Gasseling, T. "Compact Transistor Models: The Roadmap to First-Pass Amplifier Design Success", Microwave Journal, March 2012. Available online: http://www.microwavejournal.com/articles/17138-compact-transistor-models--the-roadmap-to-first--pass-amplifier-design-success [Accessed 9-December-2012]

[4] Victory, J.J.; Sanchez, J.J.; DeMassa, T.A.; Welfert, B.D.; , "A static, physical VDMOS model based on the charge-sheet model," Electron Devices, IEEE Transactions on , vol.43, no.1, pp.157-164, Jan 1996

[5] Forestier, S.; Gasseling, T.; Bouysse, Ph.; Quere, R.; Nebus, J.M.; , "A new nonlinear capacitance model of millimeter wave power PHEMT for accurate AM/AM-AM/PM simulations," Microwave and Wireless Components Letters, IEEE , vol.14, no.1, pp. 43- 45, Jan. 2004

[6] Baylis, C.; Marks, R.J.; Martin, J.; Miller, H.; Moldovan, M.; , "Going Nonlinear," *Microwave Magazine, IEEE* , vol.12, no.2, pp.55-64, April 2011

[7] Wood, John and Root, David E. "Fundamentals of Nonlinear Behavioural Modeling for RF and Microwave Design," Arctech House. ISBN 1-58053-775-8

[8] J. Verspecht, "Large-Signal Network Analysis – 'Going Beyond S-Parameters'", 62nd ARFTG Conference Short Course Notes, December 2003

[9] Jan Verspecht, David E. Root, "Poly-harmonic Distortion Modeling", IEEE microwave magazine 1527-3342/06, June 2006

[10] J. Verspecht, M. Vanden Bossche, and F. Verbeyst, "Characterizing Components under Large Signal Excitation: Defining Sensible 'Large Signal S-Parameters' ?!" 49th ARFTG Conf. Digest, June 1997, pp. 109-117.

[11] J. Verspecht, "Large-Signal Network Analysis – 'Going Beyound S-Parameters'," 62nd ARFTG Conference Short Course Notes, December 2003.

[12] Online: http://cp.literature.agilent.com/litweb/pdf/N5242-90007.pdf [Accessed 04-Aug-2012]

[13] D. Root, J. Horn, L. Betts, C. Gillease, and J. Verspecht, "X-parameters: The new paradigm for measurement, modeling, and design of nonlinear RF and microwave components," Microwave Eng. Eur., vol. 51, no. 12, pp.16–21, Dec. 2008

[14] Online: http://www.nmdg.be/jump.php?category=home [Accessed: 9-December-2012]

[15] Myslinski, M.; Verbeyst, F.; Bossche, M.V.; Schreurs, D.; , "S-functions behavioral model order reduction based on narrowband modulated large-signal network analyzer measurements," Microwave Measurements Conference (ARFTG), 2010 75th ARFTG, vol., no., pp.1-6, 28-28 May 2010

[16] Baylis, C.; Marks, R.J.; Martin, J.; Miller, H.; Moldovan, M.; , "Going Nonlinear," Microwave Magazine, IEEE , vol.12, no.2, pp.55-64, April 2011

[17] Bretscher, Otto "Linear Algebra With Applications", 3rd ed. 1995. Upper Saddle River NJ: Prentice Hall

[18] Simpson, G.; Horn, J.; Gunyan, D.; Root, D.E.; , "Load-pull + NVNA = enhanced X-parameters for PA designs with high mismatch and

technology-independent large-signal device models," ARFTG Microwave Measurement Symposium, 2008 72nd, vol., no., pp.88-91, Dec. 2008

[19] Root, D.E.; Xu, J.; Horn, J.; Iwamoto, M.; Simpson, G.; , "Device modeling with NVNAs and X-parameters," Integrated Nonlinear Microwave and Millimeter-Wave Circuits (INMMIC), 2010 Workshop on , vol., no., pp.12-15, 26-27 April 2010

[20] Qi, H.; Benedikt, J.; Tasker, P.; , "Direct extraction of large-signal table-based behavioural models from time-domain voltage and current waveforms," High Frequency Postgraduate Student Colloquium, 2005

[21] Hao Qi; Benedikt, J.; Tasker, P.J.; , "Nonlinear Data Utilization: From Direct Data Lookup to Behavioral Modeling," Microwave Theory and Techniques, IEEE Transactions on, vol.57, no.6, pp.1425-1432, June 2009

[22] P. Wright, A. Sheikh, C. Roff, P. J. Tasker, and J. Benedikt, "Highly efficient operation modes in GaN power transistors delivering upwards of 81% efficiency and 12W output power," in IEEE MTT-S Int. Microwave Symp. Dig., June 15–20, 2008, pp. 1147–1150.

[23] Woodington, S.; Williams, T.; Qi, H.; Williams, D.; Pattison, L.; Patterson, A.; Lees, J.; Benedikt, J.; Tasker, P.J.; , "A novel measurement based method enabling rapid extraction of a RF Waveform Look-Up table based behavioral model," Microwave Symposium Digest, 2008 IEEE MTT-S International , vol., no., pp.1453-1456, 15-20 June 2008

[24] Woodington, S. P.; Saini, R. S.; Willams, D.; Lees, J.; Benedikt, J.; Tasker, P. J.; , "Behavioral model analysis of active harmonic load-pull measurements," Microwave Symposium Digest (MTT), 2010 IEEE MTT-S International, vol., no., pp.1, 23-28 May 2010

[25] Bell, J.J.; Saini, R.; Woodington, S.; Lees, J.; Benedikt, J.; Cripps, S.; Tasker, P.J.; , "Behavioral model analysis using simultaneous active fundamental load-pull and harmonic source-pull measurements at X-band," Microwave Symposium Digest (MTT), 2011 IEEE MTT-S International, vol., no., pp.1-4, 5-10 June 2011

Chapter 4 – An Intelligence Driven Active Load-Pull System

4.1 Introduction

This chapter describes how an application of the PHD model can add intelligence to an open loop active load-pull system. The approach that will be demonstrated improves prediction of the operating conditions required to emulate a specified load during open-loop active load-pull and thereby allowing more efficient use to be made of a measurement system. The work discussed in this chapter was summarised by the author in [1].

As mentioned in the literature review of chapter 2, source and load-pull measurement systems are widely used in the design of power amplifiers to deduce regions of operation that correspond to optimum efficiency, gain, linearity and output power and hence to make the design choices; hopefully leading to arrival at a solution for a particular set of requirements in a timely manner.

In open loop active load-pull systems, load emulation of the target reflection coefficient ($\Gamma_{T,h}$) is achieved by solving (4-1). Subscript h indicates the harmonic index. Since there is no prior knowledge of the function $b_{2,h}(.)$,

the open loop system is iterative in nature and typically a solution to (4-1) is found a using a numerical technique.

$$a_{2,h} - \Gamma_h b_{2,h}\left(a_{2,1}, a_{2,2}, ..., a_{2,h}\right) = 0 \tag{4-1}$$

This chapter is based around measurements carried out using an automated open loop active load-pull system, developed at Cardiff University as discussed in Chapter 2. The receiver used was a 4-channel Tektronix oscilloscope [2]-[3] in this setup as shown in Figure 4-30.

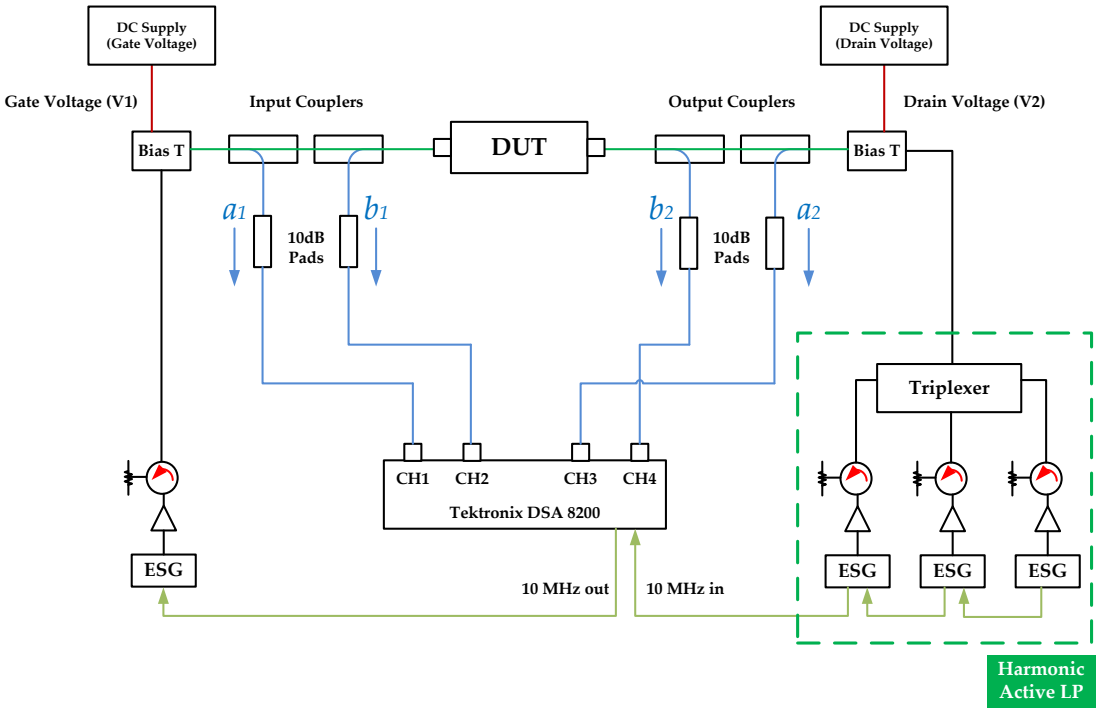

Figure 4-30: Open loop active load-pull system using a Tektronix oscilloscope

Automated load-pull measurements were achieved by custom-written software which managed all the relevant instrumentation to provide calibrated datasets during each device characterisation.

This software was written by the author using Microsoft C# as discussed and illustrated in Appendix A.

4.2 The load-pull error model

The model below is based on the work presented by D.J. Williams [4] to provide a mechanism of maintaining constant reflection coefficients at the fundamental and harmonic tones as input drive power, bias and frequency are varied. During measurements, acquired error-corrected data from the receiver is utilised to generate the magnitude and phase of the electronic signal generator required to set arbitrary load impedances at each frequency of interest thus generating the signal, $a_{pset,h}$ *(p=port Index, h = harmonic index)*. This signal is then amplified or attenuated and the incident wave, $a_{p,h}$ presented to the DUT.

Figure 4-31: Active load-pull error model

The magnitude and phase of the required generator's signal $a_{pset,\ h}$ is calculated in an iterative convergence process to achieve the desired reflection coefficient, based on the error model shown in Figure 4-31 and described by equations (4-2) to (4-3).

$$a_{pset,h} = \frac{b_{p,h}(\Gamma_{Tp,h} - \Gamma_{p,h})}{T_{sp,h}} \qquad (4\text{-}2)$$

$$T_{sp,h} = \frac{a_2 - \Gamma_{pL,h} b_2}{a_{pset,h}} \qquad (4\text{-}3)$$

In this error model:

i. $\Gamma_{pL,h}$ represents the system reflection coefficient for the specified port and harmonic network. This coefficient can be measured after calibration of the system and values stored for each harmonic.

ii. $T_{sp,h}$ represents the transmission coefficient; accounting for the loss or gain in the specified port network between the generator and the DUT. During the iterative convergence process, this coefficient is continuously measured using equation (4-3) from the magnitude and phase of the measured data and the RF signal of the generator. The continuous measurement is required to account for the non-linear behaviour of the amplifiers used in the system.

iii. $a_{pset,h}$ is a definition of the magnitude and phase energy generated by the generator. During the iterative convergence process, this signal is continuously computed using equation (4-2), usually via a numerical technique.

iv. $\Gamma_{Tp,h}$ is the desired reflection coefficient that the system iterates to.

A summary of the iterative loop is shown in the flow chart below, illustrating the steps required for fundamental load-pull. At the start, an initial measurement is taken to determine the present impedance state of the DUT. Based on the RF signal settings of the generator, an updated value of the $T_{sp,h}$ coefficient is then determined. The value of $a_{pset,h}$ is then calculated and uploaded to the signal generator. Resulting from the new signal, a further measurement is required to determine the error in the

convergence between the target load impedance ($\Gamma_{Tp,h}$) and the present load impedance ($\Gamma_{p,h}$). If this error meets the required tolerance set by the user, the system stops the iterations. Otherwise, it carries out further iterations until the convergence is attained or the loop count times out.

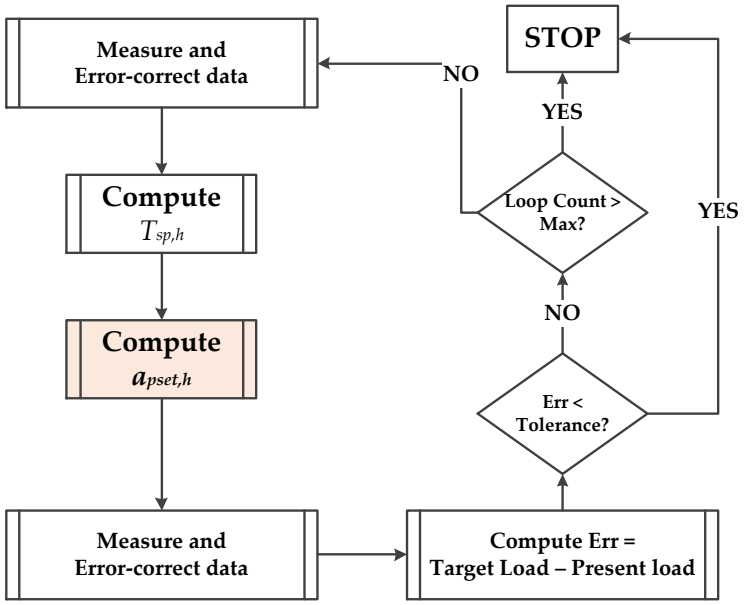

Figure 4-32: The load-pull iterative loop

4.3 Finding the solution using the Newton-Raphson Algorithm

The computation of $a_{pset,h}$ was carried out using a numerical technique based on the Newton-Raphson (NR) [5] root finding technique in the original open loop active load-pull software implementation [4]. This is an *open* method; that is one that requires one or more starting values, but not necessarily the root of the function. For example, a plot of the function $f(x)$ is shown in Figure 4-33. From this figure, it can be see that an initial guess of the root of the function $f(x)$ is given by x_i.

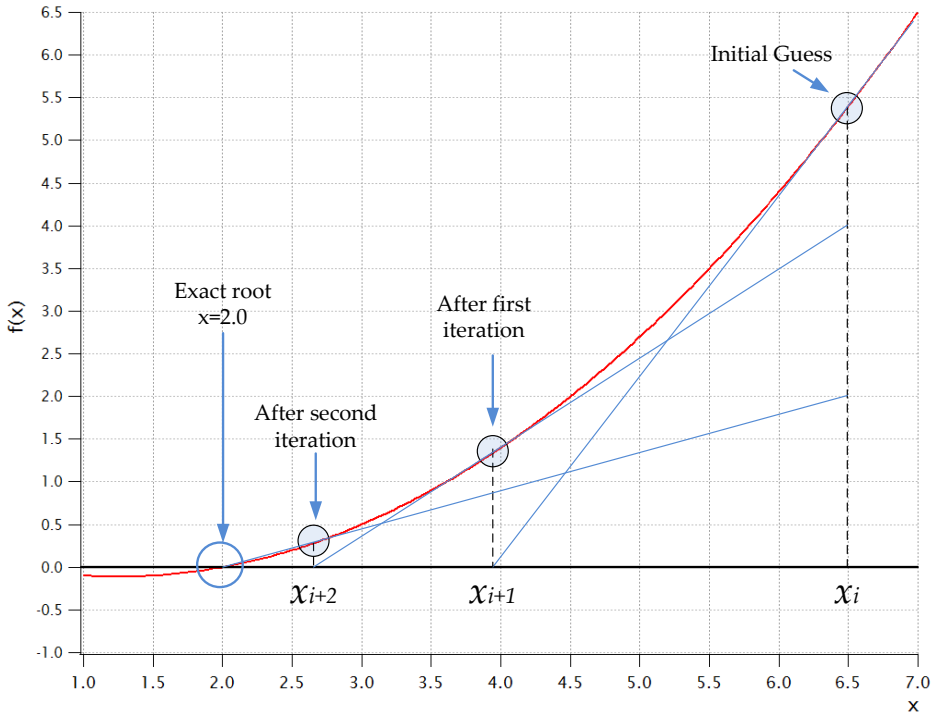

Figure 4-33: Solving for function *f(x)* using the NR technique

Extending a tangent from this point i.e. [x_i, $f(x_i)$], a better estimate of the root is found at the position where the tangent intercepts the x-axis (x_{i+1}). The above process is repeated until the exact solution is found. Therefore, the generalized equation for the Newton-Raphson method as examined by Epperson [6] is given in (4-4).

$$x_{i+1} = x_i - \frac{f(x_i)}{f'(x_i)} \qquad (4\text{-}4)$$

In this form, there are various drawbacks of this numerical technique. Firstly, computation of a derivative is required before the function can be used. Secondly, the formulation is also prone to numerical oscillations whereby the root of the solution oscillates around a point of inflexion. In order to make practical use of the technique, a weighting factor w was used (4-5)-(4-9).

Considering the function:

$$f(x) - x = 0 = g(x) \tag{4-5}$$

$$\frac{g(x)}{x_i - x_{i+1}} = \frac{\partial g^i}{\partial x} \tag{4-6}$$

$$x_i - x_{i+1} = \frac{g(x_i)}{\partial g^i / \partial x} \tag{4-7}$$

$$\therefore \frac{\partial g}{\partial x} = \frac{\partial f}{\partial x} - 1 \tag{4-8}$$

$$x_{i+1} = x_i - \frac{f(x_i) - x_i}{\frac{\partial f}{\partial x} - 1} \tag{4-9}$$

The final NR equation is highlighted in (4-10) and based on the load-pull error model in (4-2); the calculation of $a_{pset,h}$ is shown in (4-11).

$$x_{i+1} = (w) f(x_i) + (1-w) x_i \tag{4-10}$$

$$a_{pset,h} = (w) \frac{b_{p,h}(\Gamma_{Tp,h} - \Gamma_{p,h})}{T_{sp,h}} + (1-w) a_{pset\_old,h} \tag{4-11}$$

In this form, the value of $a_{pset,h}$ in the next iteration depends on the present value of $a_{pset,h}$ and a weighting factor w. The value of w can be set at the start of a measurement (between 0 and 1), giving more control of the convergence by reducing numerical oscillations and protecting the device from unpredictable impedance terminations. The smaller the weighting factor, the longer a convergence process takes.

4.3.1 ALP measurements using the NR numerical technique

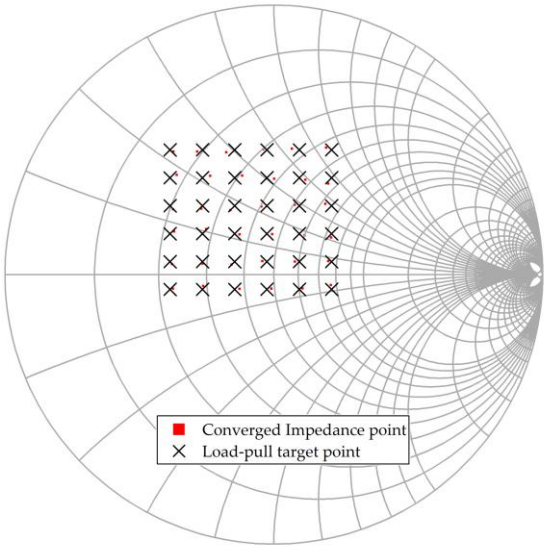

Figure 4-34: A 6x6 Grid of target reflection coefficients for load-pull

A demonstration of the quality of convergence was shown by active load-pull measurements carried out on a 10x75µm GaAs pHEMT device, operating at 3 GHz with Class-B biasing conditions. In this example, a 6x6 grid of target reflection coefficients is utilised; centred on the device optimum for power. The load-pull sweep was carried out at the 1dB compression point. All higher harmonics e.g. second (2F0) and third (3F0) were terminated into 50 ohms. Figure 4-34 shows the results of this convergence.

On analysing the results, as shown in Figure 4-35, 114 iterations were required to complete the process in order to achieve a pre-set error tolerance of less than 5%. Note that this load-pull measurement was carried out at a single power level and bias point. Typically, such device characterisations are done over a range of independent variables such as input power, frequency and bias settings. With each independent variable being swept independently, this process is very time consuming.

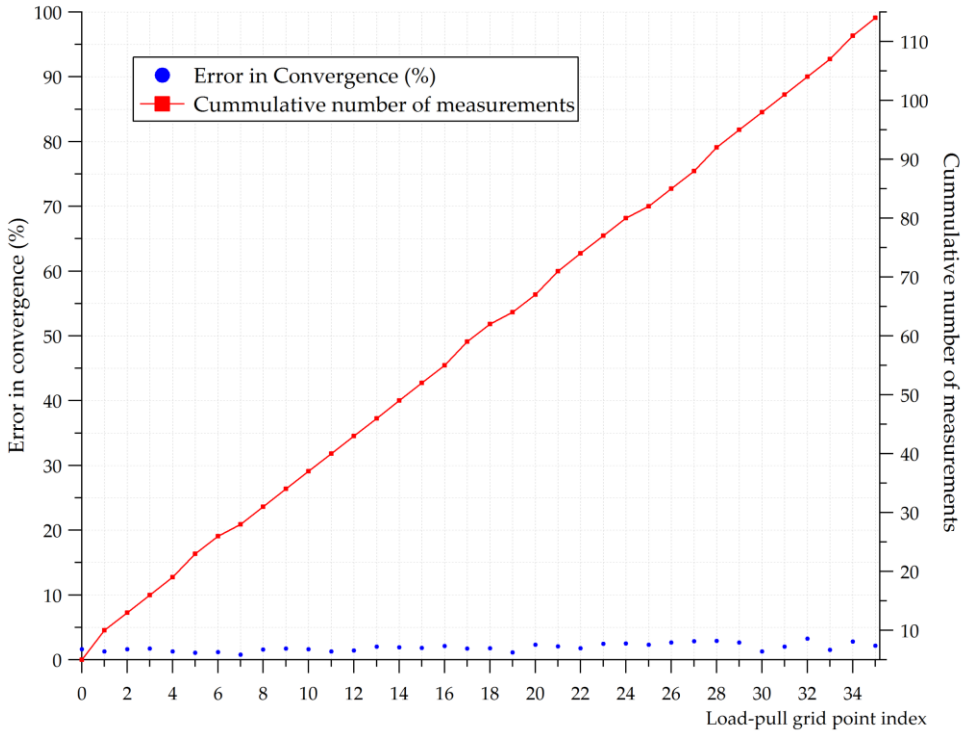

Figure 4-35: Plot of convergence error and cumulative iterations

4.3.2 Utilisation efficiency of a measurement system (η_{meas})

In open loop active load-pull measurements, we can classify the measurements in two categories. Redundant measurements ($M_{redundant}$) aid the measurement system to achieve a load-emulation target. In the model driven load-pull approach, these measurements are used in computing the localised X-parameter models. Useful measurements (M_{useful}) are those taken once the target load emulation point is within the error tolerance as set by the user. The utilisation efficiency (η_{meas}) therefore quantifies the ratio of useful to the total number of measurements as shown in (4-12). An ideal system, 100% efficient would require only one measurement per load point.

$$\eta_{meas} = \frac{M_{useful}}{M_{useful} + M_{redundant}} * 100 \qquad (4\text{-}12)$$

For the above load-pull sweep, the efficiency of the algorithm using the NR numerical technique is therefore 31.5%. (Number of points: 36, Number of measurements: 114).

4.4 Theory and design of a model-based algorithm

The Poly Harmonic Distortion modelling (PHD) technique [7], as discussed in Chapter 3, provides a mathematical framework for describing the response, $b_{2,h}$ of a non-linear system as a function of the respective injection signals (4-14). Combining this with (4-13) thus allows for the formulation of a new open loop load-pull algorithm with improved load emulation capability. A singular approximation to the solution of (4-13) can therefore be reached; which is valid locally in the region that it is determined.

$$a_{2,h} - \Gamma_h b_{2,h}\left(a_{2,1}, a_{2,2}, ..., a_{2,h}\right) = 0 \tag{4-13}$$

$$b_{2,h} = S_{21}\left(\left|A_{11}\right|\right)A_{11} + \sum_h S_{22}\left(\left|A_{11}\right|\right)A_{2,h} + \sum_h T_{22}\left(\left|A_{11}\right|\right)A_{2,h}^{\ *} \tag{4-14}$$

As already discussed in the literature review of Chapter 3, (4-14) can be modified by describing P and Q as input and output a-wave harmonic phase operators, leading to the generalized solution shown in (4-15)-(4-17).

$$b_{2,1} = P_1 . g\left(V_{1,0}, \left|A_{1,1}\right|, V_{2,0}, \left|A_{2,1}\right|, Q_1 \big/ P_1\right) \tag{4-15}$$

$$K_{p,h,m} = g\left(V_{1,0}, \left|A_{1,1}\right|, V_{2,0}, \left|A_{2,1}\right|\right) \tag{4-16}$$

$$b_{p,h} = P_1^{\,h} . \left(\sum_{m=-(w-1)/2}^{m=+(w+1)/2} K_{p,h,m} \left(Q_1 \big/ P_1\right)^m \right) \tag{4-17}$$

Adapting this generalized formulation and assuming that the magnitude of the input signal ($|a_{11}|$) during this process is held constant; we can simplify it to (4-18) by considering only the linear third order mixing terms. This is analogous to X-parameter™ [8] formulation, also described in Chapter 3. The equivalent X-parameter equation is shown in (4-19).

$$b_{2,h} = K_{2,0,h} + K_{2,1,h}\left(|a_{2,1}|\right)\left(\frac{Q}{P}\right) + K_{2,-1,h}\left(|a_{2,1}|\right)\left(\frac{P}{Q}\right) \qquad (4\text{-}18)$$

$$b_{2,h} = X_{2,h}^{(F)} + X_{2,h}^{(S)} a_{2,h} + X_{2,h}^{(T)} a_{2,h}^{*} \qquad (4\text{-}19)$$

The extraction of the required X-parameters, practical considerations and finally testing of the model-based algorithm is covered in the rest of this chapter.

4.4.1 Measurement of X-parameters

The measurement of the X-parameters during load-pull follows the technique explained in [7]. The parameter $X_{2,h}^{(F)}$ can be deduced from the output response of the fundamental input drive $|A_{11}|$ at the harmonic being load-pulled.

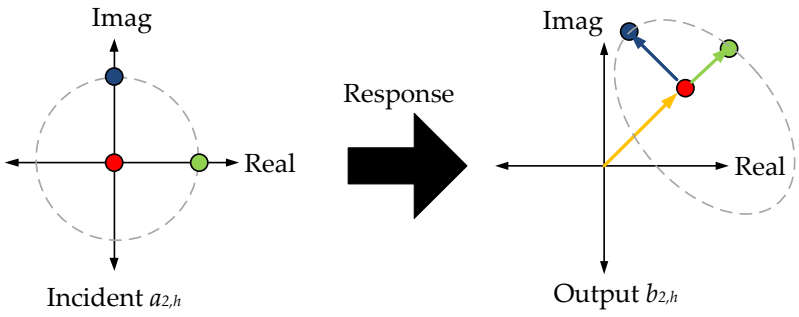

Figure 4-36: Extraction of $X_{2,h}^{(S)}$ and $X_{2,h}^{(T)}$

As shown in Figure 4-36, the parameters $X_{2,h}^{(S)}$ *and* $X_{2,h}^{(T)}$ are extracted by applying a perturbation signal to the incident a_{21} wave, first of all with a

zero-degree phase and then followed by the same signal with a 90-degree shift, keeping the input drive signal, $|a_{11}|$, constant in both cases. By utilizing the measured values of a_{2h} and b_{2h} at the centre and offset points (indicated by the subscripts 0, 1 and 2) we can then calculate these parameters using equation set (4-20)-(4-23).

$$\Delta_1 = a_{2,h,1} - a_{2,h,0} \qquad \Delta_2 = a_{2,h,2} - a_{2,h,0} \tag{4-20}$$

$$X_{2,h}^{(S)} = \frac{(\Delta_2{}^*)(b_{2,h,1} - b_{2h,0}) - (\Delta_1{}^*)(b_{2,h,2} - b_{2,h,0})}{(\Delta_1)(\Delta_2{}^*) - (\Delta_1{}^*)(\Delta_2)} \tag{4-21}$$

$$X_{2,h}^{(T)} = \frac{b_{2,h,1} - b_{2,h,0} - X_{2,h}^{(S)}(\Delta_1)}{(\Delta_1{}^*)} \tag{4-22}$$

$$X_{2,h}^{(F)} = b_{2,h,0} - X_{2,h}^{(S)}(a_{2,h,0}) - X_{2,h}^{(T)}(a_{2,h,0}{}^*) \tag{4-23}$$

4.4.2 Application of the measured X-parameters

Since the target load emulation point (Γ_T) is known during the automated load-pull process, the injected signal $a_{2,h}$ can be calculated analytically by the solution to (4-24) – this has been simplified for only the fundamental injected signal at the output (a_{21}). A derivation of this formulation is included in Table 4-1.

$$a_{2,1} = \frac{X_{2,1}^{(T)}.X_{2,1}^{(F)} * \left|\Gamma_T\right|^2 - \left(X_{2,1}^{(S)}\Gamma_T - 1\right) * \Gamma_T.X_{2,1}^{(F)}}{\left|X_{2,1}^{(F)}.\Gamma_T - 1\right|^2 - \left|X_{2,1}^{(T)}.\Gamma_T\right|^2} \tag{4-24}$$

Considering fundamental load-pull at port 2,

Given that the reflection coefficient, $\Gamma_{2,1}$ is defined by:

$$\Gamma_{2,1} = \frac{a_{2,1}}{b_{2,1}}$$

the output response, $b_{2,1}$ given by the X-parameter formulation is

$$b_{2,1} = X_{2,1}^{(F)} + a_{2,1}X^{(S)} + X_{2,1}^{(T)}a_{2,1}^{*}$$

Hence:

$$\Gamma_{2,1} = \frac{a_{2,1}}{X_{2,1}^{(F)} + X_{2,1}^{(S)}a_{2,1} + X_{2,1}^{(T)}a_{2,1}^{*}}$$

$$a_{2,1} = \Gamma_{2,1}\left(X_{2,1}^{(F)} + X_{2,1}^{(S)}a_{2,1} + X_{2,1}^{(T)}a_{2,1}^{*}\right)$$

$$\Gamma_{2,1}X_{2,1}^{(F)} + a_{2,1}\left(\Gamma_{2,1}X_{2,1}^{(S)} - 1\right) + \Gamma_{2,1}X_{2,1}^{(T)}a_{2,1}^{*} = 0$$

$$\Gamma_{2,1}^{*}X_{2,1}^{(F)^{*}} + a_{2,1}^{*}\left(\Gamma_{2,1}X_{2,1}^{(S)} - 1\right)^{*} + \Gamma_{2,1}^{*}X_{2,1}^{(T)^{*}}a_{2,1} = 0$$

$$\begin{bmatrix} \Gamma_{2,1}X_{2,1}^{(F)} \\ \Gamma_{2,1}^{*}X_{2,1}^{(F)^{*}} \end{bmatrix} + \begin{bmatrix} X_{2,1}^{(S)}\Gamma_{2,1} - 1 & X_{2,1}^{(T)}\Gamma_{2,1} \\ X_{2,1}^{(T)^{*}}\Gamma_{2,1}^{*} & \left(X_{2,1}^{(S)}\Gamma_{2,1} - 1\right)^{*} \end{bmatrix} \begin{bmatrix} a_{2,1} \\ a_{2,1}^{*} \end{bmatrix} = 0$$

$$\begin{bmatrix} -X_{2,1}^{(F)}\Gamma_{2,1} \\ -X_{2,1}^{(F)^{*}}\Gamma_{2,1}^{*} \end{bmatrix} = \begin{bmatrix} X_{2,1}^{(S)}\Gamma_{2,1} - 1 & X_{2,1}^{(T)}\Gamma_{2,1} \\ X_{2,1}^{(T)^{*}}\Gamma_{2,1}^{*} & \left(X_{2,1}^{(S)}\Gamma_{2,1} - 1\right)^{*} \end{bmatrix} \begin{bmatrix} a_{2,1} \\ a_{2,1}^{*} \end{bmatrix}$$

$$\begin{bmatrix} a_{2,1} \\ a_{2,1}^{*} \end{bmatrix} = \frac{1}{\left|X_{2,1}^{(S)}\Gamma_{2,1} - 1\right|^2 - \left|X_{2,1}^{(T)}\Gamma_{2,1}\right|^2} \begin{bmatrix} \left(X_{2,1}^{(S)}\Gamma_{2,1} - 1\right)^{*} & -X_{2,1}^{(T)}\Gamma_{2,1} \\ -X_{2,1}^{(T)^{*}}\Gamma_{2,1}^{*} & \left(X_{2,1}^{(S)}\Gamma_{2,1} - 1\right)^{*} \end{bmatrix} \begin{bmatrix} -X_{2,1}^{(F)}\Gamma_{2,1} \\ -X_{2,1}^{(F)^{*}}\Gamma_{2,1}^{*} \end{bmatrix}$$

$$\begin{bmatrix} a_{2,1} \\ a_{2,1}^{*} \end{bmatrix} = \begin{bmatrix} \dfrac{-\left(X_{2,1}^{(S)}\Gamma_{2,1} - 1\right)^{*}\Gamma_{2,1}X_{2,1}^{(F)} + X_{2,1}^{(T)}\left|\Gamma_{2,1}\right|^2 X_{2,1}^{(F)^{*}}}{\left|X_{2,1}^{(F)}\Gamma_{2,1} - 1\right|^2 - \left|X_{2,1}^{(T)}\Gamma_{2,1}\right|^2} \\ \dfrac{X_{2,1}^{(T)^{*}}\left|\Gamma_{2,1}\right|^2 X_{2,1}^{(F)} - \left(X_{2,1}^{(S)}\Gamma_{2,1} - 1\right)\Gamma_{2,1}^{*}X_{2,1}^{(F)^{*}}}{\left|X_{2,1}^{(S)}\Gamma_{2,1} - 1\right|^2 - \left|X_{2,1}^{(T)}\Gamma_{2,1}\right|^2} \end{bmatrix}$$

Replacing $\Gamma_{2,1}$ by the desired target reflection coefficient, Γ_T

$$a_{2,1} = \frac{X_{2,1}^{(T)}X_{2,1}^{(F)^{*}}\left|\Gamma_T\right|^2 - \left(X_{2,1}^{(S)}\Gamma_T - 1\right)^{*}\Gamma_T.X_{2,1}^{(F)}}{\left|X_{2,1}^{(F)}.\Gamma_T - 1\right|^2 - \left|X_{2,1}^{(T)}.\Gamma_T\right|^2}$$

Table 4-1: Derivation of load-pull algorithm

4.5 Implementation and use in open loop active load-pull measurements

4.5.1 The active load pull error model

The predicted signal computed using (4-24) does not take into account non-ideal behaviours of open loop active load-pull characterisation. This is best described by the error model discussed earlier, in Figure 4-31. In order to present the desired value of $a_{2,h}$ to the device, the parameters $T_{sp,h}$ (transmission coefficient i.e. loss/gain of the amplifier and hybrid couplers) and $\Gamma_{sp,h}$ (impedance of the measurement system) need to be accounted-for and thus aid the synthesis of the necessary RF signal by the generator ($a_{pset,h}$). This calculation can be carried out using (4-2) and (4-3).

4.5.2 Range of a local model

As three distinct measurements are required to compute the local model, it is necessary to maximize the use of an existing set of X-parameters (a local model), provided the input drive ($|a_{11}|$) or biasing conditions have remained unchanged. If the new load position is found to be within the acceptable tolerance of the target load, the existing model would have converged without requiring an update; this is particularly beneficial during load pull of an impedance grid. Each of the measurements carried out to compute the local models are regarded as "redundant" since they are aiding the measurement system to achieve an emulation target. The efficiency of the measurement system can therefore be quantified by comparing the number of useful to redundant measurements.

4.5.3 Summary of the load emulation process

The flow chart in Figure 4-37 summarises the implementation of the algorithm, including the re-use and adjustment steps.

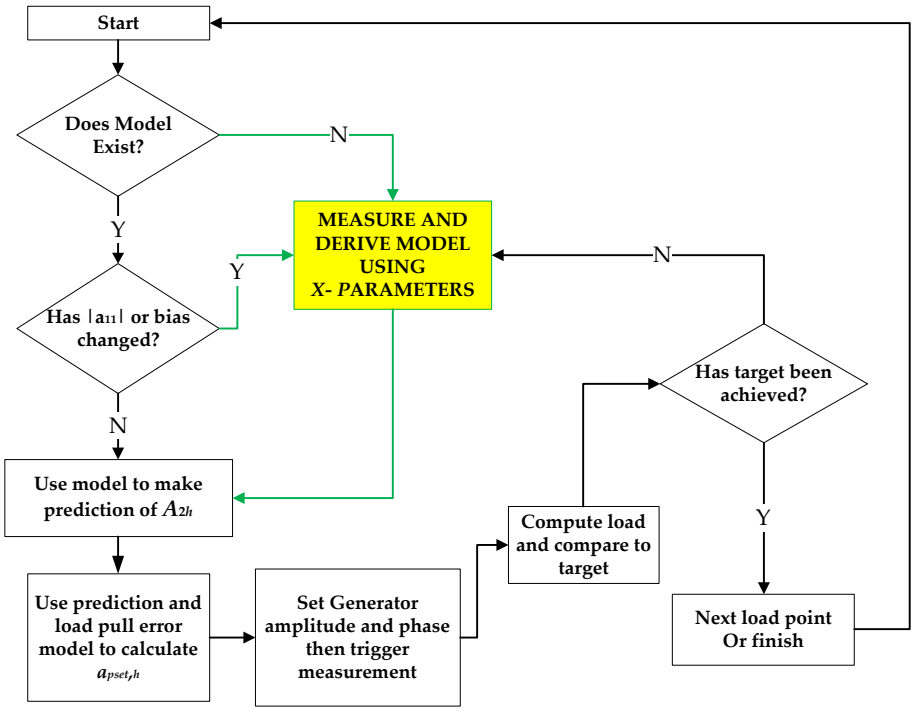

Figure 4-37: Flow chart showing the steps in the load emulation process

At the start, a query is carried out to find an available model for the measurement conditions defined (Such as equal input power, bias settings and frequency). If a suitable model is found, a prediction of the injected signal $a_{2,h}$ is then calculated using this; and further adjusted for the transmission coefficient ($T_{sp,h}$) and impedance of the measurement system ($\Gamma_{sp,h}$). The algorithm also checks if the measurement system or model generated is in an "error state". If this is safe to continue, the compensated value ($a_{pset,h}$) is then uploaded to the signal generators and a measurement is carried out. Using the data generated from this measurement, the value of the actual load at the present position is calculated and compared with the target.

If this target is within the tolerance level set by the user, the convergence is now complete. However, if it is higher than the tolerance level, a new set of X-parameters is then calculated to derive a fresh local model and the whole prediction process is carried out again.

4.6 Testing the algorithm

In order to illustrate how the target load is attained, a single point was initially considered. This was followed by carrying out measurements on a sweep plan of multiple target points. All measurements were carried out on a 10x75µm GaAs pHEMT, operating at 3.0GHz with Class-B biasing conditions. These measurements were carried out on the automated load-pull system, described earlier and based on the Tektronix oscilloscope as the primary receiver.

4.6.1 "Single-point" load-pull

In this test, a single load emulation point was considered as a target and the path taken by the algorithm to achieve this is shown in Figure 4-38.

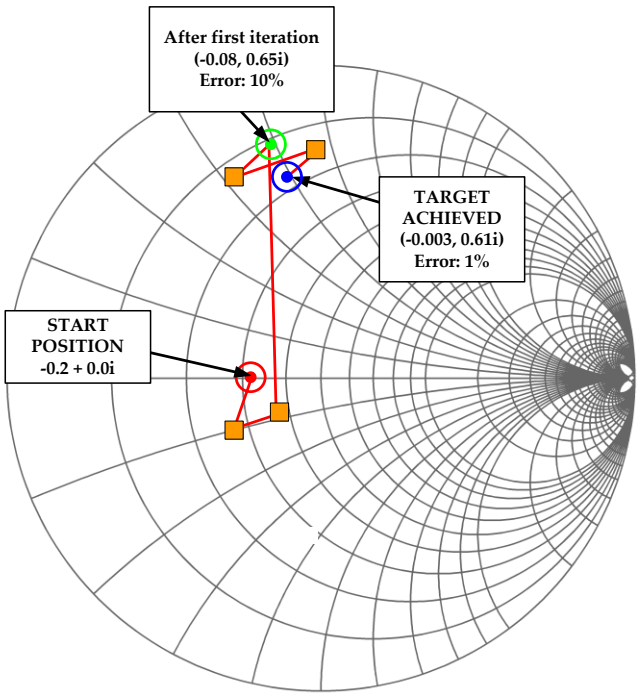

Figure 4-38: Single point load-pull

The measured starting position of the load pull was recorded as a reflection coefficient of -0.2+0.0i. The target load emulation point required to be achieved was a reflection coefficient of 0.0+0.6i and the tolerance set was 6%. At the starting point (-0.2+0i), a query is carried out to find any local models. In this case, the query does not return any models since the measurement criteria do not exist in its database. As a result, two perturbations are made to the $a_{2,1}$ injection signal; thereby creating the two offset points (indicated by orange square-shaped markers) which allow the calculation of a local model. The local model is then used to compute a value of $a_{pset,h}$; this moves the load to a new position (-0.08+0.65i), which in this case is not within the tolerance range set by the user. The algorithm therefore requires the model to refresh itself with a new set of X-parameters at this stage, hence the additional set of offset points. The final reflection coefficient obtained (-0.003+0.61i) was within 1% of the target load emulation point (0+0.6i); implying the algorithm had now converged to a solution.

4.6.2 "Swept-mode" load-pull at single power level

In this measurement configuration, a 6x6 impedance grid was centred on the optimum of the device and the target emulation points matched the ones used in the review of the Newton Raphson numerical technique discussed earlier, in section 4.3.1 of this chapter. Figure 4-39 shows results of this characterisation. The measurement results show that the algorithm improved the utilisation efficiency to 78.3%. (Total number of points: 36, Total number of measurements: 46). A summary of the iterations required in this characterisation as well as the convergence error per point has been plotted in Figure 4-40.

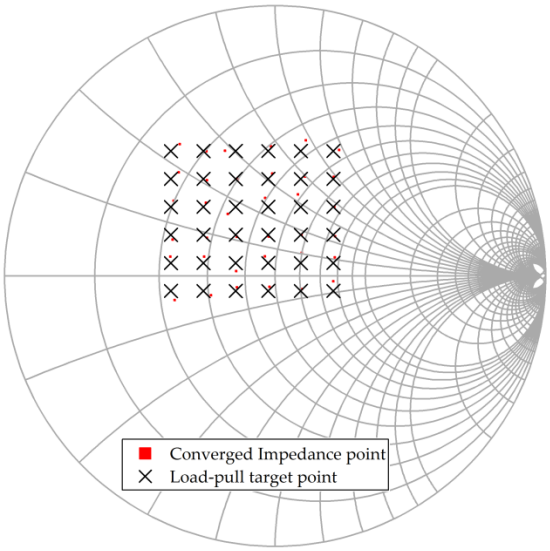

Figure 4-39: Results from a load-pull characterisation using the model-based technique at a single power level

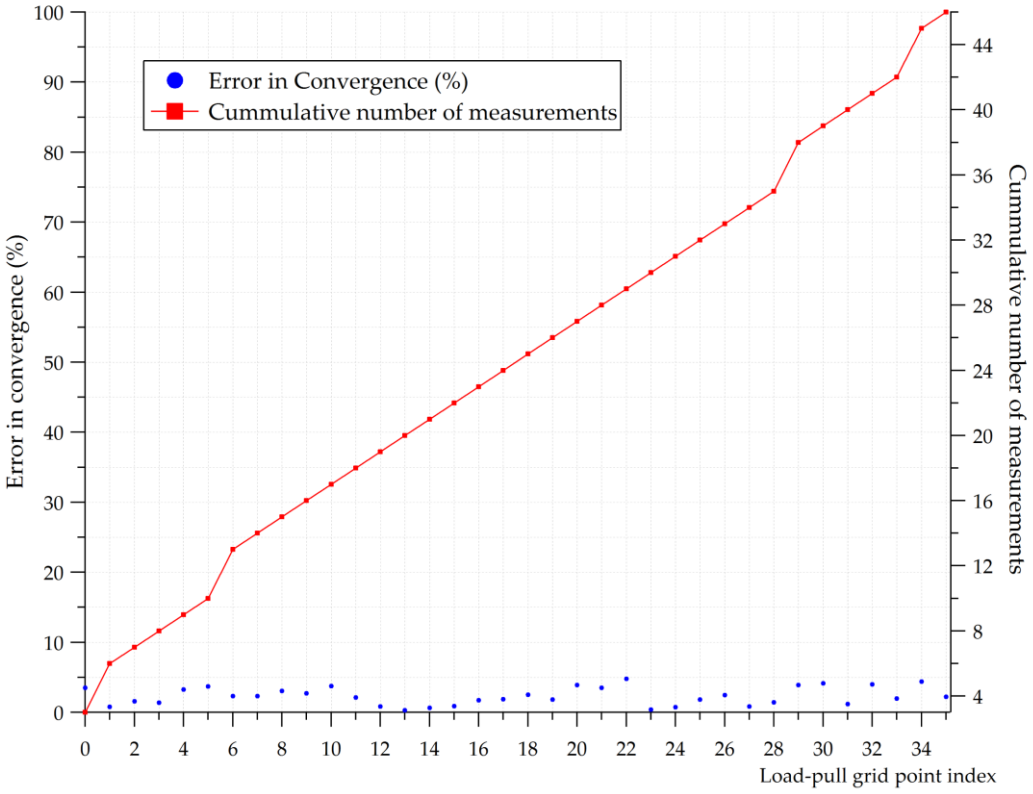

Figure 4-40: Plot of error in convergence and number of measurements

4.6.3 "Swept-mode" load-pull in a power sweep

The real benefit of this algorithm is during load and power sweeps. Since the intelligence is consistently being built throughout the sweep, the efficiency and speed of measurement improves gradually.

In order to illustrate this, measurements were carried out around the optimum of the device, with a load emulation error tolerance of 5%. They were also configured with a large power sweep plan, with a dynamic range featuring 28 input power levels in 0.5dB steps and 25 impedance target points (a total of 700 load-pull points). Results from this measurement are shown on the smith chart in Figure 4-41.

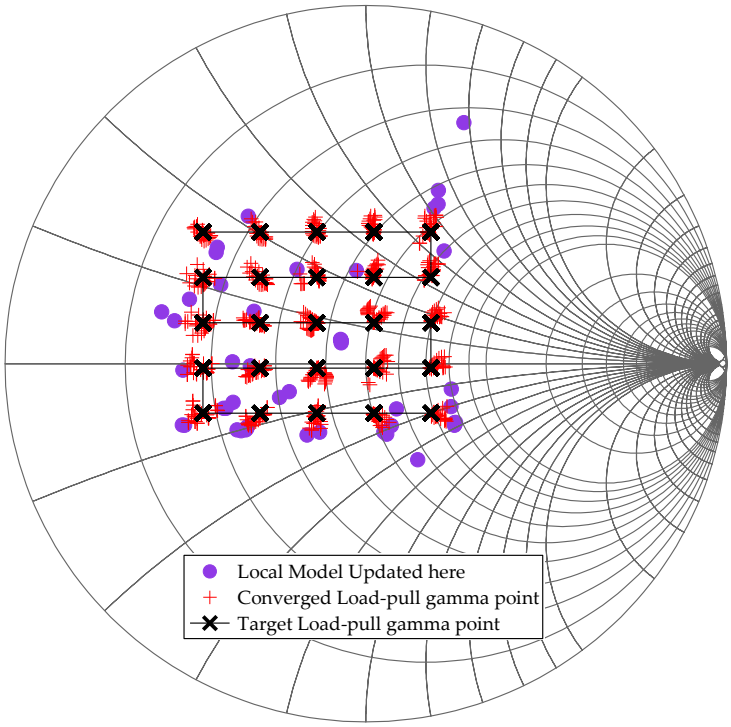

Figure 4-41: Load-pull characterisation using the model based technique

In this figure, the points where the load-pull algorithm required a recalculation of the X-parameters are also highlighted. Figure 4-42 shows the cumulative number of measurements required in the convergence of the sweep plan. The percentage error between the target and attained values of the load are also shown in this figure. For this sweep, the

measurement system managed to achieve all the load points to within the required error tolerance value (5%); with an average value of 2.11%.

For the above example, efficiency of the measurement system was 90% (778 measurements were carried out for 700 load pull target points) as existing models were re-used during the power sweeps. This result, when compared to a typical value previously of only 10-30% using a numerical algorithm, is a significant improvement in the measurement efficiency of the open loop active load-pull system.

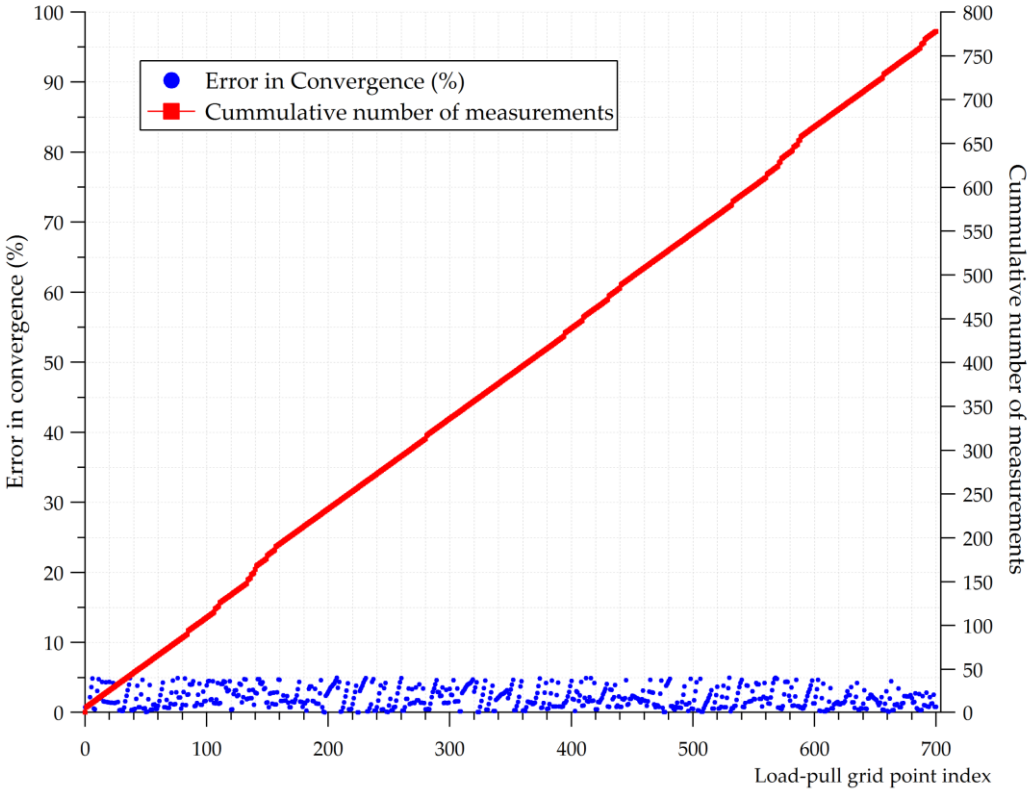

Figure 4-42: Cumulative number of measurements and convergence error in each measurement

4.7 Further Improvements

In order to further reduce the number of iterations in the system, it is important to analyse the range of the local model versus the changing behaviour of the measurement system. This phenomenon is inherent in the fact that the gain ($T_{sp,h}$) of the system amplifier in the active load-pull loop may be changing (due to AM-AM or AM-PM distortion characteristics of the system amplifier) as the system attempts to converge onto a target load emulation point.

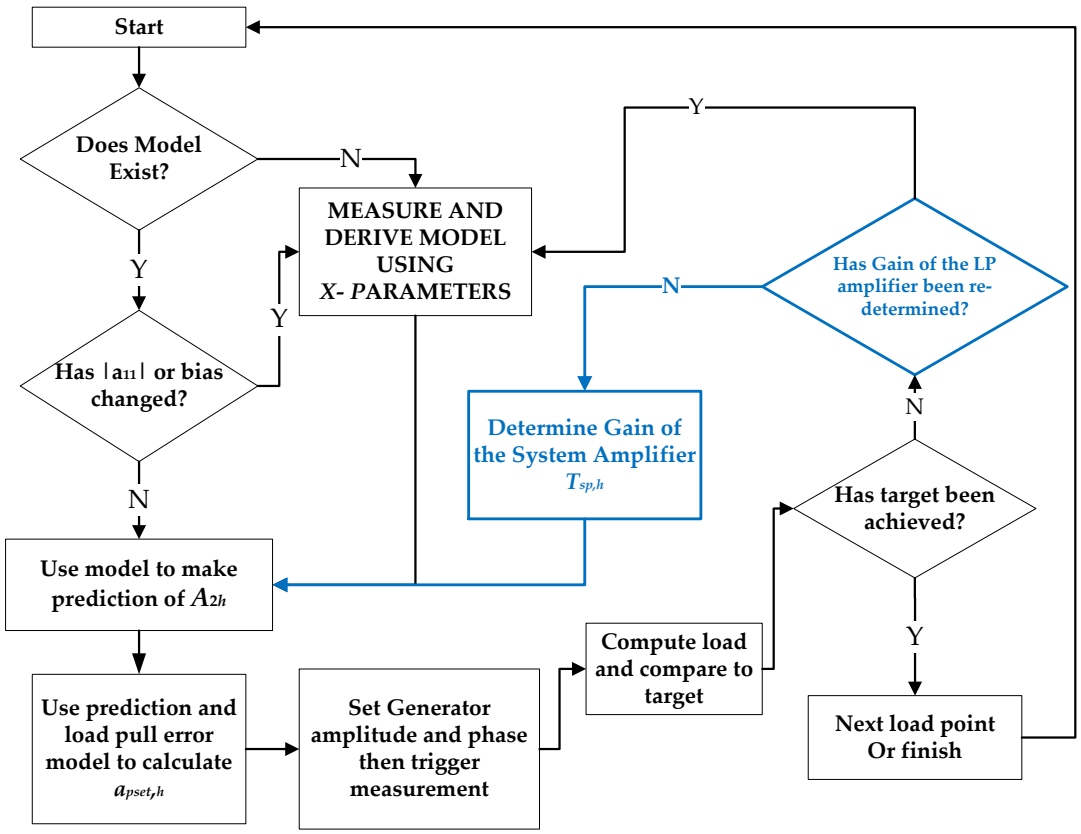

Figure 4-43: An improved LP Flow

This may trigger a fresh local model generation as the achieved gamma point may not be within the error tolerance. However the range of the model may still be valid and thus all that was required of the algorithm

was a refreshed determination of $T_{p,sh.}$ This determination however does not require an iterative step and can be calculated from the known values of $a_{pset,h}$. This check can be included in the flow graph described in Figure 4-37. The resulting flow chart is shown in Figure 4-43.

4.8 Summary

A discussion of the load-pull error model in open loop active load-pull measurement systems was used to examine the iterative nature of such a system. This was followed by discussions of the existing numerical techniques e.g. the Newton-Raphson technique used to compute the active load-pull signal required for load emulation and their associated problems. An illustration of the iterative system was carried out by load-pull measurements on a 10x75μm device running at 3 GHz. The utilisation efficiency of the system when using the Newton-Raphson numerical technique was found to be 31.5% hence the rest of the measurements were iterations to achieve load emulation targets.

As a solution to the above problem, a new approach was introduced which utilised the X-parameter formulations for carrying out load-pull predictions. A locally derived X-parameter model was shown to be capable of adding intelligence to an open loop active load-pull system. This approach enabled a significant improvement in the system's ability to provide the desired load emulation capability. The algorithm was also optimised to maximise the use of locally generated X-parameters. Hence the measurement system utilisation efficiency was greatly improved for realisation of the desired load conditions, with less than 5% error in the achieved load-impedances. For multi-variable sweeps such as power and load-pull sweeps, the algorithm proved to be very effective with utilisation efficiency of 90% for 700 load-pull target points.

Suggestions for an improved algorithm were also discussed whereby the local model generation and thus the redundant measurement step can be minimised by using an updated value of the gain of the system amplifier.

References

[1] R. S. Saini, S. Woodington, J. Lees, J. Benedikt, and P. J. Tasker,"An Intelligence driven active load-pull system," in Proc. 75th Microwave Measurements Conf. (ARFTG), pp. 1–4, May 2010.

[2] D. Williams, P. Hale, K. A. Remley, "The sampling oscilloscope as a microwave instrument," IEEE Microwave Mag., vol. 8, no. 4, pp. 59–68, Aug. 2007.

[3] Tasker, P.J, "Practical Waveform Engineering", Microwave Magazine, IEEE, Volume 10, Issue 7, pp 65-76, December 2009

[4] Williams D.J., "Non-linear Measurement System and Techniques for RF Power Amplifier Design", PhD Thesis Cardiff University 2003.

[5] C. Chapra, Raymond P. Canale, "Numerical methods for Engineers", 6-ed McGraw-Hill Higher Education (2010).

[6] Epperson, James F., "An Introduction to Numerical Methods and Analysis", Wiley 2002, pp 89

[7] Jan Verspecht, David E. Root, "Poly-harmonic Distortion Modeling", IEEE microwave magazine 1527-3342/06, June 2006.

[8] Jason Hom, Daniel Gunyan, Loren Betts, Chad Gillease, Jan Verspect, David E. Root, "Measurement-Based Large-Signal Simulation of Active Components from Automated Nonlinear Vector Network Analyzer Data via X-Parameters", COMCAS 2008,13-14 May 2008 Page(s):1 - 6, IEEE

Chapter 5 – High speed non-linear device characterisation and uniformity investigations exploiting behavioural models

5.1 Introduction

This chapter investigates a non-linear measurement approach suitable for wafer mapping and technology screening applications. It is shown how rapid characterisation and uniformity investigations of non-linear devices are possible through the use of an intelligence driven, open-loop active load-pull measurement system which uses localised behavioural models to improve speed of device characterisation and thus measurement system utilisation efficiency. The work in this chapter was presented by the author in [1].

At the present time, significant interest and effort has been devoted to the realisation of Monolithic Microwave Integrated Circuits (MMICs) for high power and high efficiency applications such as mobile telecommunications, radar and satellite communications [2]. Thorough

optimisation of transistor technology is thus required along with the availability of accurate CAD device models. An ideal CAD device model is one that describes transistor behaviour across the entire range of external terminal parameters such as DC bias, input drive and input/output VSWR. Traditionally, analytical modelling techniques are generally employed in developing foundry Process Design Kits (PDKs). These models, when used in large signal simulations, rely on the extrapolations of the DC and small signal measurements. While these extrapolations are successful in certain regions of large-signal operation, they fail in others. Experimental validation of the predicted behaviour of such a CAD model is thus required before the device can be used for MMIC design. Such an experimental validation is carried out via load-pull measurements, as explained in Chapters 2-4.

The constraint on measurement time is critical in non-linear device characterisation and therefore, parameters measured during load-pull are often focussed towards optimising key performance parameters such as optimum power, efficiency, gain etc. This is in contrast to more detailed device characterisation routines which involve extracting relevant non-linear parameters required for process optimisation. Therefore in addition to the evolution of measurement hardware new techniques for system control, analysis and modelling of measured large signal parameters are required if such measurement systems are to be utilised most efficiently.

5.2 Intelligence driven load-pull measurements

As described in Chapter 4, intelligence can be added to an open loop active load-pull load emulation process, thereby reducing the number of iterations required during such measurements. While capturing the desired device performance data, the load-pull system also incrementally built a database of localised X-parameter models which were archived and re-used. This proved beneficial when a "batch" of target load emulation points were measured over a large power sweep.

A more important consequence of the above technique is during a non-linear wafer mapping process. Moving from device to device or wafer to wafer, each captured set of local models can be used in rapidly attaining non-linear data under the same excitation conditions, making most efficient use of the measurement system and thus further minimising the need for iterative load-pull in the open-loop technique.

5.2.1 X-Band device comparison measurement strategy

High efficiency power amplifier modes of operation are governed by maximising DC-to-RF conversion. A deduction from the detailed consideration of the time-varying voltage *v(t)* and current *i(t)* waveforms shows that by driving the device hard into compression and presenting favourable impedances at the fundamental (e.g. the optimum impedance point for efficiency) and harmonic frequencies, designers can synthesize these waveforms for high efficiency modes of operation [3]-[6] e.g. Class-B, Class-F and Class F^{-1}.

Based on the above discussion, the load-pull impedance space required for comparison of devices and later on model generation was to be focused around the relevant optimum impedance emulation points such as for power and efficiency. The devices under test were four 10x75µm GaAs

pHEMT devices (named *D1, D2, D3, D4*) all operating in class-AB biasing conditions at 9 GHz. Initially, it was necessary to find the output fundamental impedance point which corresponded to the load for maximum power (Z_{opt}) for one of these devices. The approximate value of Z_{opt} can be predicted by using the Cripps' load technique which uses an estimation of the measured transfer characteristic of the DUT [7]. An alternative is to use a PDK model which, if available in CAD, can be configured with the same measurement conditions (e.g. bias, frequency and drive) as the load-pull characterisation to provide an initial estimate of Z_{opt}.

Using the latter approach, load-pull simulations on the PDK model were carried out in AWR Microwave Office Design Environment (AWRDE) with predicted power contours at the P-1dB compression point, highlighting the area of interest for the non-linear comparison analysis and model generation. These contours are shown in the Figure 5-44.

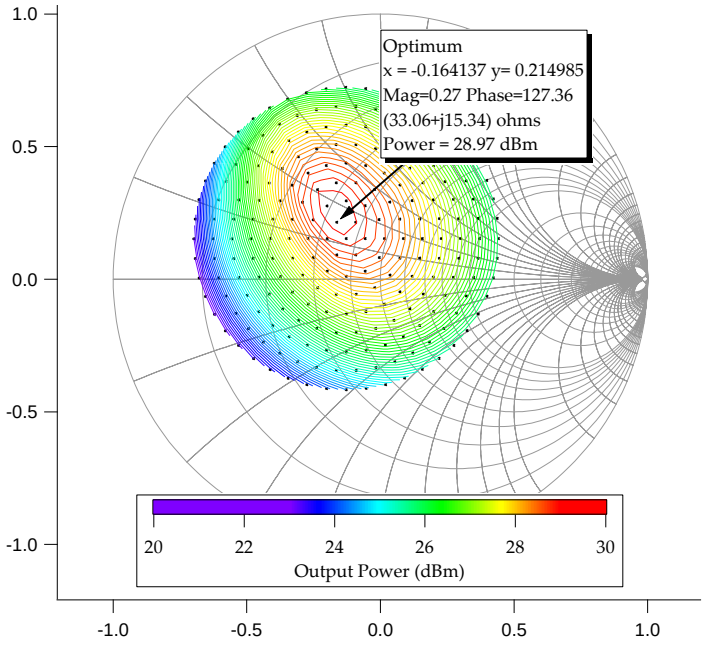

Figure 5-44: Predicted power contours achieved by carrying out load-pull on PDK using AWRDE

Applying the intelligence driven technique to active load-pull measurements, locally computed X-parameter models were used to aid the measurement of the above impedance space for the first device (*D1*).

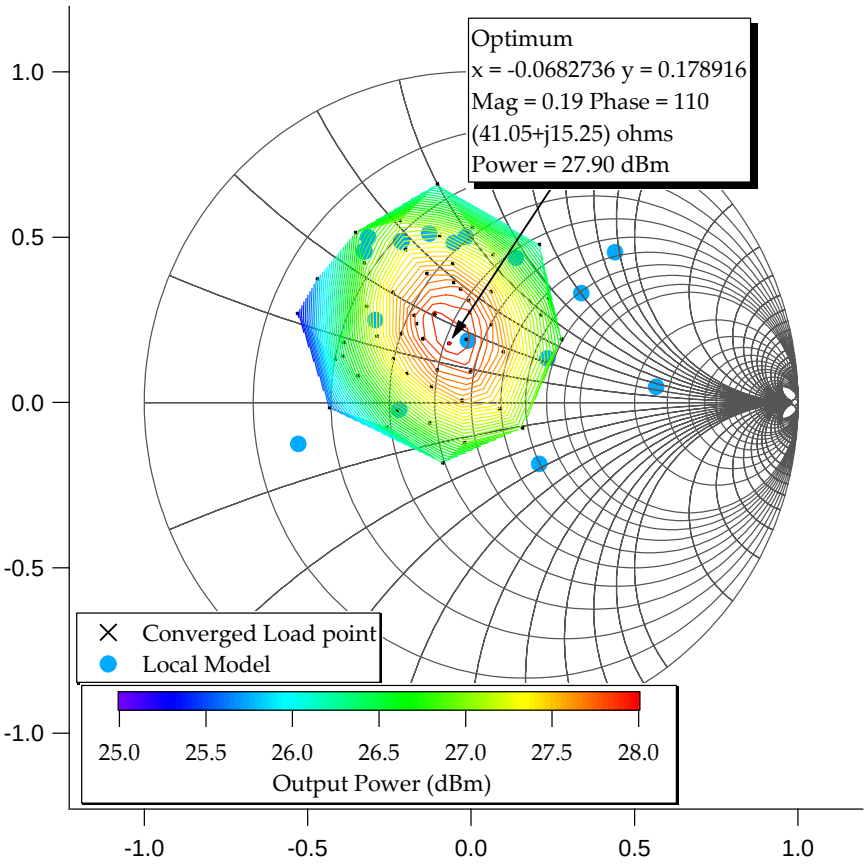

Figure 5-45: Measured power contours on device *D1*

The resulting power contours are shown in Figure 5-45, highlighting the points where the local model required an update. The convergence error tolerance for this load-pull grid was set to 6%. The measurement utilisation efficiency for this characterisation was 70%; requiring 12 local models to achieve the target grid. The characterisation time for the above was 30 minutes.

5.2.2 Optimising the use of measurement conditions

In order to further improve the utilisation efficiency and taking note of the fact that all DUTs to be compared are of the same device technology and geometry (10x75 GaAs PHEMTs), there were two options to be considered.

i. For all subsequent device measurements, the local models can be re-used from the characterisation of device *D1* to speed up the load pull process.

ii. The measurement stimulus (A_{11}, A_{21}, V_{ds}, V_{gs} and fundamental frequency) archived for converged load impedances in the characterisation of *D1* can be re-used for all subsequent device to device measurements.

As a consequence of ii), no further iterations nor local model generation is necessary in the device comparison process, thus potentially improving the measurement system utilisation efficiency to 100% for all subsequent load pull measurement sequences.

5.2.3 Summary of measurement results

Table 5-2 is a summary of the comparison measurements, showing the variation in output power and optimum impedance for maximum power ($\boldsymbol{Z}_{OPT}$). It can be seen from these results that the position of $\boldsymbol{Z}_{OPT}$ is very similar for these devices (Real: 41.2 ± 0.5 Ω and imaginary: 16.0 ± 2 Ω). The variation in output power was 28.0 ± 0.3dBm. There is however a notable 0.8 dB offset between the measurement results and the predictions from the PDK analytical model.

Device	Max. Power (dBm)	Z_{OPT} (Ω)	Z_{IN} (Ω)	Time (min)
PDK Model	28.90	33.06 + j15.34	4.66 - j9.00	--
D1	27.90	41.05 + j15.25	4.94 - j10.00	30

D2	28.23	41.73 + j16.16	4.21 - j12.23	7
D3	28.03	41.52 + j16.68	4.16 - j12.58	7
D4	27.75	41.50 + j17.33	4.36 - j13.22	7

Table 5-2: Comparison of device measurements

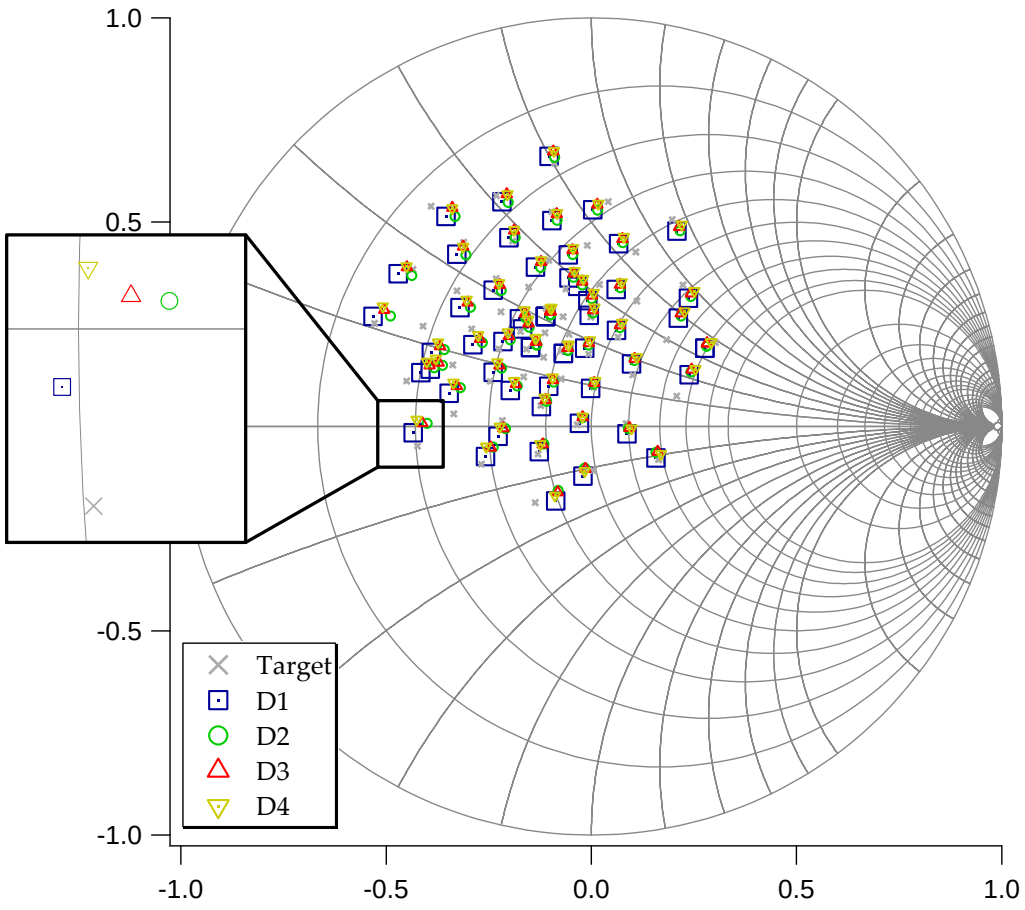

Figure 5-46: Results from measuring all 4 DUTs with the same stimuli as device *D1*

By using the archived set of measurement stimulus, the characterisation time required to achieve the target load emulation points for all subsequent devices was 7 minutes (23% of the original time taken). Figure 5-46 shows results of applying the same stimuli on all the other DUTs (*D2*, *D3*, and *D4*). As shown in the figure, a consequence of this approach is that device to device variation has caused a small scatter in the measurement impedance locations.

5.3 Model generation for use in CAD tools

Once the device measurements were complete, the next task was to archive the device-to-device behaviour in a format that is elegant for CAD use. For the above experiment, two main techniques were considered:

i. Data look-up models
ii. Behavioural models

In a data look-up model e.g. Cardiff DWLUT model [8], there are various disadvantages. First of all, as discussed in Chapter 3, the data collected is not truly a model i.e. it is only valid in the region that it was measured. Any interpolation or extrapolation is entirely left to the robustness of the CAD simulator. A more critical point is that the data is required to be placed on a *standard grid* thus the scatter created by device variations requires additional mathematical processing so that all the device look-up tables are represented by the same impedance grid. Finally, data mining is required to quantify device-to-device or wafer-to-wafer variations based on variables such as output power, efficiency etc.

In behavioural models e.g. Cardiff Behavioural Model [9], the measured data is transformed into an equivalent set of coefficients grouped by parameters such as frequency, temperature, bias and input drive. Using such a modelling technique,

i) Multiple models based on random look-up can account for device-to-device variations
ii) The model can incorporate these variations in the extracted coefficient space

5.3.1 Cardiff Behavioural model extraction

For each of the devices, a fundamental behavioural model based on the technique in [9] and discussed in the literature review of Chapter 3 was extracted. The generalised equation for a fundamental model using this technique is shown in (5-1). A 6-term behavioural model was extracted from the measurement data via a Least Means Squares (LMS) function. The coefficient set used is shown in Figure 5-47.

$$B_{p,h} = P_1^h \cdot \left(\sum_{m=-(w-1)/2}^{m=+(w+1)/2} K_{p,h,m} \left(Q_1 / P_1 \right)^m \right) \qquad K_{p,h,m} = g\left(V_{1,0}, \left|A_{1,1}\right|, V_{2,0}, \left|A_{2,1}\right| \right)$$

$$\text{Whereby} \quad P_1 = \angle A_{1,1} = \frac{A_{1.1}}{\left|A_{1,1}\right|} \qquad Q_1 = \angle A_{2,1} = \frac{A_{2.1}}{\left|A_{2,1}\right|}$$

(5-1)

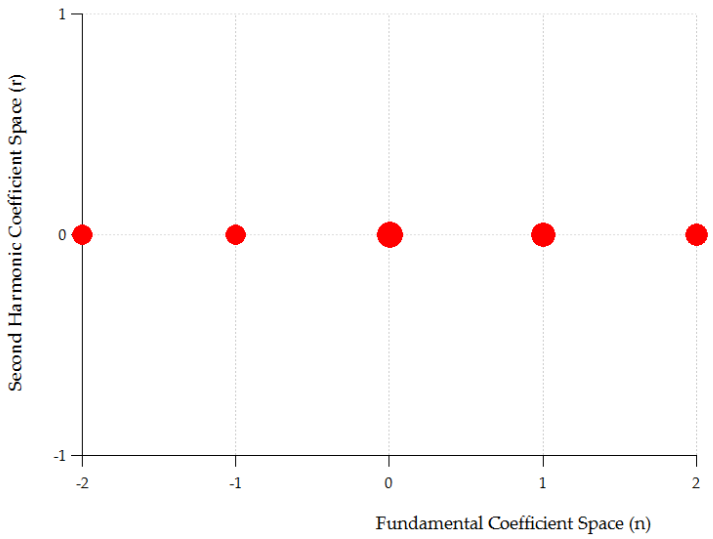

Figure 5-47: Coefficient set used in parameter extraction

5.3.2 Model verification

Using the same measurement stimulus e.g. input power, bias and frequency, the response from the generated model for device *D1* when compared to the original measurement data was used to verify accuracy in the parameterised approach. Table 5-3 shows a summary of the error in the response at each harmonic for this verification. From the results it can be seen that for the fundamental model, the average model accuracy is based on measured and modelled b_{21} waves is 99.8%. The Smith chart in Figure 5-48 shows this prediction in terms of fundamental (F0) and second harmonic (2F0) gamma.

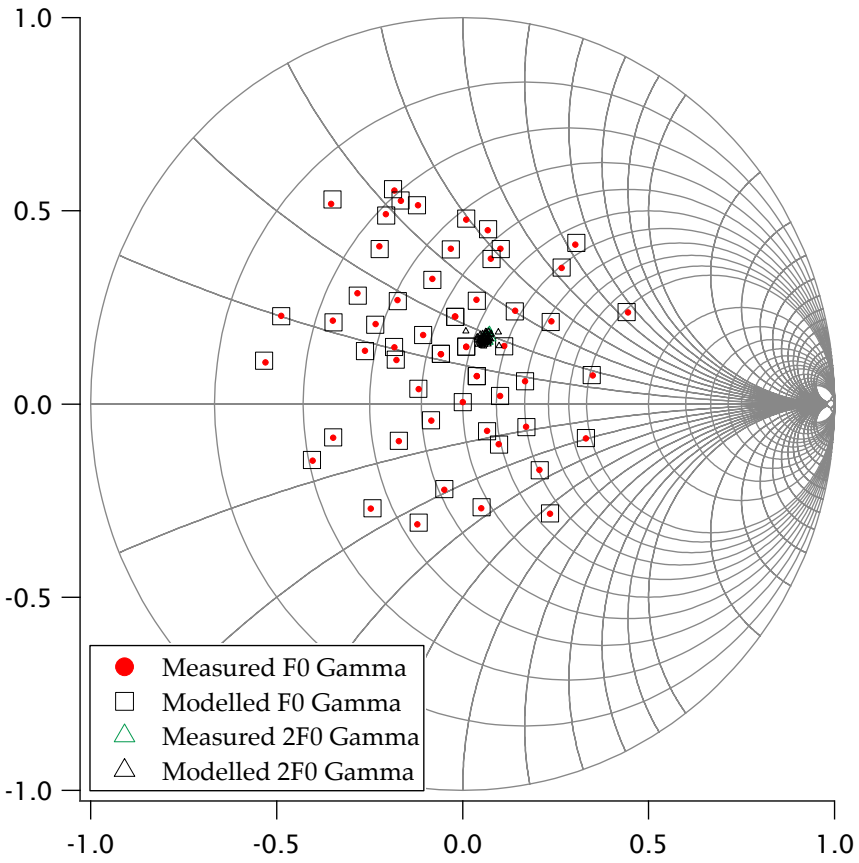

Figure 5-48: Model coefficients applied on entire dataset

Variable	Min Error (%)	Max Error (%)	Average Error (%)
b_{21}	0.0064	0.59	0.19
b_{22}	0.05	2.08	0.64
b_{23}	0.08	7.12	1.83
b_{12}	0.005	1.87	0.44
b_{13}	0.02	5.8	1.38

Table 5-3: Verification of parameterised model for device D1

5.3.3 Usage and validation in CAD

The model coefficients for each device were imported into AWR Microwave Office Design Environment (AWRDE) via its APLAC simulator interface [10]. Simulations were run using the Frequency Domain Device component (FDD). A load-pull simulation in AWRDE is shown in Figure 5-49 whereby the DUT has been setup as a net list which imports the Cardiff model file. It features a harmonic balance tuner which can set impedances at the fundamental and harmonics. The simulation was automated via a script to emulate load pull functionality such as target load impedances, bias points, frequency and input power. A total of 780 load-pull target emulation points were chosen for the fundamental sweep plan.

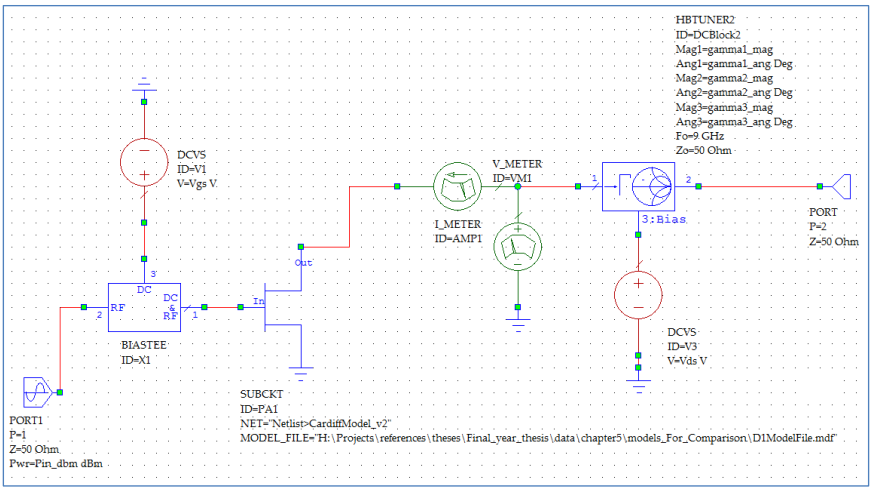

Figure 5-49: Load-pull simulations in AWRDE

Results from the simulation showed good agreement between measured and modelled power contours as shown in Figure 5-50.

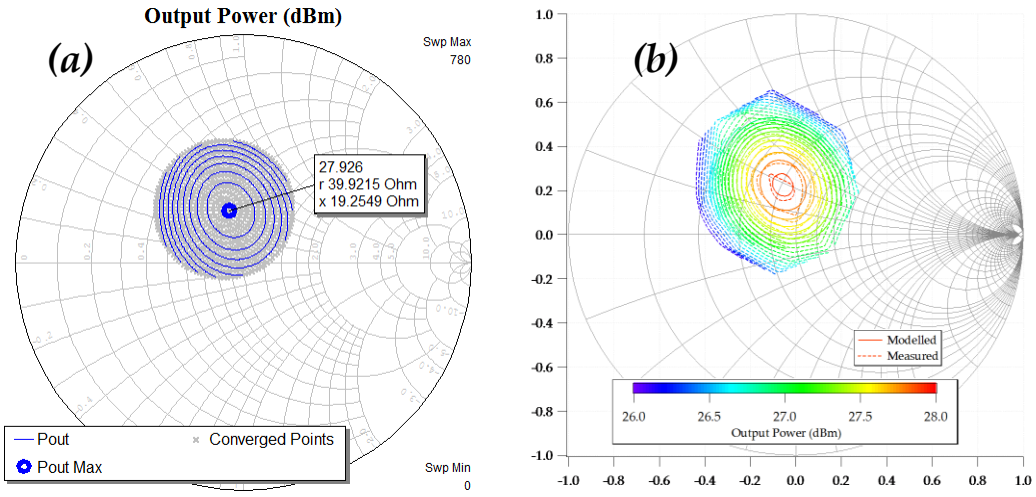

Figure 5-50: (a) Output from AWRDE load-pull simulation. (b) Comparison of load-pull simulation and measurement data on device D1

The optimum impedance (Z_{OPT}) from the simulation was (39.9+j19.25) ohms and the maximum output power was 27.92dBm. When compared to the measurement results on device D1, the output power accuracy was ±0.02dB. The position of Z_{OPT} also showed a similar position (Real: 41 ± 1Ω, Imaginary: 16 ± 3Ω). More importantly, the extracted coefficients guided the simulator to achieve an accurate interpolation. A comparison of the output power contours near the optimum impedance is shown in Figure 5-51 whereby the measured gamma points used in the model extraction are marked by (X). The simulated gamma points, as interpolated by model coefficients, are marked by (o).

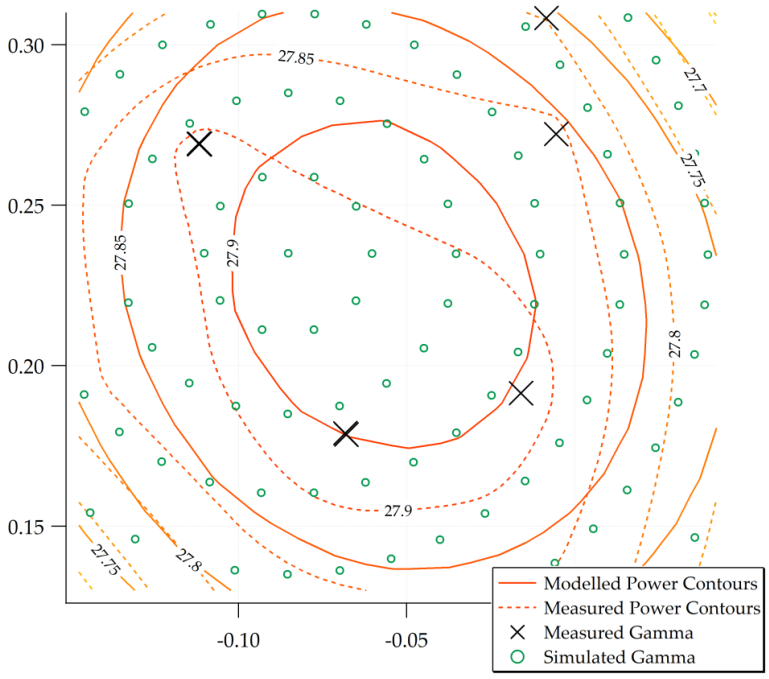

Figure 5-51: Power contours and gamma distribution around the optimum

Comparing the two contours, a *pulling* effect was noticed on the model contours. It has to be noted that this is an effect caused by the interpolation algorithm run by the plotting software and the coefficients extracted by the model are able to capture the optimal performance space accurately.

When plotting raw measurement data, this *pulling* effect on the values close to Z_{OPT} can be corrected-for by including more measurement data points around this region in the device measurements. Since the work presented in this technique is based on re-generating performance using the extracted coefficients within the simulator rather than raw data, the significance of the *pulling* effect can be ignored. Table 5-4 shows the measured and simulated results from all the device models D1-D4. The agreement between measurements and simulations is to accuracy of ± 0.02dB.

Device	**Power (dBm) Meas.**	**Power (dBm) Sim.**	**Z_{OPT} (Ω) Meas.**	**Z_{OPT} (Ω) Sim.**
PDK Model	--	28.90	33.06 + j15.34	
D1	27.90	27.92	41.05 + j15.25	39.92 + j19.25
D2	28.23	28.20	41.73 + j16.16	38.81 + j18.70
D3	28.03	28.01	41.52 + j16.68	39.90+j19.92
D4	27.75	27.78	41.50 + j17.33	38.29 + j22.55

Table 5-4: Comparison of measured and simulated performance for all devices

5.4 Analysis and application of model coefficients

The elegance of the above technique allows comparison and archiving of extracted model in a similar way to s-parameters [11]. The above technique involved generating a parameterised behavioural model containing 6 coefficients, as shown in (5-2):

$$\frac{b_{2,1}}{P_1} = K_{2,1,-2,2}\left(a_{2,1}{}^*\right)^2 + K_{2,1,-1,1}\left(a_{2,1}{}^*\right) + K_{2,1,0,0}\left(\left|a_{2,1}\right|\right)^0 + K_{2,1,1,1}\left(a_{2,1}\right) + K_{2,1,0,2}\left(\left|a_{2,1}\right|\right)^2 + K_{2,1,2,2}\left(a_{2,1}\right)^2 \quad (5\text{-}2)$$

A comparison of these model coefficients is illustrated in Table 5-5:

Coeff Number	**D1 Mag**	**D1 Phase**	**D2 Mag**	**D2 Phase**	**D3 Mag**	**D3 Phase**	**D4 Mag**	**D4 Phase**
0	39.58	64.58	39.77	54.29	38.47	54.32	38.62	51.14
1	20.56	-113.60	19.73	-126.48	18.36	-125.65	18.53	-131.92
2	28.11	-95.73	28.07	-114.68	26.71	-114.92	26.56	-114.71
3	6.58	-123.30	5.21	-110.32	5.47	-106.54	5.10	-120.54
4	21.66	35.98	23.63	6.60	22.43	4.96	22.29	1.58
5	9.47	-136.28	8.87	-164.78	7.97	-173.19	7.95	-169.32
6	15.79	17.45	15.60	18.72	14.17	19.75	13.95	23.24
7	10.88	161.47	7.78	107.38	6.36	118.39	6.27	122.85
8	-30.74	24.53	-30.80	47.97	-29.50	41.22	-29.69	54.12

Table 5-5: Comparison of magnitude and phase of coefficients

An example application of using coefficients within CAD is shown in Figure 5-52 which shows simulated time-domain waveforms for each of the device models, computed about the same impedance point. Each of these parameterised models can therefore be utilised within the CAD tool for circuit design, optimisation and sensitivity analysis.

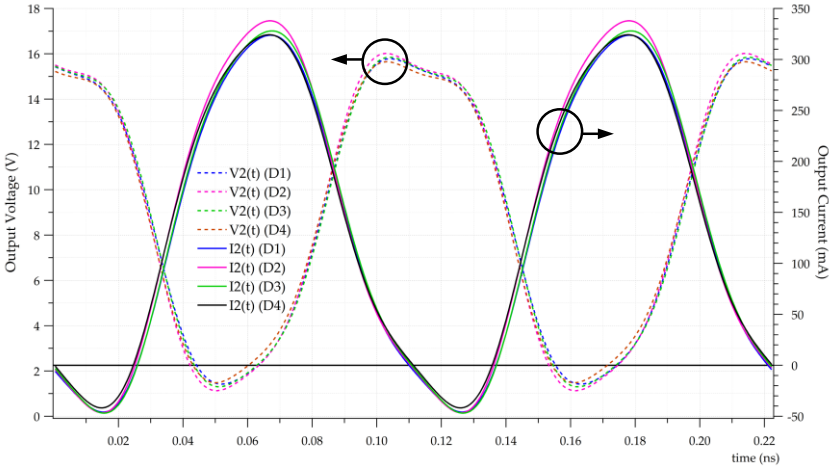

Figure 5-52: Simulated time-domain waveforms

5.5 Chapter Summary

This chapter discussed a rapid characterisation and uniformity investigation technique for measurement of non-linear devices through the use of an intelligence driven, open-loop active load-pull measurement system. The necessary improvement in measurement speed was achieved by improving the utilisation efficiency of the measurement system in two ways. Initially, locally computed X-parameters guide the active load pull system thus minimising iterations required to set the desired impedances. Simultaneously to this process, the locally computed models as well as the open-loop settings were archived. These settings were then recalled, eliminating the need for iterative load-pull and thus significantly reducing measurement time.

In order to demonstrate the procedure, a batch of 4 10x75 μm GaAs devices was measured at 9GHz. For the first device (*D1*), locally computed X-parameter models guided the load-pull measurements and achieved a target grid of 58 points in 30 minutes. Each of the remaining devices (*D2-D4*) utilised the archived open loop settings from the characterisation of *D1* to complete the same load-pull grid within 7 minutes. The four devices showed very similar characteristics in output power (28.0 ± 0.3dBm). There was however a notable 0.8 dB offset between the measurement results and the predictions from the PDK analytical model.

For exploitation within CAD tools, these load-pull measurements were used to create a 6-term parameterised behavioural model based on Cardiff Model formulations. The verification on simulation data showed a very good agreement between measurements and model accuracy. The output power was noted to be within ±0.02 dB for each of the devices. Each of these parameterised models could therefore be utilised within the CAD tool for circuit design, optimisation as well as yield analysis.

An application of this was demonstrated by simulating time-domain waveforms for each of the device models, computed about the same impedance point.

References

[1] Saini, R.S.; Bell, J.W.; Canning, T.A.J.; Woodington, S.P.; FitzPatrick, D.; Lees, J.; Benedikt, J.; Tasker, P.J.; , "High speed non-linear device characterization and uniformity investigations at X-band frequencies exploiting behavioral models," Microwave Measurement Conference (ARFTG), 2011 77th ARFTG , vol., no., pp.1-4, 10-10 June 2011

[2] Powell, J.R.; Uren, M.J.; Martin, T.; McLachlan, A.; Tasker, P.; Woodington, S.; Bell, J.; Saini, R.; Benedikt, J.; Cripps, S.C.; , "GaAs X-band high efficiency (>65%) Broadband (>30%) amplifier MMIC based on the Class B to Class J continuum," Microwave Symposium Digest (MTT), 2011 IEEE MTT-S International , vol., no., pp.1-4, 5-10 June 2011

[3] P. Wright, A. Sheikh, C. Roff, P. J. Tasker, and J. Benedikt, "Highly efficient operation modes in GaN power transistors delivering upwards of 81% efficiency and 12W output power," in IEEE MTT-S Int. Microwave Symp. Dig., June 15–20, 2008, pp. 1147–1150.

[4] P. Wright, J. Lee, P. J. Tasker, J. Benedikt, and S. C. Cripps, "An efficient, linear, broadband class-J-mode PA realised using RF waveform engineering," in IEEE MTT-S Int. Microwave Symp. Dig., June 2009, pp. 653–656.

[5] S. C. Cripps, P. J. Tasker, A. L. Clarke, J. Lees, and J. Benedikt, "A New General Formulation for High Efficiency R.F. Amplifiers," IEEE Microwave Wireless Compon. Lett., Oct. 2009.

[6] M. Sipilä, K. Lethinen, and V. Porra, "High-frequency periodic time-domain waveform measurement system," IEEE Trans. Microwave Theory Tech., vol. 36, no. 10, pp.1397–1405, Oct. 1988.

[7] S. C. Cripps, "RF Power Amplifiers for Wireless Communications," Norwood, MA: Artech House, 1999.

[8] Qi, H.; Benedikt, J.; Tasker, P.; , "Direct extraction of large-signal table-based behavioural models from time-domain voltage and current waveforms," High Frequency Postgraduate Student Colloquium, 2005

[9] Woodington, S. P.; Saini, R. S.; Willams, D.; Lees, J.; Benedikt, J.; Tasker, P. J.; , "Behavioral model analysis of active harmonic load-pull measurements," Microwave Symposium Digest (MTT), 2010 IEEE MTT-S International, vol., no., pp.1, 23-28 May 2010

[10] Online: http://www.awrcorp.com/products/innovative-technologies/aplac [Accessed 22-Nov-12]

[11] Online: http://cp.literature.agilent.com/litweb/pdf/5965-7742E.pdf [Accessed 12-Jan-13]

Chapter 6 – Interpolation and Extrapolation Capabilities of Non-Linear Behavioural Models

6.1 Introduction

This chapter describes how an application of the Poly Harmonic Distortion (PHD) modelling framework, the Cardiff Behavioural model [1], is effective in its ability to interpolate or extrapolate non-linear measurement data and thereby improve the quality and speed of measurement systems. The analysis included testing the interpolation capability of a fundamental-only model. This was followed by using measurement data to examine the extrapolation and interpolation capabilities of a second harmonic model. The work in this chapter was presented by the author in [2].

As discussed in Chapter 2, load-pull is the direct measurement of key non-linear performance parameters such as output power, gain, efficiency and linearity as a function of load impedance, input drive, frequency, bias and temperature. With the rise in demand for system requirements, PA designers have to seek high efficiency modes of operation

e.g. Class-F, Class-J, Class F^{-1} [3]-[4]. As a consequence of the requirements to achieve such modes, precision in setting very specific impedance terminations at the fundamental and harmonic tones is required. This process is iterative and often leads to time-consuming measurements due to the number of tune-able variables. A fast and efficient non-linear measurement system is therefore critical for such a PA design lifecycle.

The various commercially available techniques for achieving fundamental and harmonic load-pull all have their benefits and short-comings. In passive systems [5]-[6], the more commonly available solution, mechanical stub tuners are used to achieve the desired impedance. Multiple stub tuners are also available for simultaneous fundamental and harmonic load-pull. The losses inherent in these systems mean that the available coverage of the impedance plane is limited and practically achieving high gamma terminations (typically $|\Gamma| > 0.9$) is very difficult or impossible. Active load-pull systems [7] are able to overcome these losses by amplifying the injected wave hence allowing unrestricted coverage of the smith-chart. As discussed in Chapter 2 and 4, they are prone to an iterative loop leading to a longer measurement time.

Previous work based on the Cardiff Behavioural model has shown that by considering higher order mixing terms in the PHD formulation, a model can be developed which is globally accurate over a range of fundamental and harmonic impedance points. Such a model can also be utilised to improve the quality and speed of measurements as well as the ability to overcome limitations of load-pull systems discussed above.

Interpolation carried out on measurement data can reduce the density of impedance grids hence reducing measurement time. Load-pull systems that cannot achieve a high enough impedance termination at higher harmonics can take advantage of harmonic extrapolation to achieve

these values. In this chapter, the benefits of the Cardiff Behavioural model will be demonstrated in various ways:

i) Interpolation accuracy of a fundamental load-pull grid

ii) Interpolation and extrapolation accuracy of the second harmonic load-pull grid.

Model generation analysis carried out in this chapter was achieved using custom-written software developed by the author using Microsoft C#. A description of this software is attached in Appendix B.

6.2 Cardiff Behavioural Modelling formulations

As shown in Chapter 3, an equivalent Fourier series description of the measured behaviour of a DUT (6-1) can be described whereby the coefficients $K_{p,h,m}$ and the necessary mixing order, ω can be determined via a least-squares fit of all the measurement data (6-2).

$$B_{2,1} = P_1 . g\left(V_{1,0}, \left|a_{1,1}\right|, V_{2,0}, \left|a_{2,1}\right|, Q_1 \middle/ P_1 \right)$$

whereby

$$P_1 = \angle a_{1,1} = \frac{a_{1.1}}{\left|a_{1,1}\right|}$$

$$Q_1 = \angle a_{2,1} = \frac{a_{2.1}}{\left|a_{2,1}\right|}$$

(6-1)

$$B_{p,h} = P_1^h . \left(\sum_{x=0}^{x=m} \sum_{m=-(\omega-1)/2}^{m=+(\omega+1)/2} K_{p,h,m,x} \left(Q_1 \middle/ P_1 \right)^m \left(\left| a_{p,h} \right| \right)^x \right)$$

whereby

$$K_{p,h,m} = g\left(V_{1,0}, \left|a_{1,1}\right|, V_{2,0} \right)$$

h = harmonic index, p = port index

m = phase index,

x = magnitude index

(6-2)

A further reduction in the complexity of (6-2) can be achieved as shown in (6-3). This includes variation of the coefficients $K_{p,h,m}$ as a function of the measured fundamental gamma $\Gamma_{2,1.}$ Fundamental load interpolation can be achieved by this simplified equation, due to its ability to interpolate in both polar co-ordinates (i.e. magnitude $|\Gamma_{2,1}|$ and phase Q_1/P_1).

$$B_{p,h} = P_1^h \cdot \left(\sum_{x=|m|}^{x=|m|+2q} M_{p,h,m,x} \left(\left| \Gamma_{2,1} \right| \right)^x \right)$$

whereby

m = phase index

x = magnitude index

(6-3)

6.3 X-Band measurements for fundamental and harmonic analysis

Open-loop active load-pull measurements for these investigations were carried out on a 0.5W 10x75µm GaAs PHEMT device, operating at 9GHz and biased in Class-B conditions. The device was measured at the P-2dB compression point for the entire analysis. The X-Band harmonic load-pull and source-pull measurement system utilised for this objective was developed at Cardiff University [8] and discussed in Chapter 2. In order to achieve the desired open-loop load-pull control at X-Band frequencies, the system featured a number of modifications:

i) The MTA receiver in [8] was replaced by a 4-channel Tektronix DSA8200 sampling oscilloscope [9]. This contained sampling modules with an electrical bandwidth of DC-70GHz. The unit also contained *remote* samplers which could be mounted directly onto the measurement couplers to reduce losses in cables and to achieve an accurate calibration.

ii) At X-band and higher frequencies, controlling the harmonic signals actively with just a 10MHz lock created significant drift in phase. Thus achieving active control at harmonic frequencies e.g. 18GHz was very difficult. A coherent carrier distribution system was therefore realised, as described in [10].

A schematic of the X-band system is shown in Figure 6-53. The entire system was automated using custom written software, written by the author in Microsoft C# as described in Appendix A.

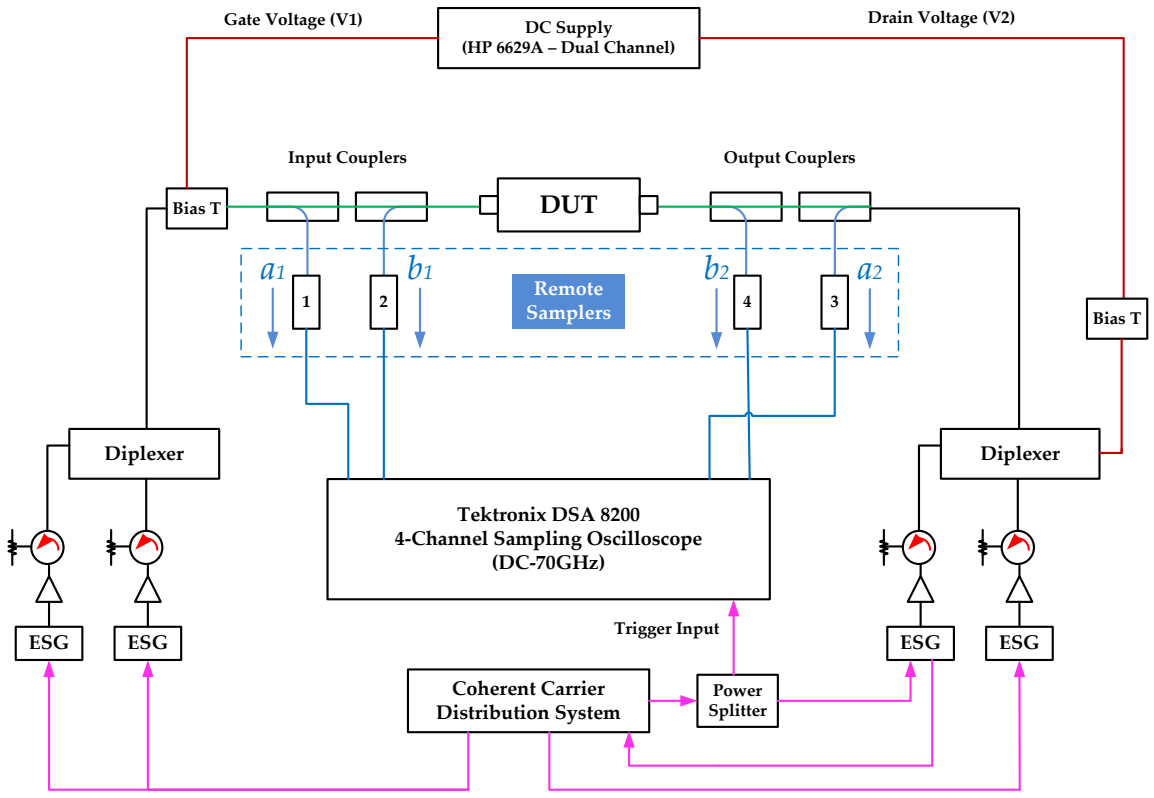

Figure 6-53: X-Band harmonic load-pull measurement system setup

6.4 Fundamental load-pull interpolation analysis

In order to investigate the quality of interpolation for the fundamental grid, various sets of fundamental gamma (Γ_{21}) were measured. Theoretically, the minimum number of measurements required for the least-squares algorithm to extract i coefficients is i measurements. In order to allow for inaccuracies in the practical measurement scenario and for redundancy in the measurement, 2*i measurements can be considered as a recommended minimum set. The target emulation grid, with 56 points, was centred on the device optimum gamma for maximum output power (Γ_{OPT}). All higher harmonics e.g. 2-F0 were held constant at 50 ohms. Throughout this analysis, the fundamental frequency, bias and drive level were held constant. Once the measurements were complete, the measured gamma points were grouped-by and contained within datasets of the measured output power contours in 0.5dB steps up-to 3.5dB from the optimum. This measurement result is shown in Figure 6-54.

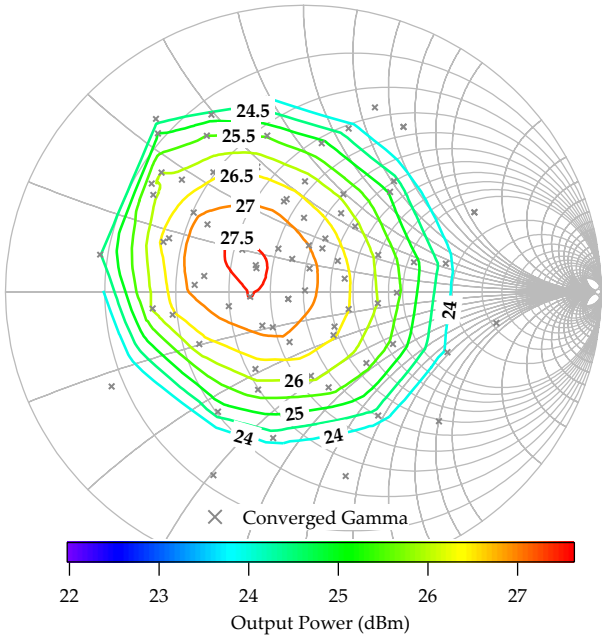

Figure 6-54: Gamma points grouped-by and contained within datasets of the measured output power contours (0.5 dB steps)

6.4.1 Model generation and analysis

Behavioural models of increasing order, defined by changing ω in (6-2) were used to capture the non-linear behaviour for each of these gamma subsets.

Table 6-6 shows the resulting polynomial equations for the calculation of the response signal, $b_{2,1}$ using each of these model coefficient sets.

Coefficients	Equation
3	$\frac{b_{2,1}}{P_1} = K_{2,1,-1,1}\left(a_{2,1}^{*}\right) + K_{2,1,0,0}\left(\left\|a_{2,1}\right\|\right)^0 + K_{2,1,1,1}\left(a_{2,1}\right)$
4	$\frac{b_{2,1}}{P_1} = K_{2,1,-1,1}\left(a_{2,1}^{*}\right) + K_{2,1,0,0}\left(\left\|a_{2,1}\right\|\right)^0 + K_{2,1,1,1}\left(a_{2,1}\right) + K_{2,1,0,2}\left(\left\|a_{2,1}\right\|\right)^2$
6	$\frac{b_{2,1}}{P_1} = K_{2,1,-2,2}\left(a_{2,1}^{*}\right)^2 + K_{2,1,-1,1}\left(a_{2,1}^{*}\right) + K_{2,1,0,0}\left(\left\|a_{2,1}\right\|\right)^0 + K_{2,1,1,1}\left(a_{2,1}\right) + K_{2,1,0,2}\left(\left\|a_{2,1}\right\|\right)^2 + K_{2,1,2,2}\left(a_{2,1}\right)^2$
7	$\frac{b_{2,1}}{P_1} = K_{2,1,-2,2}\left(a_{2,1}^{*}\right)^2 + K_{2,1,-1,1}\left(a_{2,1}^{*}\right) + K_{2,1,0,0}\left(\left\|a_{2,1}\right\|\right)^0 + K_{2,1,1,1}\left(a_{2,1}\right) + K_{2,1,0,2}\left(\left\|a_{2,1}\right\|\right)^2 + K_{2,1,2,2}\left(a_{2,1}\right)^2 + K_{2,1,0,3}\left(\left\|a_{2,1}\right\|\right)^3$
8	$\frac{b_{2,1}}{P_1} = K_{2,1,-2,2}\left(a_{2,1}^{*}\right)^2 + K_{2,1,-1,1}\left(a_{2,1}^{*}\right) + K_{2,1,0,0}\left(\left\|a_{2,1}\right\|\right)^0 + K_{2,1,1,1}\left(a_{2,1}\right) + K_{2,1,0,2}\left(\left\|a_{2,1}\right\|\right)^2 + K_{2,1,2,2}\left(a_{2,1}\right)^2 + K_{2,1,0,3}\left(\left\|a_{2,1}\right\|\right)^3 + K_{2,1,3,3}\left(a_{2,1}\right)^3$

Table 6-6: Description of each coefficient set

Results from this analysis are shown in Figure 6-55, comparing the error in re-generating b_{21} with the varying model complexity. The error function used in this calculation is shown in the equation (6-4) below.

$$Errb_{p,h} = \frac{\left(\left|b_{p,h,meas}\right| - \left|b_{p,h,mdel}\right|\right)}{\left|b_{p,h,meas}\right|} * 100\% \qquad (6\text{-}4)$$

From the figure, it can be seen that the model complexity required to accurately capture impedances local to the optimum (within 0.5dB) requires a polynomial with only 3 model coefficients. However, in order to accurately capture the design space defined by the entire fundamental grid (0.5-3.5dB) a higher-order polynomial is required (6-8 coefficients).

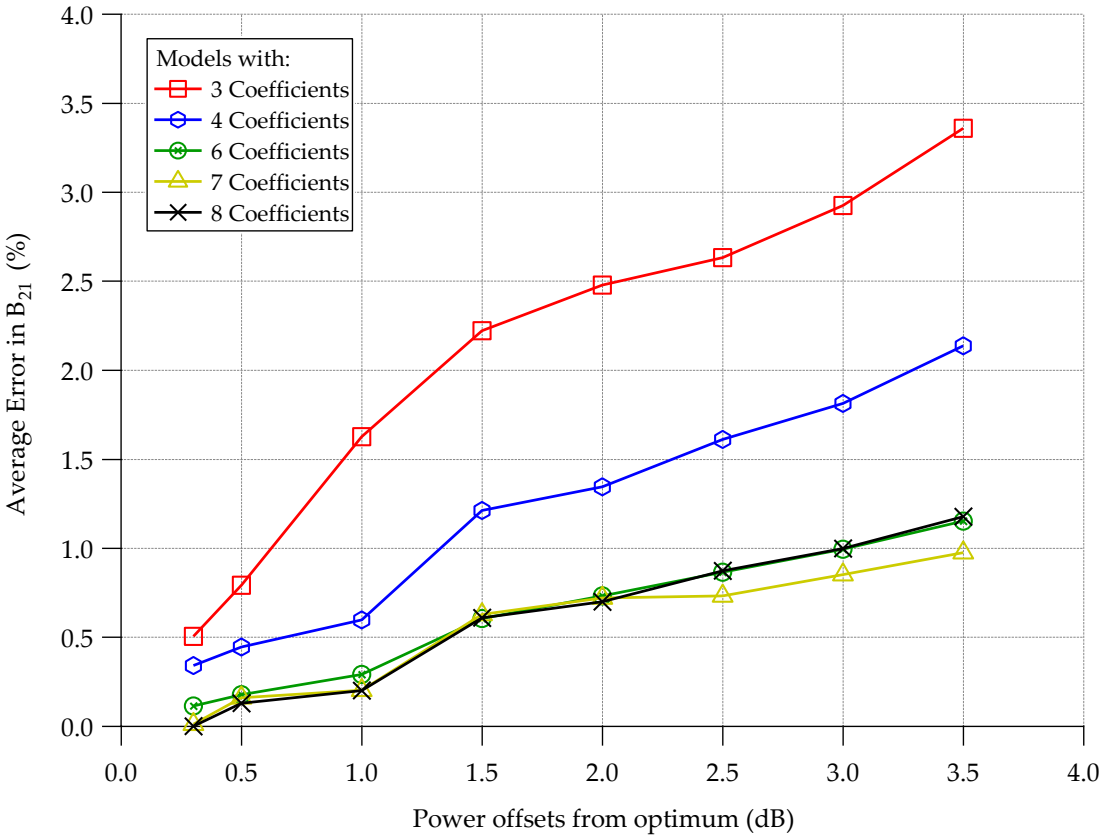

Figure 6-55: Error in B_{21} with increasing model complexity

6.4.2 Sensitivity analysis

An analysis was carried out on conjugate coefficient term ($K_{2,1,-1,1}(a_{2,1}^*)$) in order to determine its accuracy at each level of the power contour. Three data sets of the magnitude of this term were plotted against the power offsets from the optimum. The first was extracted from a model which contained only 3 coefficients, the second with 6 coefficients and the third with 7 coefficients. A comparison of the magnitude of this term in each of the coefficient sets confirms the findings in the above experiment. Very

close to the optimum i.e. near the 0.5dB power contour, the magnitude of the coefficient as calculated in each of the sets is very similar (±0.1 dB). Going further away from this point indicates divergence in this magnitude value (±0.5 dB) in a similar way to the error graph shown in Figure 6-55 above. This behaviour is shown in Figure 6-56.

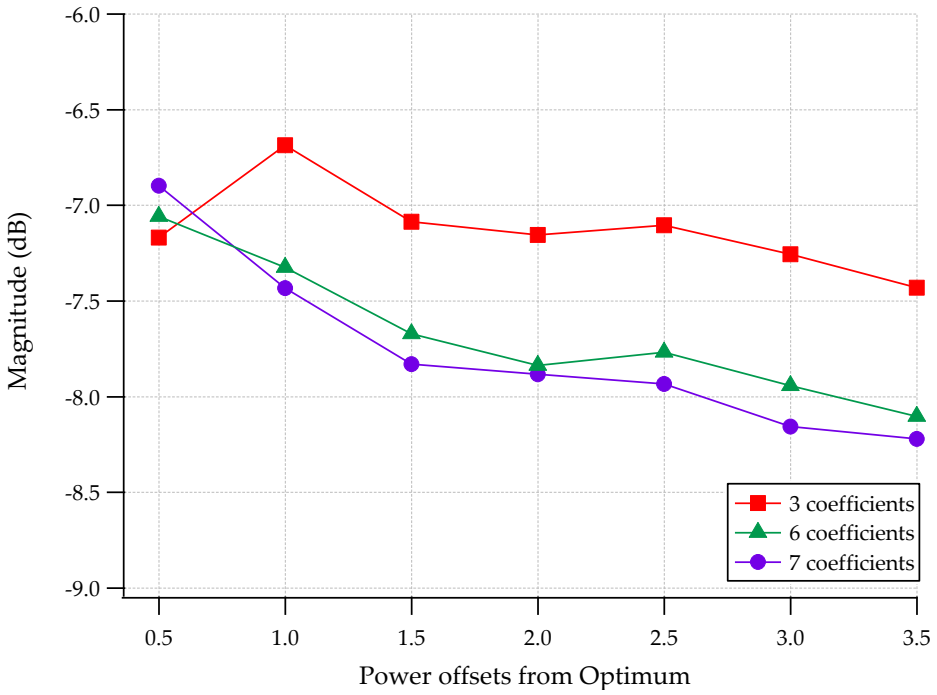

Figure 6-56: Sensitivity analysis on the magnitude of $K_{2,1,-1,1}(a_{2,1}^*)$

6.4.3 Application of Fundamental interpolation for Load-refitting

Applying the above findings, fundamental load interpolation was demonstrated practically via two sets of measured load-pull grids (see Figure 6-57). The first set (a); contained a *fine* distribution and second (b); with a *sparse* distribution of gamma emulation targets. In the first case, a grid of 100 points (*fine*) was measured around the optimum of the device. In the second case, a grid of 15 points (*sparse*) was measured in the same region. Fundamental frequency, bias conditions and drive level were held constant for both measurements.

Data collected from measurements on the sparse grid was then used to extract a behavioural model suitable for load-refitting using (6-3). The resulting polynomial is shown in (6-5); using 7 model coefficients.

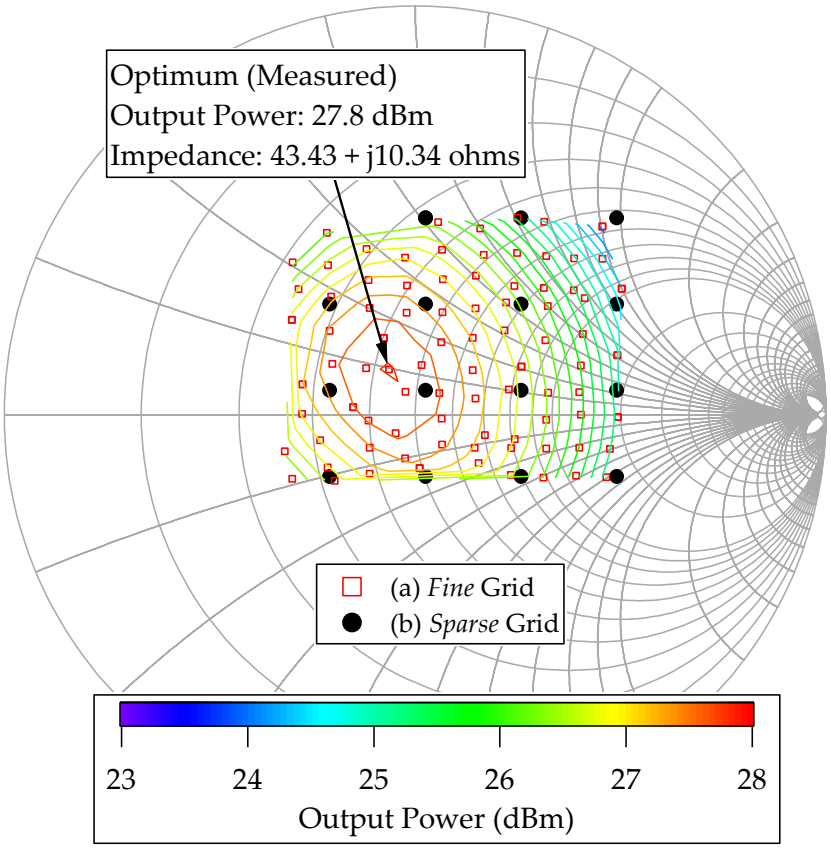

Figure 6-57: Sets of fundamental measurement grids with a) fine distribution of gamma b) sparse distribution of gamma

$$\frac{b_{2,1}}{P_1} = M_{2,1,-2,2}\left(\Gamma_{2,1}^{\ *}\right)^2 + M_{2,1,-1,1}\left(\Gamma_{2,1}^{\ *}\right) + M_{2,1,0,0}\left(\left|\Gamma_{2,1}\right|\right)^0 + M_{2,1,1,1}\left(\Gamma_{2,1}\right) + M_{2,1,0,2}\left(\left|\Gamma_{2,1}\right|\right)^2 + M_{2,1,2,2}\left(\Gamma_{2,1}\right)^2 + M_{2,1,0,3}\left(\left|\Gamma_{2,1}\right|\right)^3 \quad (6\text{-}5)$$

Interpolated data was then verified against measured data on the *fine* grid. Figure 6-58 illustrates an error contour plot, with the predictions of the model when compared to measurement data on the fine grid.

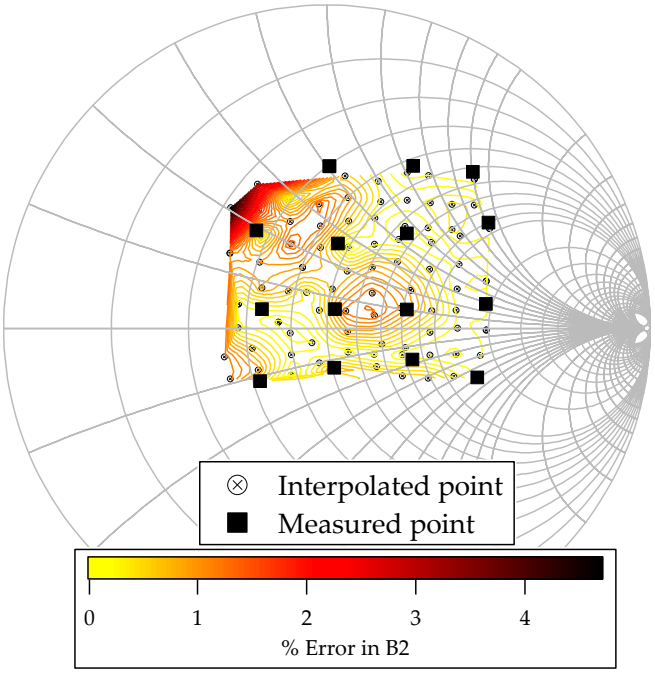

Figure 6-58: Contours of percentage error between interpolated points and measured data

The average error in predicting the response signal, b_{21} for this analysis was 0.6% and the worst-case error was 4.2%. The above coefficients from the *sparse* grid were then used to refit the data onto an "ideal" grid for use in the simulator, using (6-4) – this allows raw measurement data in the form of a lookup-table usable within the simulator without the necessity of a dense grid. The results of this load-pull simulation, when run in AWRDE Microwave office 2011, are shown in Figure 6-59.

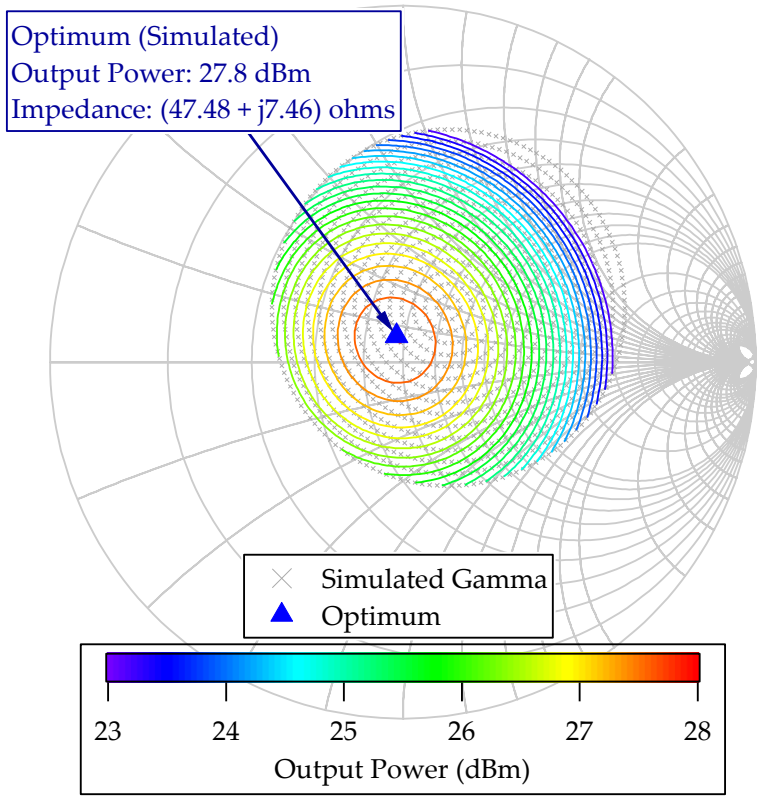

Figure 6-59: Load-pull simulation output from AWRDE

The above simulated result (Z_{opt}: (47.48+j7.46) Ω and maximum output power: 27.8dBm) shows reasonable agreement with measurement data in Figure 6-57 as the measured Z_{opt} was (43.4+j10.3) Ω and the measured maximum output power was 27.8dBm.

The interpolation technique described above shows a significant reduction in the total number of measurements required for fundamental behavioural model generation, compared to traditional look-up table approaches. It also highlights that the measurement system no longer needs to place gamma emulation targets on a "fixed-grid". For open loop active load-pull systems, this causes a reduction in load-convergence iterations and hence significant increasing their utilisation efficiency.

6.5 Second harmonic (2F0) interpolation and extrapolation analysis

With the presence of an active load-pull system capable of harmonic tuning, it was now possible to achieve high 2F0 reflection coefficients ($|\Gamma_{22}|>1$). Varying Γ_{22} in magnitude and phase thus allowed the measurement of a dense 2F0 impedance grid. This provided a platform for investigation of harmonic- interpolation and extrapolation.

For this analysis, the fundamental tone was kept at a constant reflection coefficient, corresponding to the device optimum for efficiency. All higher harmonics, except the second (2F0), were terminated into 50 ohms. External variables such as input drive and bias were held constant. The dataset utilised for this analysis included measured Γ_{22} points ranging from $|\Gamma_{22}|=0$ to $|\Gamma_{22}|=1$ with gamma targets placed on concentric circles, providing for maximum coverage of the smith chart. Figure 6-60 illustrates this sweep plan.

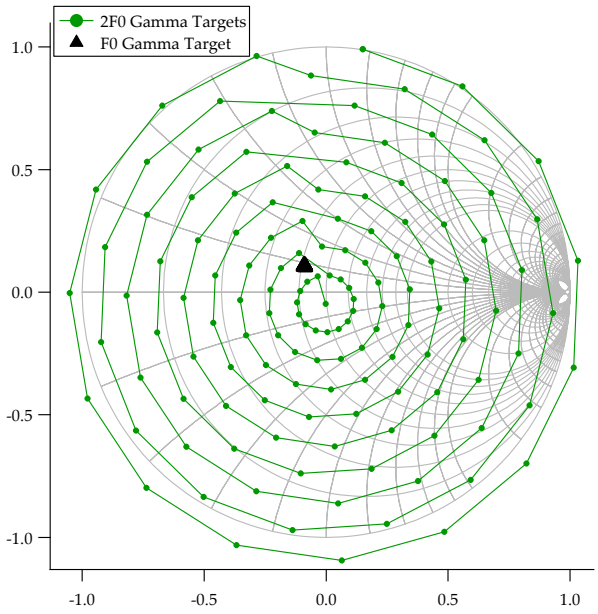

Figure 6-60: Gamma targets for second harmonic analysis

6.5.1 Second harmonic interpolation analysis

Data contained within subsets of measured 2F0 gamma were filtered and grouped by varying values of $|\Gamma_{22}|$. Models of an increasing order, defined by changing ω in (6-2) were used to capture the behaviour for each of these subsets. Results from this analysis are shown in Figure 6-61, comparing the error in re-generating b_{22} with increasing model complexity. From the above result, it was shown that a relatively low model complexity is required to capture an accurate 2F0 model to within an error tolerance of 0.7%. Accuracy is however improved if the number of coefficients is increased; especially for measurement data that includes reflection coefficients with a high magnitude ($|\Gamma_{22}| > 0.7$).

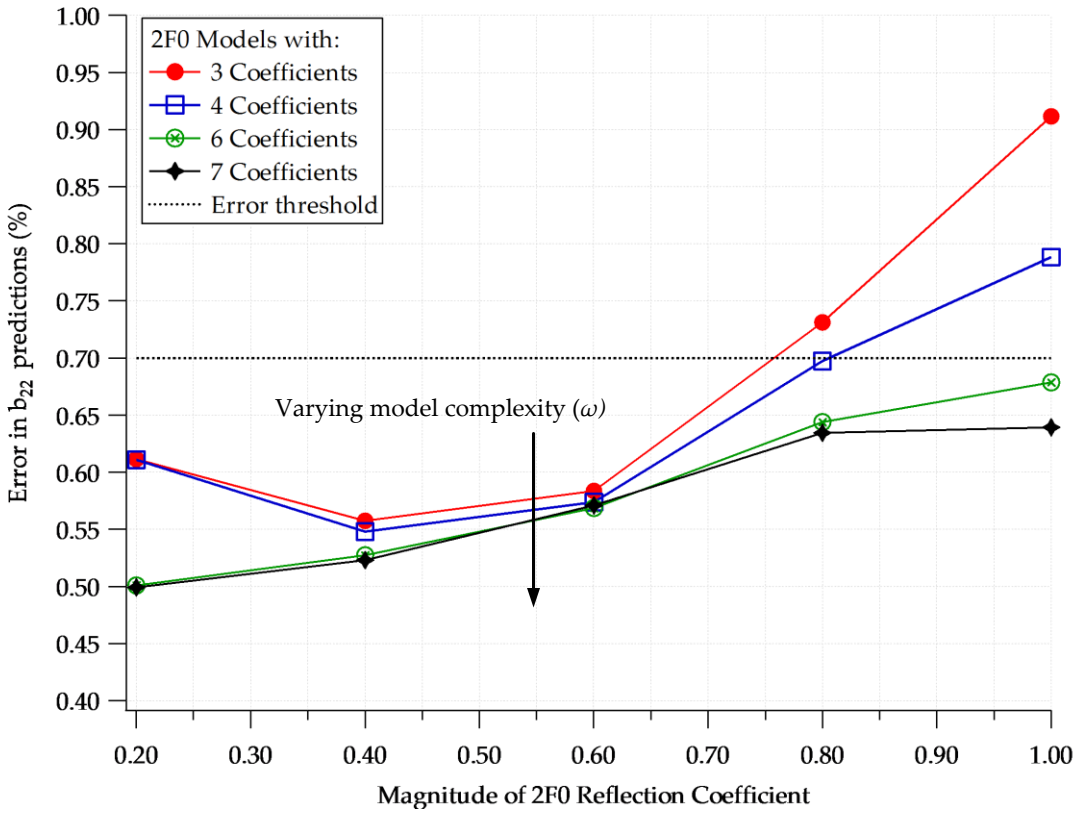

Figure 6-61: Average errors in b_{22} predictions with varying model complexity

6.5.2 Second harmonic extrapolation analysis

Results from the interpolation analysis above indicate that a behavioural model with 6 coefficients was ample to capture the entire 2F0 impedance space, as shown in the equation.

$$\frac{b_{2,1}}{P_1} = K_{2,2,-2,2}\left(a_{2,1}{}^*\right)^2 + K_{2,2,-1,1}\left(a_{2,1}{}^*\right) + K_{2,1,0,0}\left(\left|a_{2,2}\right|\right)^0 + K_{2,2,1,1}\left(a_{2,2}\right) + K_{2,2,0,2}\left(\left|a_{2,2}\right|\right)^2 + K_{2,1,2,2}\left(a_{2,2}\right)^2 \quad (6\text{-}5)$$

In order to test the 2F0 model extrapolation behaviour, these 6 coefficients were extracted from measurement data contained within two subsets:

i. For 2F0 impedances with $|\Gamma_{22}|$ <= 0.2 – [Model 'X']

ii. For 2F0 impedances with $|\Gamma_{22}|$ <= 0.7 – [Model 'Y']

These two conditions are shown in Figure 6-62. Each model was then required to predict the measured behaviour of the device on impedances spread all over the smith chart, including points at the edge of the smith chart i.e. $|\Gamma_{22}|$ <= 1.

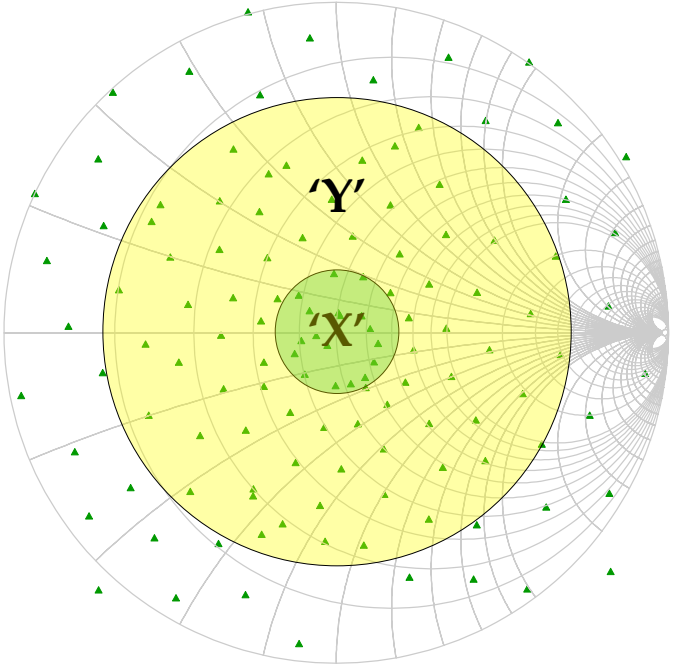

Figure 6-62: Testing for 2F0 extrapolation analysis

Predictions from simulations on Model 'X'

Figure 6-63 shows the predicted 2F0 load-pull behaviour, when compared to measured data. The average error in predicting the response signal, b_{22} was 4% however the worst-case error in the prediction was 88%. Predictions show good agreement up to $|\Gamma_{22}| <= 0.5$ (highlighted with a yellow circle in Figure 6-63). However, for values of $|\Gamma_{22}| > 0.5$, the model fails to accurately predict measured behaviour and the problem gets worse towards the edge of the smith chart.

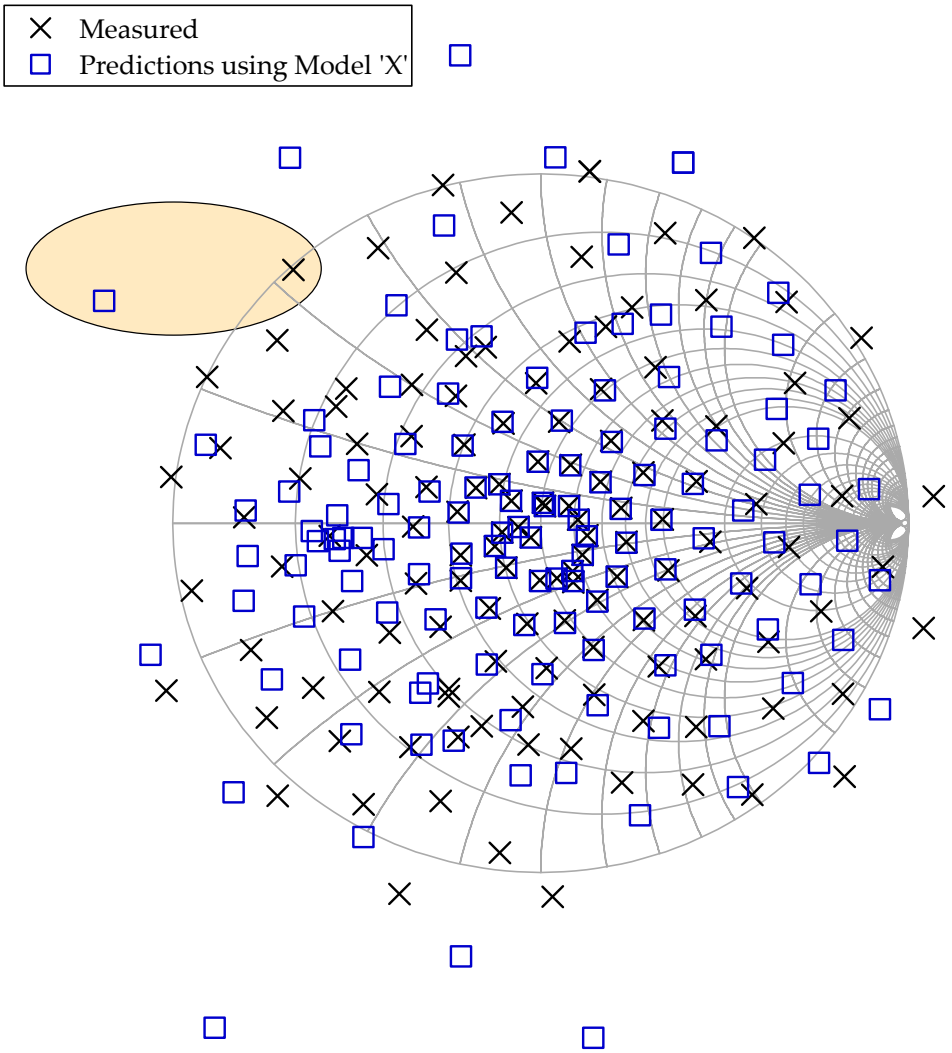

Figure 6-63: 2F0 load-pull prediction using model 'X'

Predictions from simulations on Model 'Y'

Figure 6-64 shows the predicted 2F0 load-pull behaviour, when compared with measured data. The average error in predicting the response signal, b_{22} was 1.1% and the worst-case error in the prediction was 4.6%. Load-pull predictions therefore show good agreement up to $|\Gamma_{22}|$ <= 1.0. Extrapolation results of the 2F0 load-pull behaviour were therefore found to be accurate when higher impedance terminations (e.g. $|\Gamma_{22}|$ <= 0.7) were used in the model extraction. This result is particularly beneficial for collecting harmonic load-pull data using passive tuning systems which are typically limited to a maximum achievable gamma of $|\Gamma_h|$ <= 0.9.

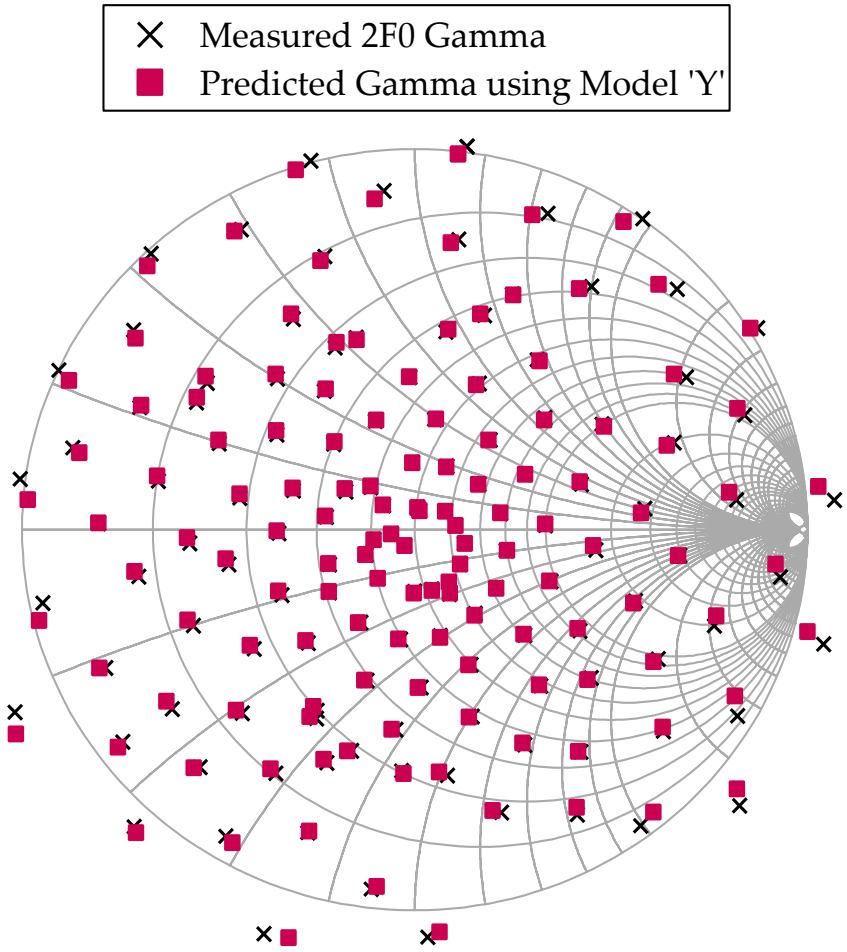

Figure 6-64: 2F0 load-pull prediction using model 'Y'

6.6 Summary

This chapter described how an application of the PHD modelling framework, the Cardiff Behavioural model was effective in its ability to interpolate or extrapolate non-linear measurement data and thereby improve the quality of measurement data and speed of measurement systems.

Fundamental interpolation was demonstrated by using the Cardiff Behavioural Modelling framework with higher order terms. It was shown that a 7-coefficient model can accurately capture a fundamental impedance space containing 15 load-pull points and interpolate the load-pull behaviour when run in the simulator environment. Its ability to refit data onto an ideal grid was verified using measured data with a dense distribution (100 points) of target emulation points within the same region. It therefore showed a significant reduction in the number of measurements required for fundamental load-pull without compromising the quality of measurements.

A comparison of the interpolation and extrapolation accuracy of the second harmonic was also investigated. It was shown that the model required to capture second harmonic behaviour was of a relatively low order. However, the quality of interpolation can be improved by including higher-order terms in the extraction. Extrapolation behaviour of the second harmonic was found to be accurate when higher harmonic terminations were included in the model extraction datasets i.e. $|\Gamma_{22}| <= 0.7$. It was shown that using such a model, second harmonic reflection coefficients of $|\Gamma_{22}| <= 1.0$ could be obtained to an average confidence of 99%. Such a result is particularly beneficial for collecting harmonic load-pull data using passive tuning systems which are typically limited to a maximum achievable gamma of $|\Gamma_h| <= 0.9$.

References

[1] Woodington, S. P.; Saini, R. S.; Willams, D.; Lees, J.; Benedikt, J.; Tasker, P. J.; , "Behavioral model analysis of active harmonic load-pull measurements," Microwave Symposium Digest (MTT), 2010 IEEE MTT-S International, vol., no., pp.1, 23-28 May 2010

[2] Saini, R.S.; Bell, J.J.; Williams, T.; Lees, J.; Benedikt, J.; Tasker, P.J.; , "Interpolation and extrapolation capabilities of non-linear behavioural models," Microwave Measurement Symposium (ARFTG), 2011 78th ARFTG , vol., no., pp.1-4, 1-2 Dec. 2011

[3] P. Wright, A. Sheikh, C. Roff, P. J. Tasker, and J. Benedikt, "Highly efficient operation modes in GaN power transistors delivering upwards of 81% efficiency and 12W output power," in IEEE MTT-S Int. Microwave Symp. Dig., June 15–20, 2008, pp. 1147–1150.

[4] P. Wright, J. Lee, P. J. Tasker, J. Benedikt, and S. C. Cripps, "An efficient, linear, broadband class-J-mode PA realised using RF waveform engineering," in IEEE MTT-S Int. Microwave Symp. Dig., June 2009, pp. 653–656.

[5] Online: http://www.maurymw.com [Accessed: 24-11-2012]

[6] Online: http://www.focusmicrowaves.com [Accessed: 24-11-2012]

[7] Online: http://www.mesuro.com [Accessed: 24-11-2012]

[8] J. Benedikt, R. Gaddi, P. J. Tasker, and M. Goss, "High-power time-domain measurement system with active harmonic loadpull for high-efficiency base-station amplifier design," IEEE Trans. Microwave Theory Tech., vol. 48, no. 12, pp. 2617–2624, Dec. 2000.

[9] D. Williams, P. Hale, K. A. Remley, "The sampling oscilloscope as a microwave instrument," IEEE Microwave Mag., vol. 8, no. 4, pp. 59–68, Aug. 2007.

[10] Bell, J.J.W.; Saini, R.; Lees, J.; Benedikt, J.; Cripps, S.; Tasker, P.J.; , "X-band behavioral model analysis using an active harmonic source-pull and load-pull measurement system," Microwave Conference Proceedings (APMC), 2011 Asia-Pacific , vol., no., pp.1430-1433, 5-8 Dec. 2011

Chapter 7 – Future Work and Conclusions

7.1 Discussion

The objective of this thesis was to provide improved load-pull measurement strategies based on an open-loop active load pull measurement system.

An in-depth literature review was presented aimed to discuss the evolution of microwave measurement systems from linear RF measurements to the non-linear RF measurement domain. The reader was thus introduced to the automated open-loop active load-pull measurement system architecture – the focus of the rest of this thesis.

Starting with a comparison of behavioural models to compact and physical models, the review of non-linear behavioural models was carried out; sighting various advantages of using this approach. The theory behind the PHD model was then described and shown how most modern frequency domain behavioural modelling implementations follow this theory. The reader was then familiarised with the Cardiff Behavioural Model formulations and examples of model coefficient extraction were

used to explain the concept and show the accuracy of the model predictions in both fundamental and harmonic load-pull.

An intelligence driven active load-pull system was presented, based on deriving local PHD models to aid the prediction of the desired active signal in order to achieve a target reflection coefficient. In order to define the problem area and derive the load-pull error model, device characterisation was tested using a numerical based algorithm. The new strategy was then designed and proved to be effective in reducing the number of iterations and thus improving the utilisation efficiency from a typical value of < 30% up-to 90%. The work was demonstrated by carrying out load-pull measurements on 0.5W Gallium Arsenide (GaAs) devices as an example.

A non-linear measurement approach suitable for wafer mapping and technology screening applications was presented as an application of the intelligence driven load-pull system described above. Rapid characterisation and uniformity investigations of non-linear devices were now possible exploiting the speed and intelligence gathered by this system. Initially, locally computed X-parameters guided the active load pull system thus minimising iterations required to set the desired impedances while simultaneously archiving locally computed models as well as the open-loop settings. These settings were then recalled for subsequent device measurements, eliminating the need for iterative load-pull altogether and thus significantly reducing measurement time. The technique showed that if the wafer mapping process is required to measure devices of similar technology and periphery, characterisation times can be significantly reduced and quantified from approximately 30 minutes to within 7 minutes per device.

For exploitation within CAD tools, these load-pull measurements were used to create a 5th order parameterised behavioural model based on Cardiff Model formulations. The verification on simulation data showed a very good agreement between measurements and model accuracy. Each of these parameterised models could therefore be utilised within the CAD tool for circuit design, optimisation as well as yield analysis providing a format and elegance to archiving the non-linear data.

In this thesis, it was shown how the Cardiff Behavioural model was effective in its ability to interpolate or extrapolate non-linear measurement data and thereby improve the quality of measurement data and speed of measurement systems. This investigation was carried out in two stages; fundamental interpolation testing and harmonic interpolation and extrapolation testing.

Fundamental interpolation was tested by using the Cardiff Behavioural Modelling framework with higher order terms. It was concluded that a 7-coefficient model can accurately capture a fundamental impedance space containing 15 load-pull points and interpolate the load-pull behaviour when run in the simulator environment. An application of the interpolation behaviour was demonstrated by performing a data refit of the sparse grid onto a denser measurement grid. This result therefore meant a significant reduction in the number of measurements required for fundamental load-pull without compromising the quality of measurements. This strategy is useful for open loop active load-pull measurement systems which are typically iterative in nature.

A comparison of the interpolation and extrapolation accuracy of the second harmonic was also investigated. It was demonstrated that the model required to capture second harmonic behaviour was of a relatively low order. However, the quality of interpolation was improved by including

higher-order terms in the extraction. Extrapolation behaviour of the second harmonic was found to be accurate when higher harmonic terminations were included in the model extraction datasets i.e. $|\Gamma_{22}| <= 0.7$. Using such a model, second harmonic reflection coefficients of $|\Gamma_{22}| <= 1.0$ could be obtained to an average confidence of 99%. This result is particularly beneficial for collecting harmonic load-pull data using passive tuning systems which are typically limited to a maximum achievable gamma of $|\Gamma_h| <= 0.9$.

7.2 Future work

The intelligence drive active load-pull system discussed in this thesis is extendable in various areas. Firstly, if a harmonic local-model is captured concurrently as the fundamental local X-parameter models, it is possible to carry out simultaneous harmonic load-pull. A drawback of this approach is that the harmonic model will only be valid for the specified fundamental impedance and this may lead to a time-consuming extraction process at each step. The problem is further compounded by the fact that if more than one harmonic is required to be load-pulled, cross products relating the fundamental to each of the harmonics makes it difficult to archive these local harmonic models.

As well as improving the speed of active load-pull algorithms, other techniques can be applied to improve the intelligence of the active load-pull measurements. An example is the prediction of stability contours presented by Peláez et al. in [1]. The locally derived X-paramters can therefore also be used to simultaneously provide the user with information about the device stability contours.

7.3 Conclusions

The objective of this thesis was to provide improved load-pull measurement strategies based on an open-loop active load pull measurement system. A solution to the iterative problems associated with open loop active load-pull systems was therefore presented. A thorough review of existing systems and investigations into their problems provided the ideal requirement specification for this development. A significant improvement to the measurement system utilisation efficiency was noticed with the development and an application of this was demonstrated using device comparison measurements as an example. Strategies for measurements using various load-pull system architectures were also investigated taking into account their inherent problems.

The author believes that the strategies presented can be extended especially for harmonic load-pull measurements and providing more algebraic expressions within the live measurement loop.

References

[1] Peláez Pérez, Ana María. "X-parameters based analytical design of non-linear microwave circuits Application to oscillator design." PhD diss., Telecomunicacion, 2012.

Appendix A - Description of Active Load-pull Software

The core functionality was to provide automated control of all instrumentation required for active load-pull control e.g. DC Supplies, RF signal generators and receivers.

Specific Software Requirements

1. Manage synchronisation and communication in all the instruments connected via a Virtual Instrument Software Architecture (VISA) connectivity [1] allowing control of instruments connected via a Local Area network (LAN), General Purpose Information Bus (GPIB) as well as Universal Serial Bus (USB). Each instrument therefore requires a specific driver written to offer the core functionality for its type. For example, a signal generator driver is required to set a given frequency, RF power level and phase offset.
2. Allow the ability to assign each discovered signal generator to a specific harmonic frequency. This step is required for simultaneous fundamental and harmonic load-pull. Up to 6 signal generators need

to be setup for concurrent source- and load-pull with a total of 3 harmonics and each port.

3. Allow setting of dc supply parameters, such as channel numbers, compliance settings as well as assignment of ports.
4. Provide a mechanism of setting the receiver parameters such as averages, number of points and trigger settings.
5. Allow for a basic measurement and acquisition of data from the signal receiver. In this case, the signal receiver was a 4-Channel Tektronix Oscilloscope (Tektronix DSA8200). Data was to be acquired in time domain and via a Fast Fourier transform, converted to the frequency domain.
6. Allow for the correction of raw measurement data at each frequency of interest such as the fundamental and harmonic frequencies. Data correction is carried out using error coefficients provided by a file generated within a calibration utility. This utility provides an 8-term error model, grouped by frequency of measurement.
7. Independently set each fundamental and harmonic signal generator to provide an active signal to set impedances at each harmonic of interest.
8. Independently set the DC bias for the device while reporting the current and voltage at each terminal of the device.
9. Automated the steps 2-8 above to provide an automated active load-pull control feature. During the process, allow user interaction such as abort, restart and pause. A "live" feedback of measurements via waveform and smith chart plots is also required.
10. Provide measurement data in a readable and expandable format.
11. Optionally provide a mechanism for uploading de-embedding data to transfer the measurement reference plane such as device fixture.

Description of the Software

The active load-pull and source-pull software was developed using the .NET framework entirely written using Microsoft C# [2]. This framework was chosen as it provides an integrated data provider, drag-and-drop components and an integrated editor which allows for rapid application prototyping. Behind the load-pull application was a database core which was implemented using SQL Server allowing for quick data saving and retrieval. Instrument control was provided for by libraries written using Interoperable Virtual Instrument (IVI) libraries [3]. This allowed for sending and receiving commands to VISA capable instruments via SCPI commands or by drivers provided by the manufacturers.

Measurements are therefore always saved into the database and the user can optionally export them into one of the defined file formats when required. The software therefore benefits from the qualities of modern relational database suites such as indexing, data backup and recovery. Data visualisation was also provided via a library of drag-and-drop components, developed by National Instruments called "Measurement Studio" [4]. Placing all these components in a software environment allowed real time control of the measurement system providing the user with a direct feedback of device performance as a grid of load-pull emulation points was achieved.

Features of the Software (Setup)

Logging-in

The software featured a user-profiling feature allowing for personalised measurements and settings. Therefore, each user was given a user name and password which was required before the software could be used.

Once logged-in all measurements carried out were only specific to the logged-in user. The login screen is shown in Figure 65.

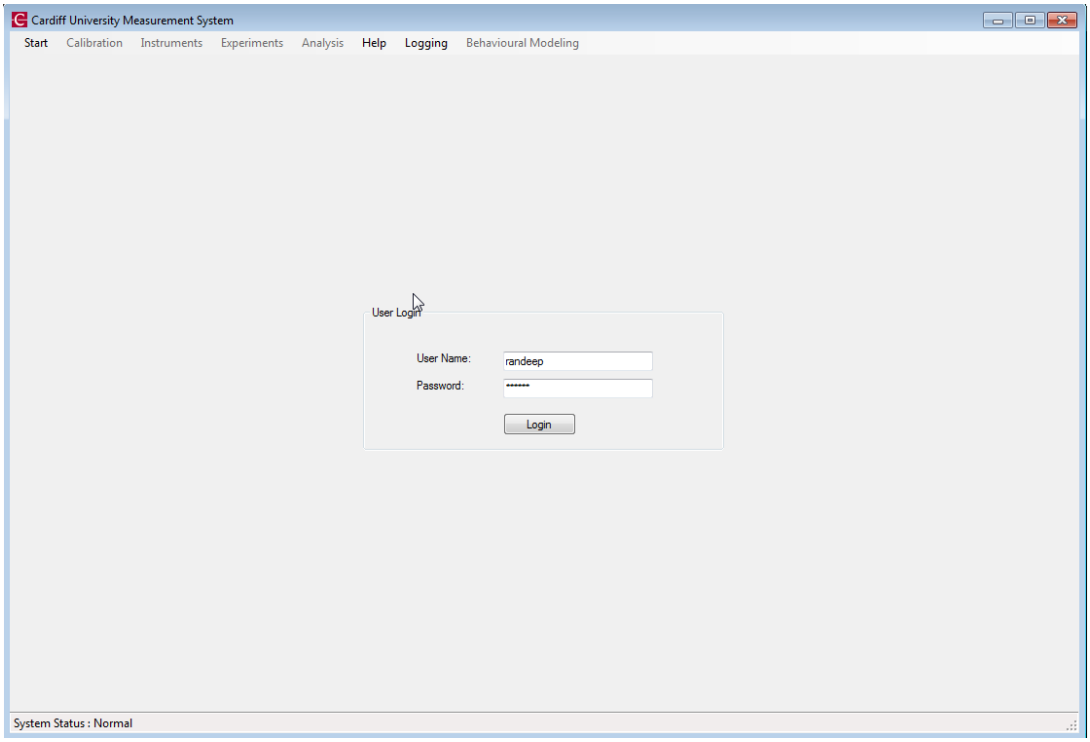

Figure 65: Login screen

Loading Calibration data

The calibration vector file generated within custom-written calibration software can be loaded into the measurement software using this tool, as shown in Figure 66.

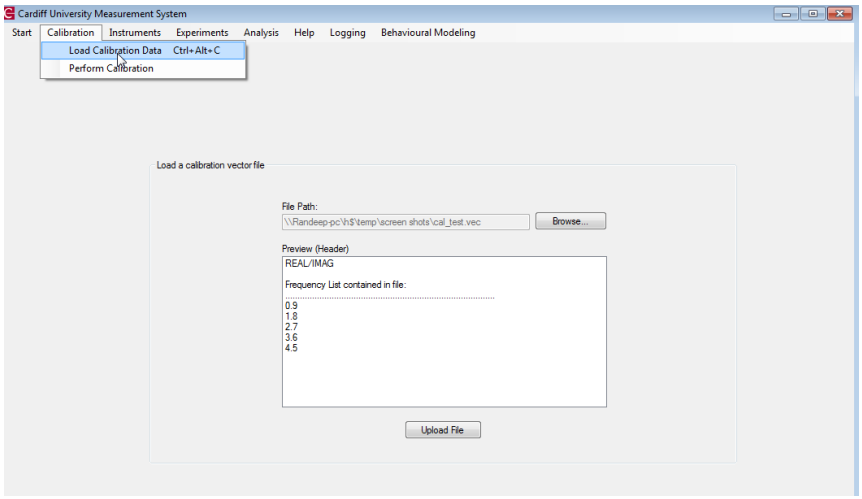

Figure 66: Loading calibration data

Instrument discovery

This tool is used to find all the available instruments on the VISA bus. Once found, an instrument needs to be tagged as of a specific type. For example, an instrument with identification string "Tektronix DSA8200" can be tagged as receiver.

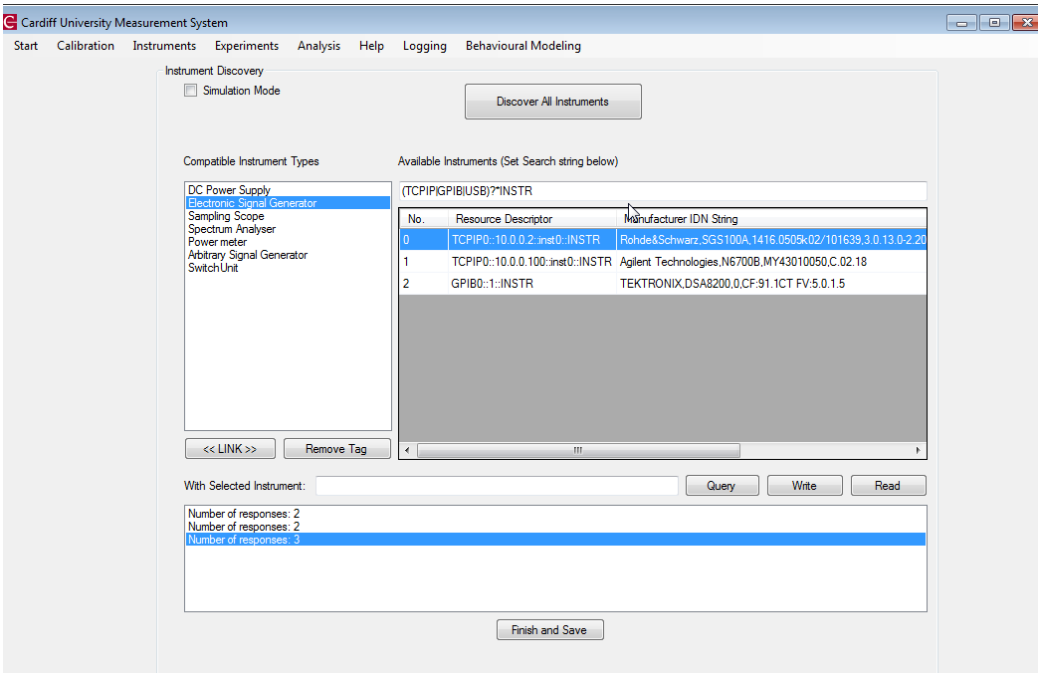

Figure 67: Instrument discovery

Assigning drivers

Since multiple models of receivers, generators and dc supplies are supported, it is vital to assign the correct driver to the discovered instrument. This is done via the settings panel shown in Figure 68.

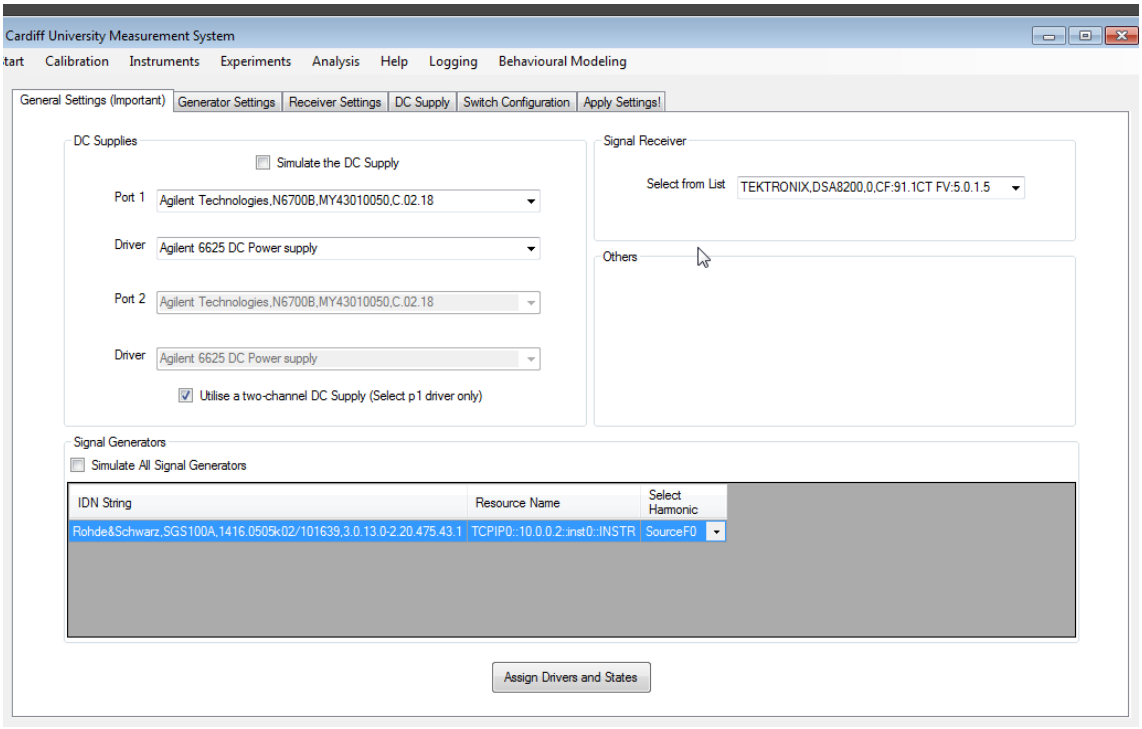

Figure 68: Driver assignment

Generator Settings

In this part of the instrument settings, the signal generators are assigned to a harmonic/port combination. For example, the signal generator responsible for the fundamental drive signal is shown in Figure 69. The fundamental frequency of measurements can also be assigned in this screen.

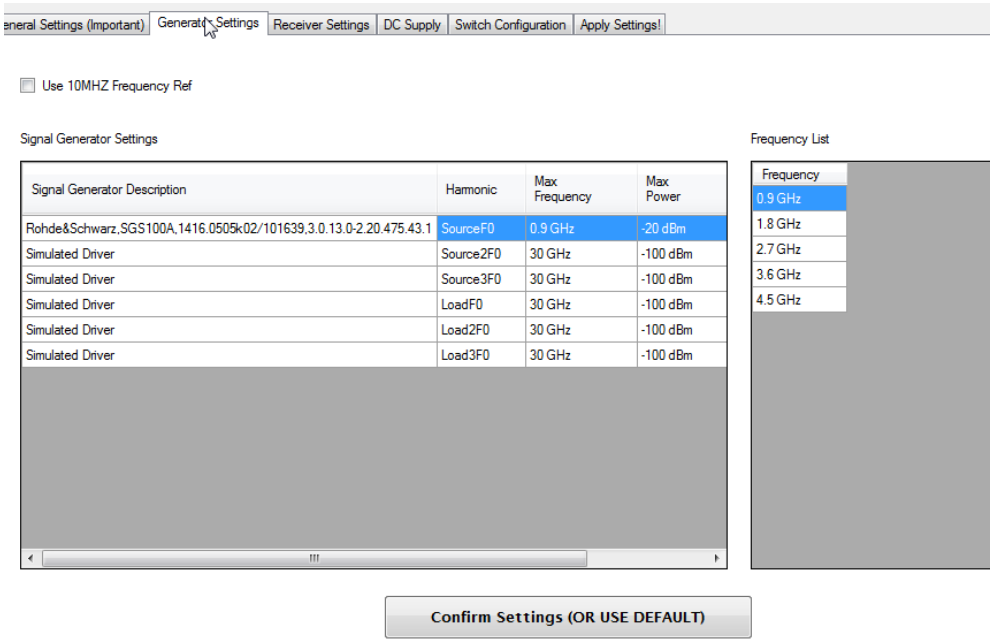

Figure 69: Signal generator settings

Receiver Settings

This screen provides a mechanism for setting the signal generator variables such as number of points, averages and trigger settings. This is shown in Figure 70.

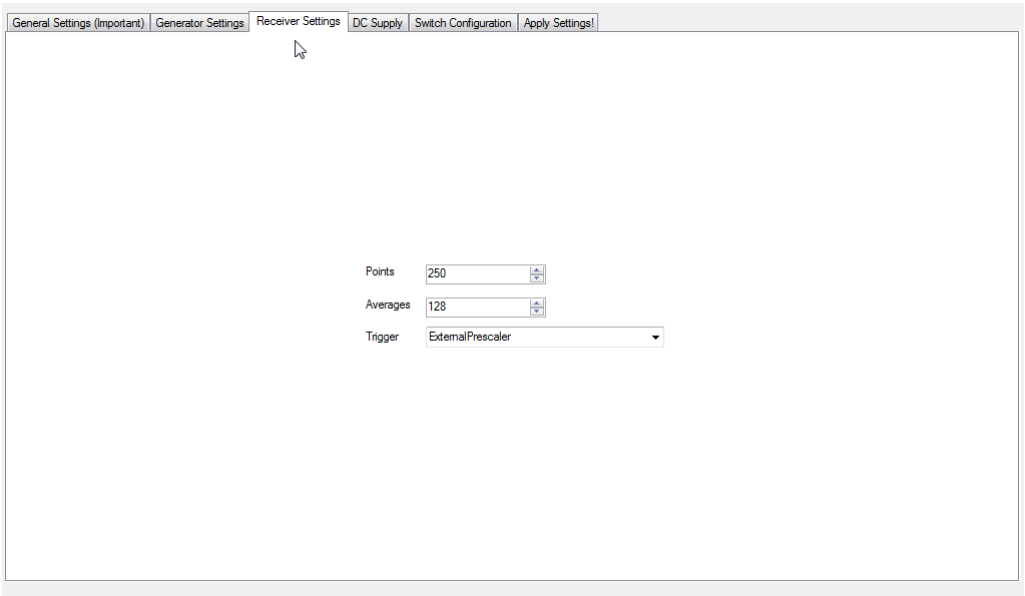

Figure 70: Receiver Settings

Device-Under-Test (DUT) Settings

This screen provides a feature that can be used to limit the maximum/minimum dc variables such as voltage and current. This is a software limit that limits the user controls from accepting out of range values.

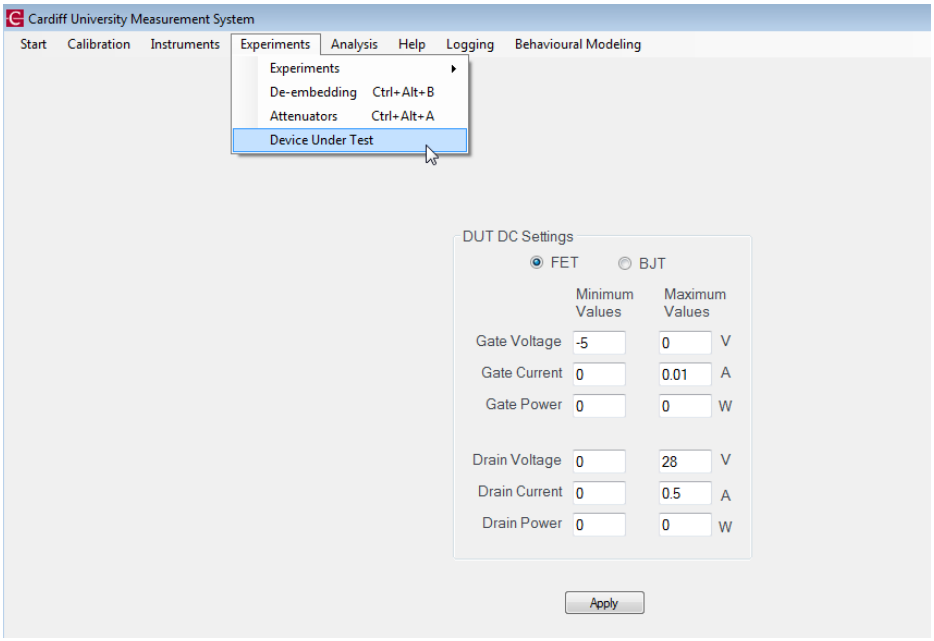

Figure 71: DUT Settings

De-embedding control

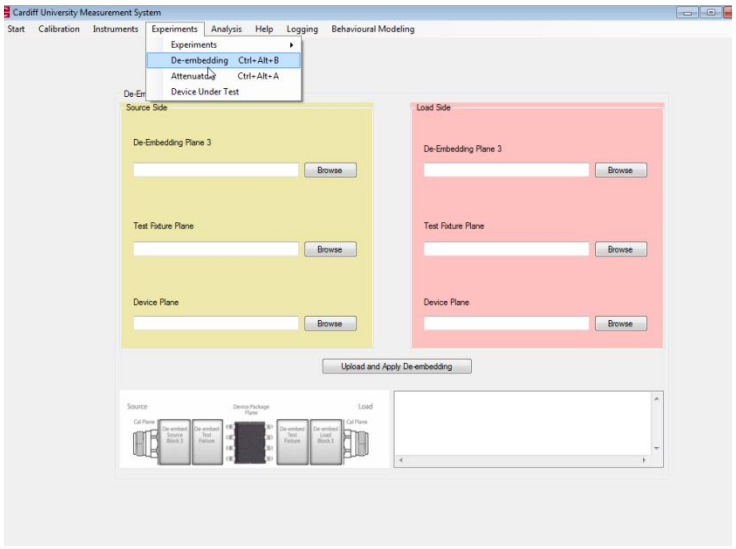

Figure 72: De-embedding control

S-parameter files for each of the reference planes such as the test fixture and device plane can be uploaded into this screen. This allows the user to carry out load-pull or visualise measurement data at the chosen plane. This is shown in Figure 72.

Attenuator settings

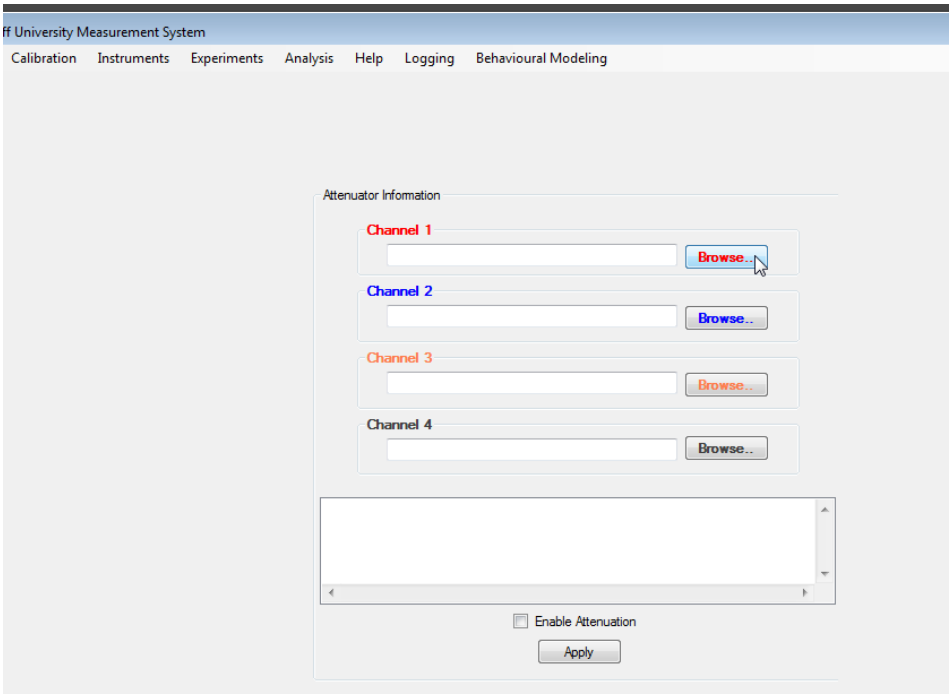

Figure 73: Attenuator Settings

This allows for high power measurements to be carried out. Once a calibration is complete, additional attenuators can be incorporated into the calibration path to protect the internal receivers of the oscilloscope. S-parameter files, containing the loss (*s21*) of each of these attenuators can be uploaded into this screen. This is shown in Figure 73.

Diagnostic test

This tool guides and checks all the settings as setup by the user. If the settings are correct, a dummy measurement is complete where by all the instruments are triggered for a measurement. If successful, the system is setup correctly and ready to measure as shown in Figure 74.

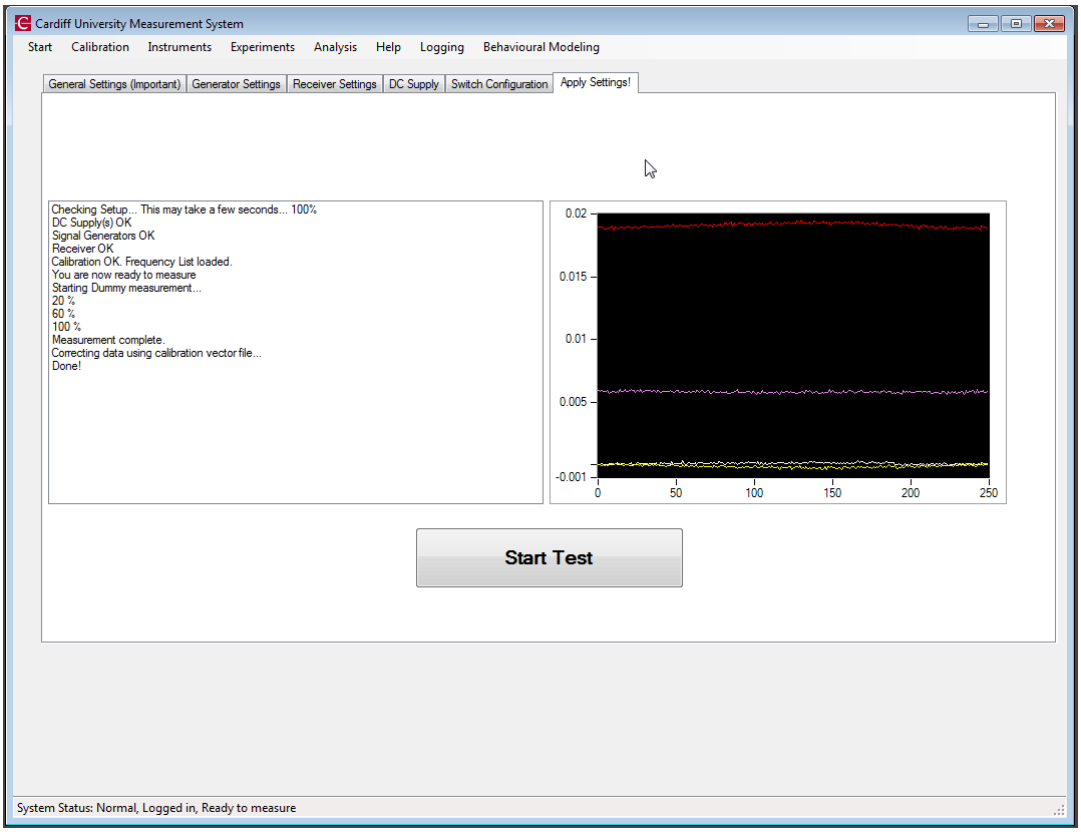

Figure 74: Diagnostic test

Features of the Software (Measurement)

The active load-pull control was developed to run in two modes. The first mode was to allow manual control by the user. The second mode can be used to carry out automated load-pull measurements such as power sweeps, bias sweeps etc.

Manual Measurement Control

In this mode, the user can set a target emulation point and then set the system to iterate to this target point by automatically setting the signal generators. The software automatically plots the new position of gamma at the harmonic being load-pulled. This is particularly useful for fine tuning. Users can also set the signal generators directly giving full manual control for control of gamma shown in Figure 75.

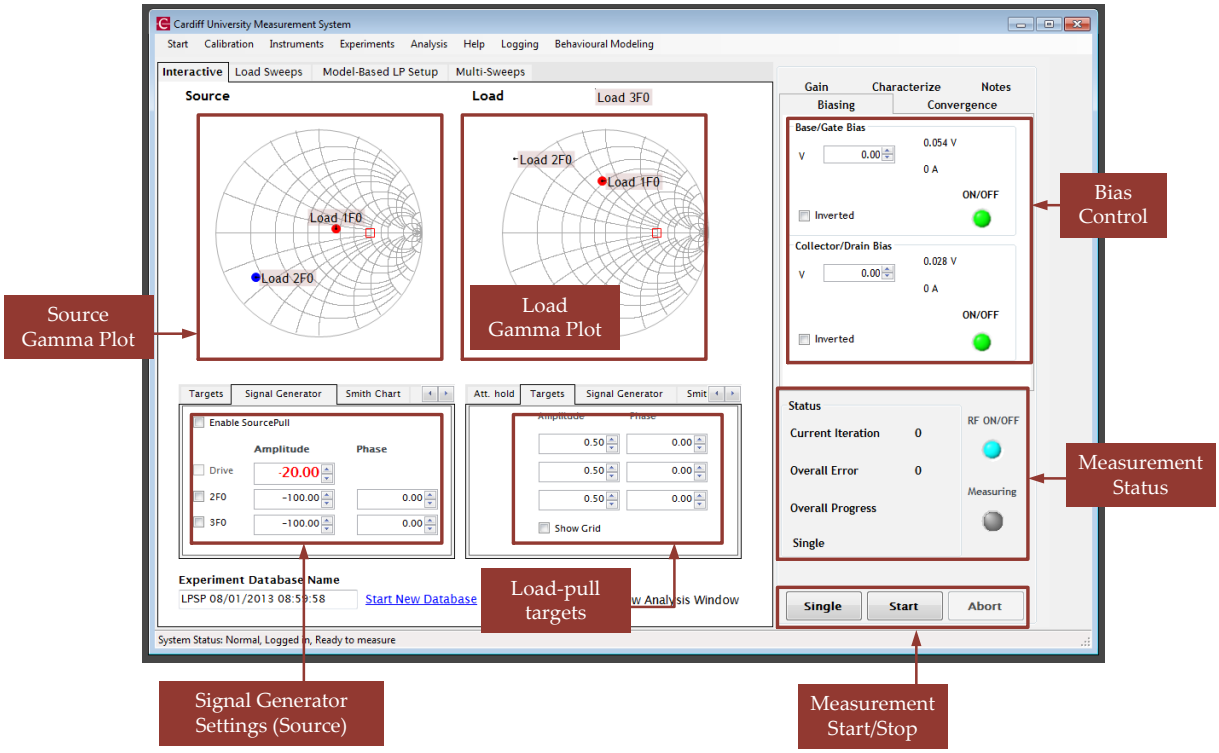

Figure 75: Measurement Control

Various settings are provided to achieve this functionality, as shown in Figure 75 and Figure 76:

- Measurement of the system characteristic impedance
- Convergence and weights settings
- An initial value for the system amplifiers
- Control for each signal generator whereby the user can set amplitude and phase.
- Ability to set the drive level and bias
- Ability to set target emulation points

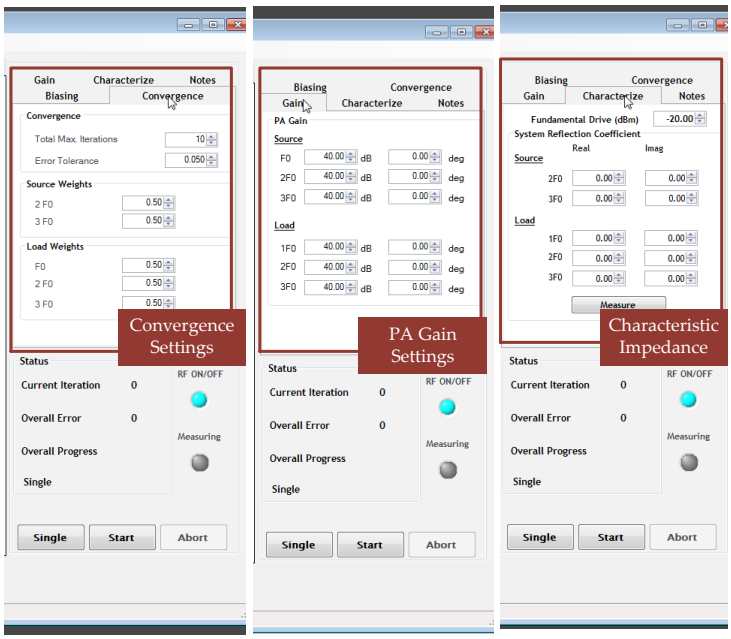

Figure 76: Convergence and Gain settings

Swept Measurement Control

This control allows setting gamma sweeps for a particular harmonic. The sweeps can be grouped by power levels, bias levels and customised in various grid shapes.

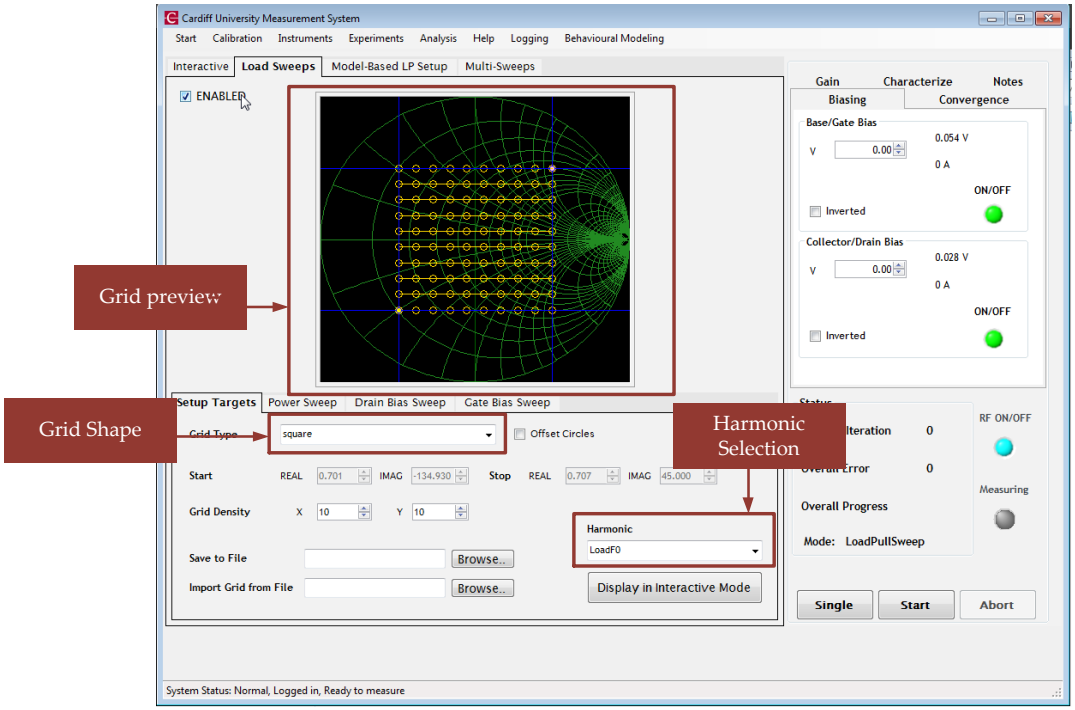

Figure 77: Sweep Control

Model-based Load-pull control

This control enables the local model based load pull control. It controls the size of the perturbation signal, allows saving of local models to a file and recalling existing models. When enabled, the active load-pull system uses locally derived x-parameters to carry out load-pull measurements.

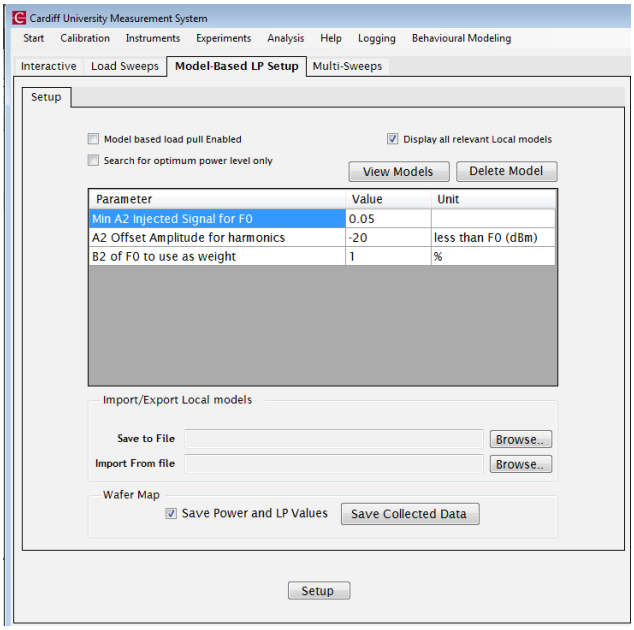

Figure 78: Model-Based LP Setup

Features of the Software (Data Viewer)

The active load-pull software features a real-time data viewer. Using this viewer, users can read off the performance information such as drain efficiency, output power, gain etc. It also displays output and input waveforms, transfer characteristics and load-lines. All of the above information can also be viewed at any of the three reference planes, in case de-embedding information was uploaded.

Selecting a sweep

This control lets the user chose a sweep from the history of experiments in the database. The entire sweep or a specific point within the sweep can also be chosen and plotted or exported. This is shown in Figure 79.

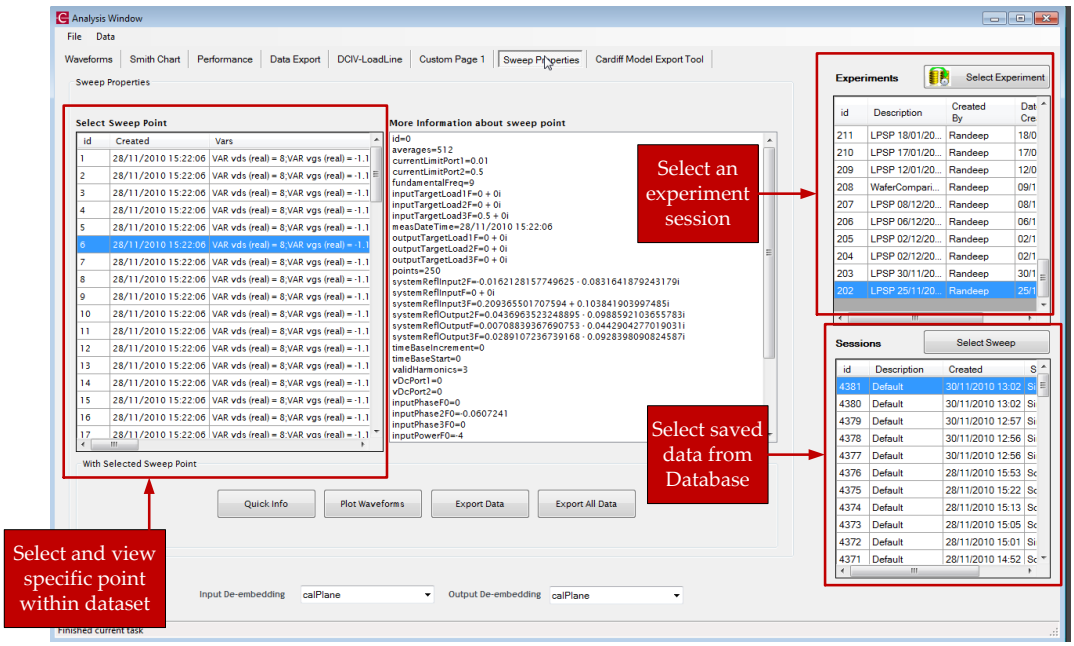

Figure 79: Selecting a sweep

Waveform plots

In this tab, the input waveforms, output waveforms, transfer characteristic and load-line plots are displayed, as shown in Figure 80.

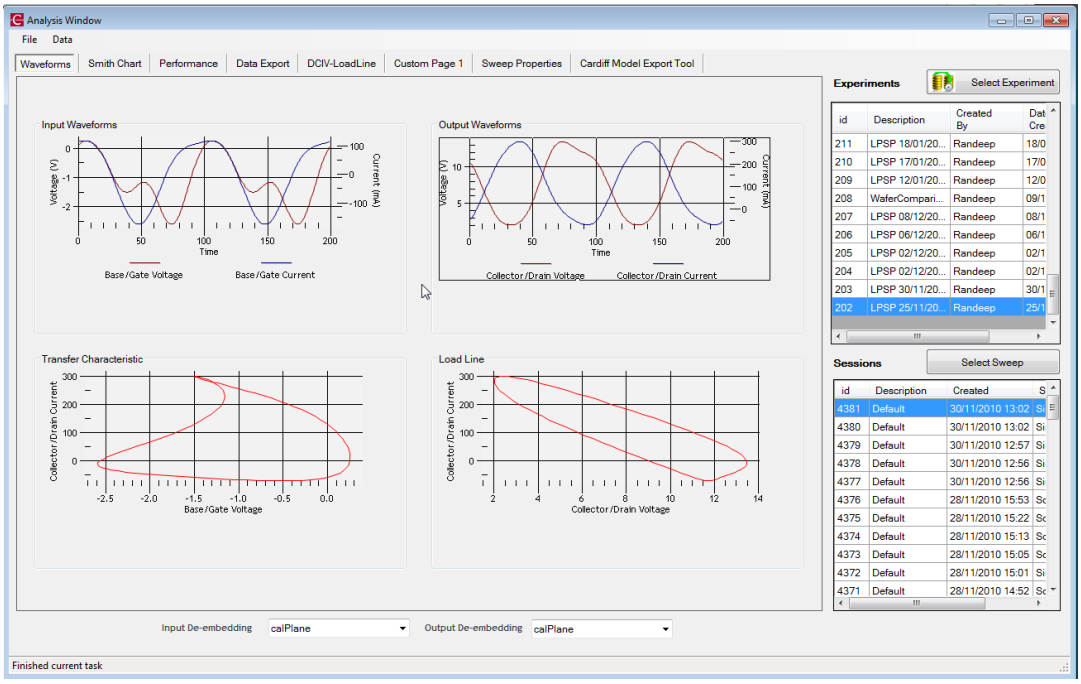

Figure 80: Waveform plots

Smith Chart Tab

This tab displays the gamma at the input and output ports for each of the harmonics being measured. This is shown in Figure 81.

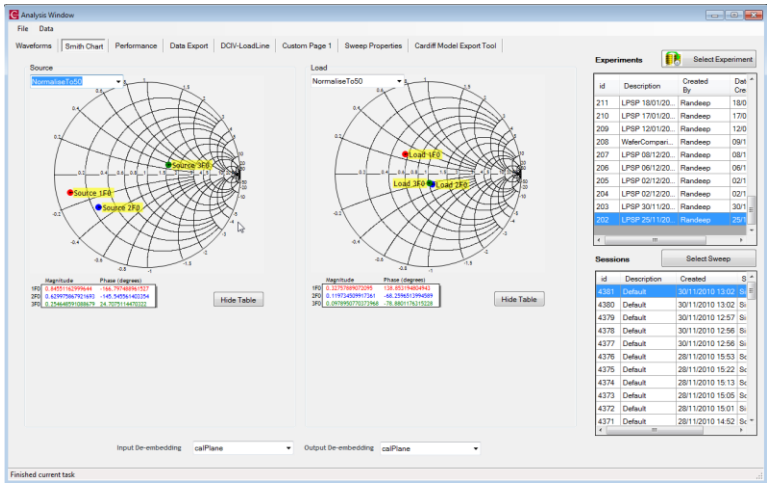

Figure 81: Smith Chart tab

Performance Tab

The device performance information such as output power, drain efficiency, power added efficiency and gain can be viewed in this tab as shown in Figure 82.

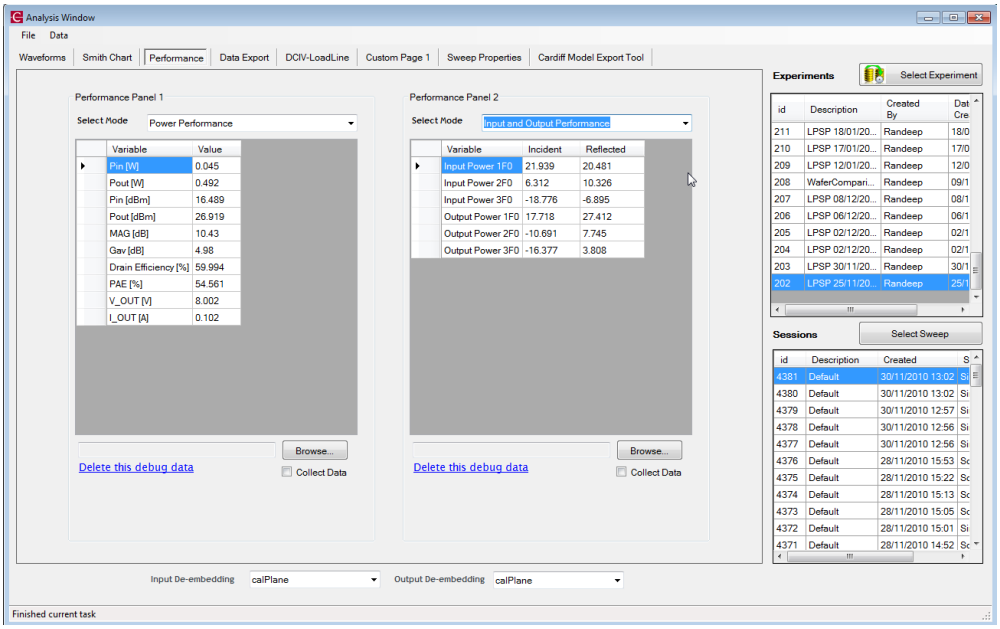

Figure 82: Performance tab

Data Export Tab

Another feature of the data viewer is that it allows the user to select any experiment from a history of archives; thus harnessing the power of using relational databases to save load-pull data. The selected sweep can be exported into a file for use in CAD tools or further processing in other software such as MATLAB™ or IGOR™. Data can be exported as a Microsoft Excel file or using the Generic MDIF file format, described below. The data export feature is shown in Figure 83.

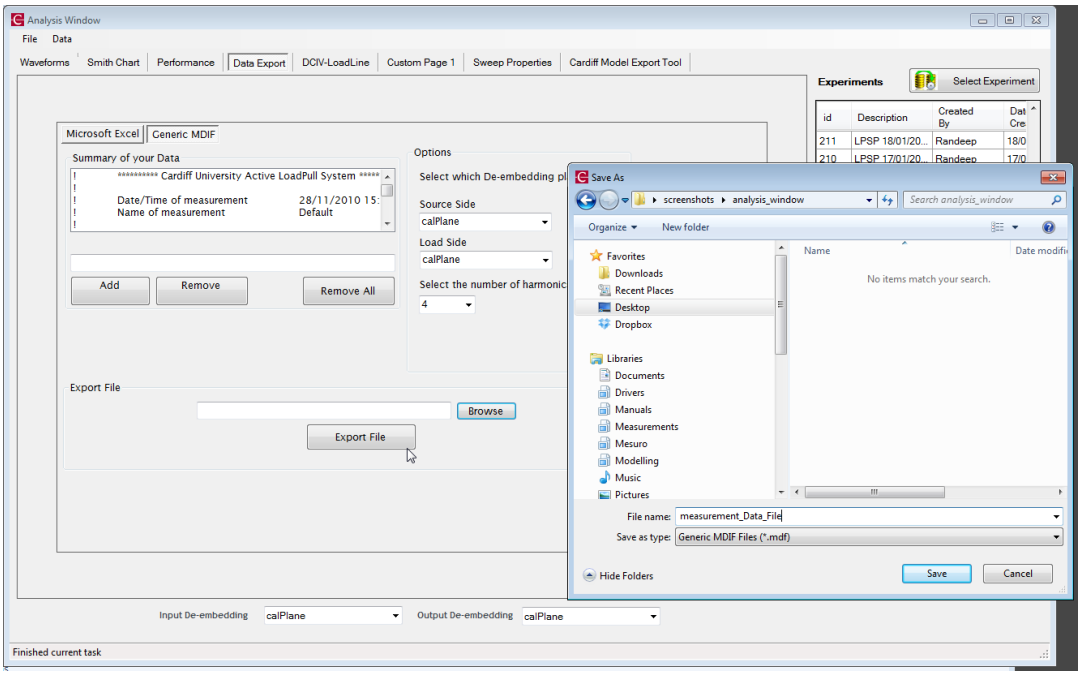

Figure 83: Data Export

The Generic MDIF File format

The Generic MDIF file format [5] is compatible with Agilent's Advanced Design System tool (ADS). This allows for raw measurement data to be directly imported into the data display window of the CAD package. This format was chosen due to its flexibility in handling numerous independent variables such as input power, frequency, load-pull targets, bias points etc. The measurement data file stored in this format therefore contains the following:

- Comments attribute including information such as the date and time the measurement was taken. This is usually started with a "!" character.
- A set of independent variables describing the conditions of each measurement point. This may include the input power level or target load emulation point.
- A data block containing the measured data point as Fourier coefficients of a and b waves as well as the v and i waves.

These are grouped by frequency with index 0 including the dc information.

A sample data block of such file formatting is shown in Figure 84.

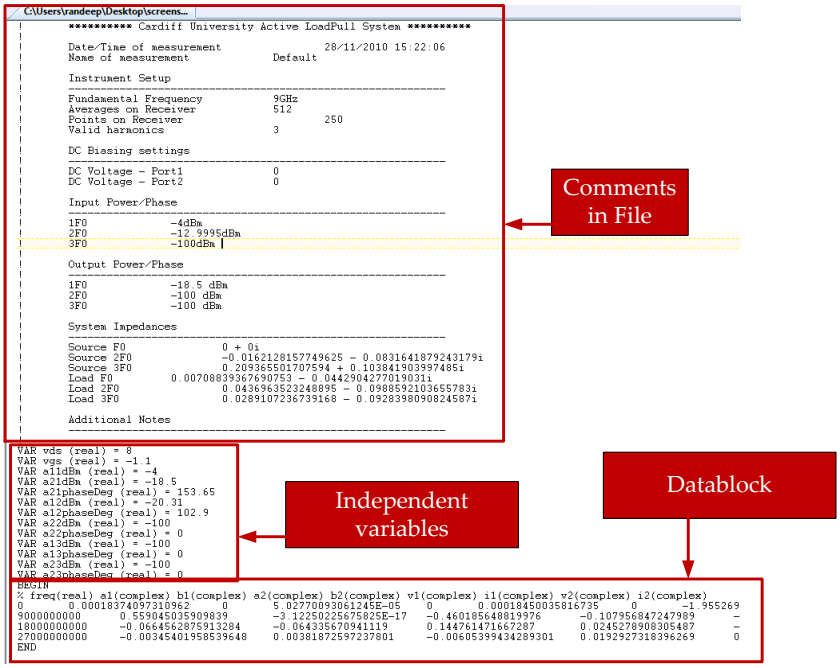

Figure 84: The Generic MDIF file format

Appendix B - Description of Model Generation Software

The Cardiff Behavioural Model generator software was also written using the .NET framework. It uses data collected by the measurement software, as stored in Generic MDIF file format. The resulting output file is compatible with both major CAD tools i.e. Agilent ADS 2009-2011 and AWR Microwave Office 2010.

Importing and filtering data

Data is imported via a Generic MDIF file loader and then filtered based on independent variables such as input power and bias. This is shown in Figure 85 (importing) and Figure 86 (filtering).

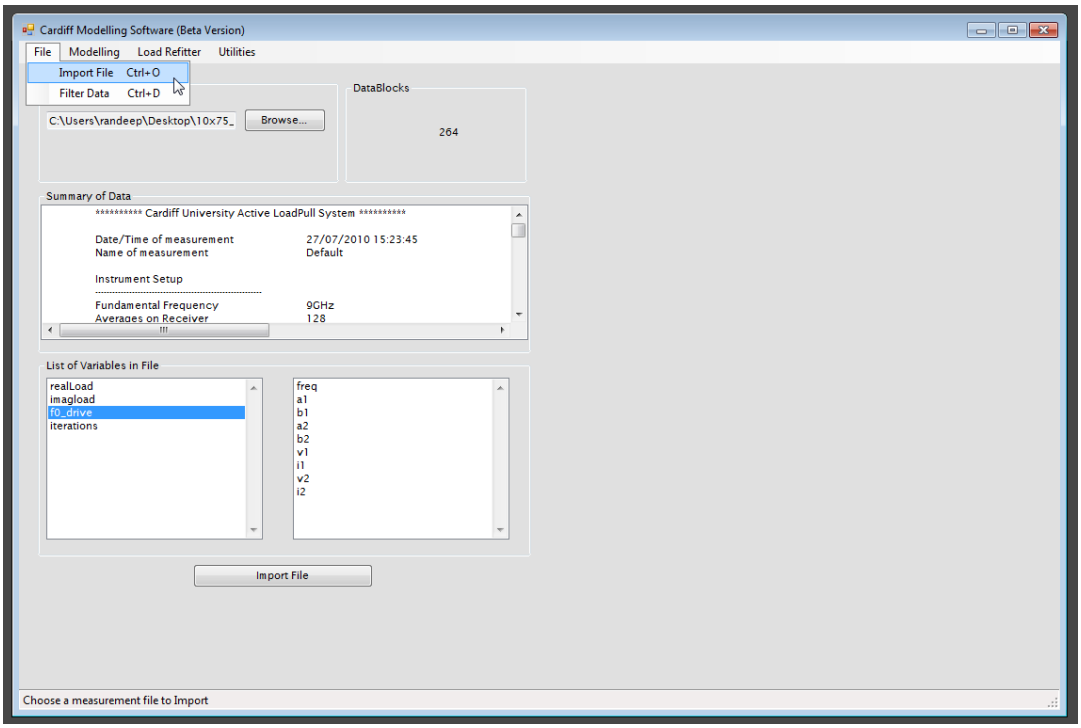

Figure 85: Importing a Generic MDIF file

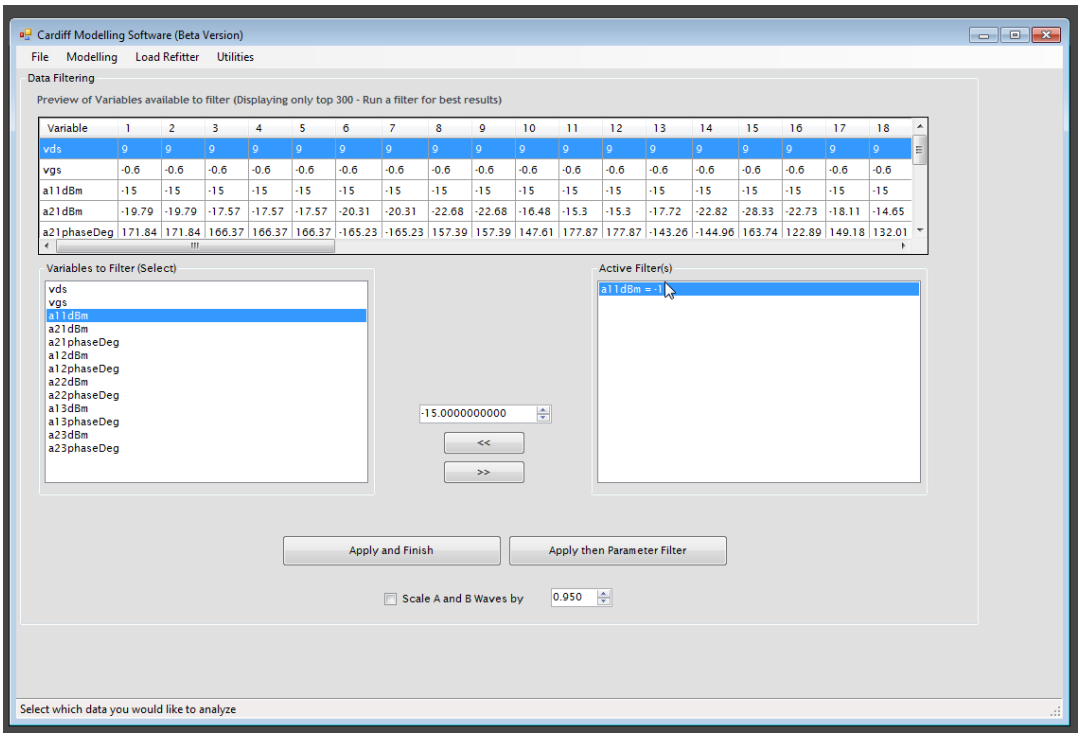

Figure 86: Filtering data

Impedance Renormalisation

This control can be used to manipulate the characteristic impedance of the A-waves (typically 50 ohms). This is shown in Figure 87.

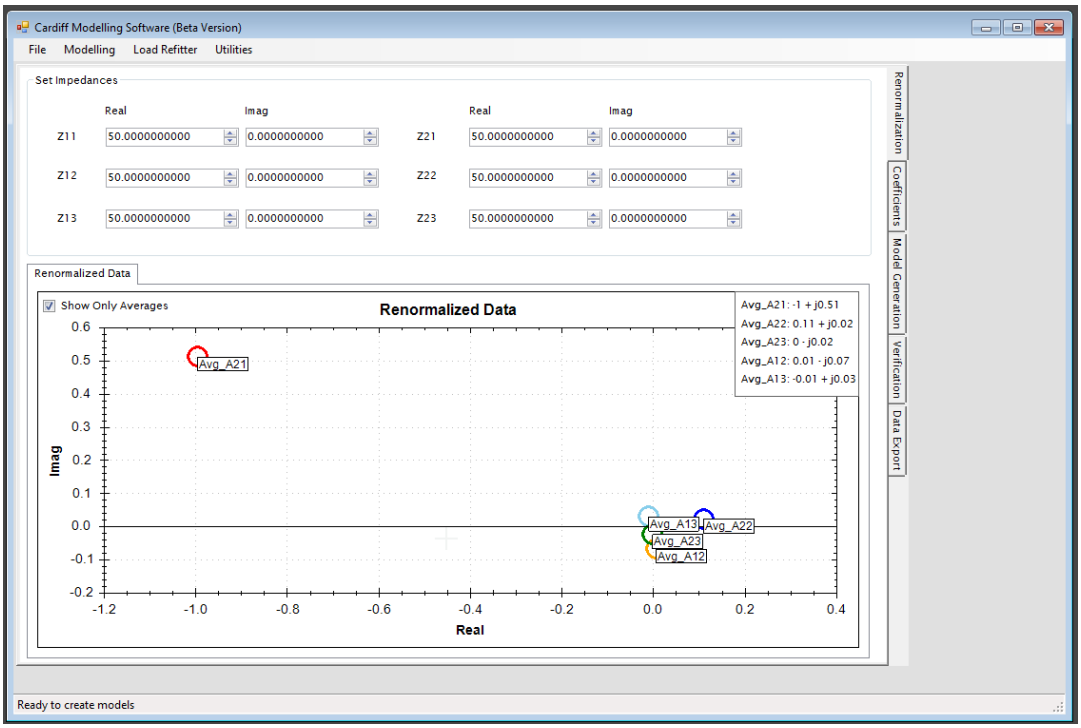

Figure 87: Impedance renormalisation

Coefficient Matrix Generator

A customisable matrix of model coefficients can be populated in this control. This is based on the magnitude and phase a-wave multipliers. Once generated, this matrix is used in the model calculations.

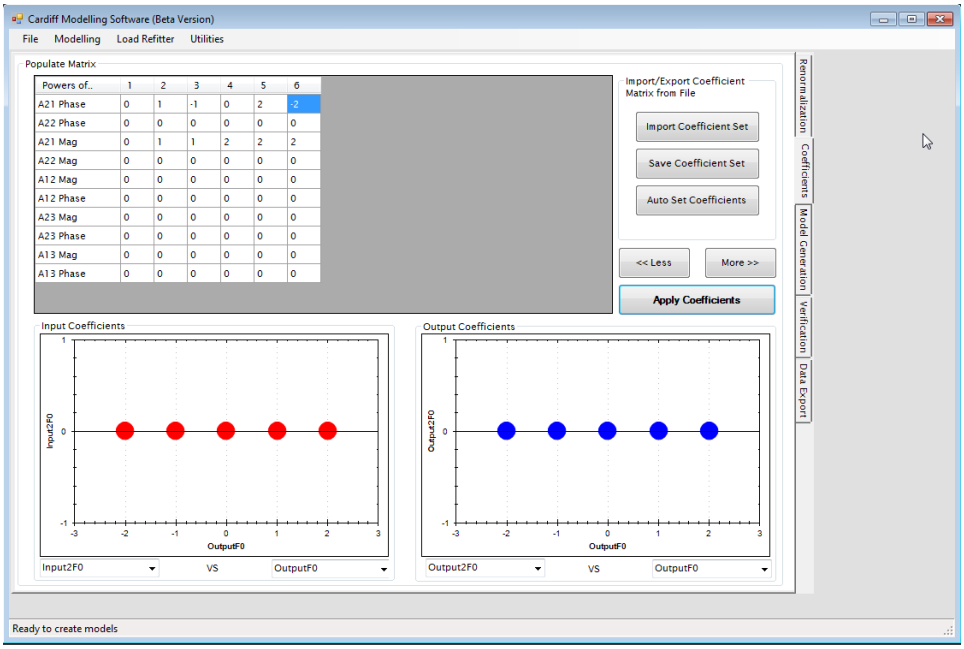

Figure 88: Coefficient Matrix generator

Model Calculation and preview

The behavioural model for the data provided can be calculated in this tab. As soon as the model has been generated, an instant preview of the measured and modelled *b* waves is shown for a quick comparison of accuracy. The window also contains a summary of the errors in the calculation; displayed as a plot as well as textual format. Within this window, models can also be archived or recalled for further analysis. This screen is shown in Figure 89.

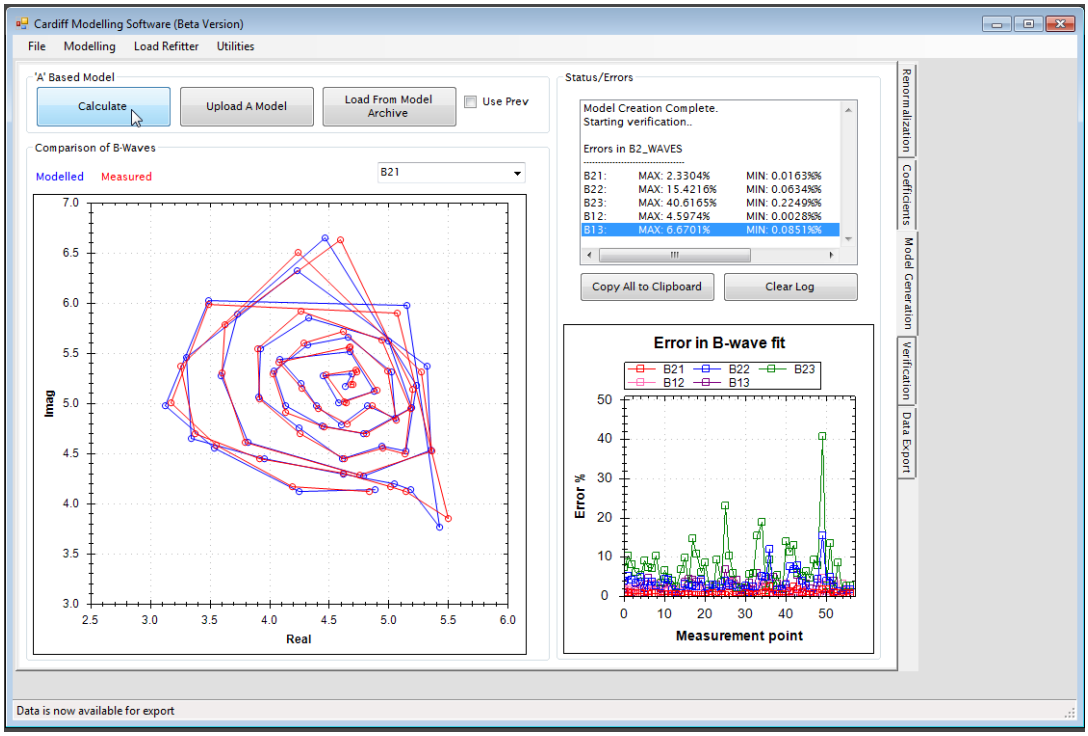

Figure 89: Generating a model

Model Verification

Model verification is carried out by comparing the input and output gamma plots of both modelled and measured points. Plots of waveforms of current and voltage at each of these points are also shown. This is an animated feature as the user can step through each point to view the corresponding waveform plots for any inaccuracies.

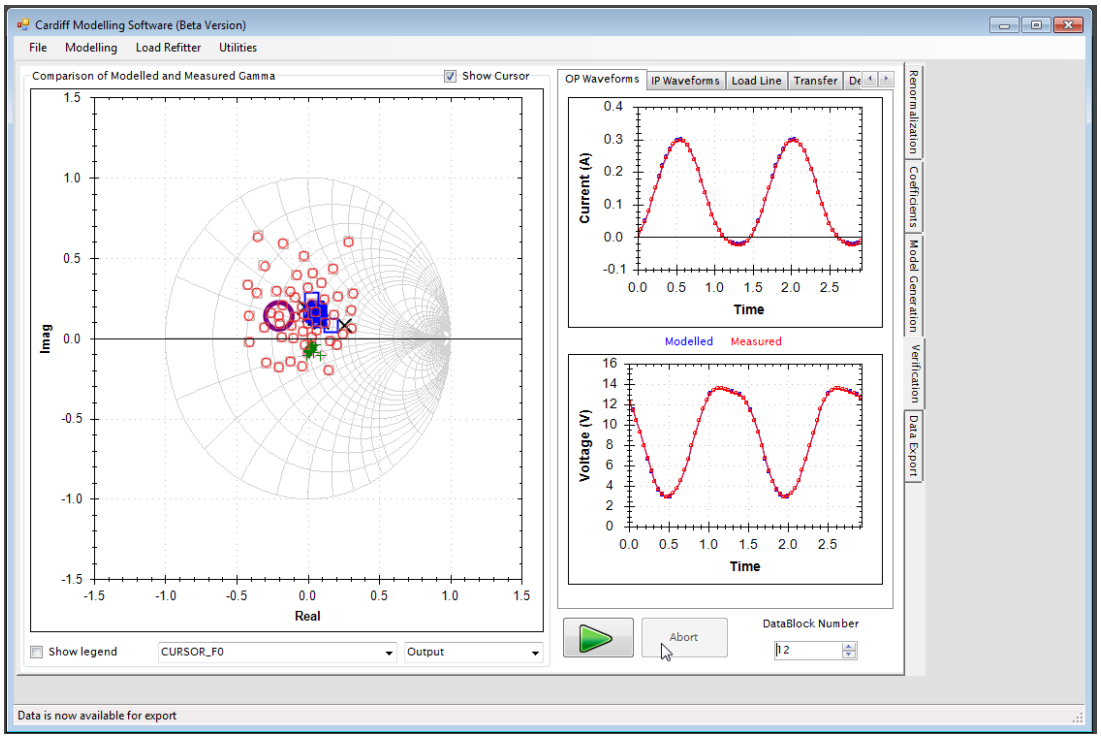

Figure 90: Verification control

Data Export

The model data can also be exported as a Generic MDIF file, readable by both Agilent ADS and AWR microwave office, as shown in Figure 91.

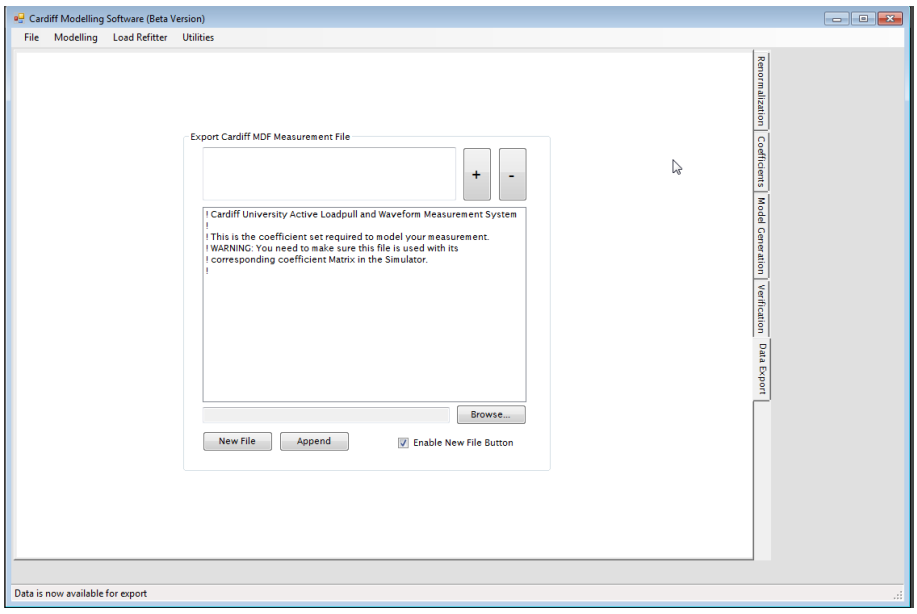

Figure 91: Data Export tool

The load-refitter control

Using this tool, users can refit a non-ideal grid onto an ideal one provided a behavioural model has been calculated. It allows the user to set a grid of gamma points overlaying the area of interest. The resulting data can then be re-exported as a measurement data file containing an ideal grid. Harmonic terminations can also be refit or an average value can be used for these.

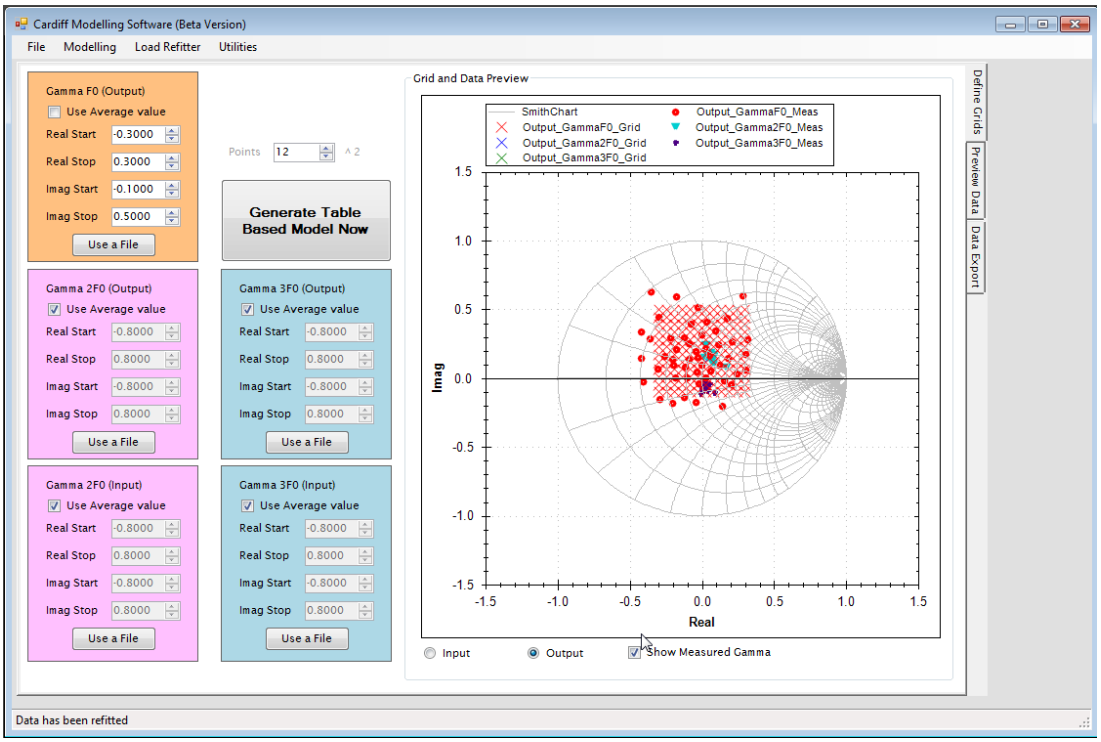

Figure 92: The load-refitter control

References

[1] Online: http://www.ni.com/visa/ [Accessed: 08-Jan-2013]

[2] Online: http://www.microsoft.com/net [Accessed: 08-Jan-2013]

[3] Online: http://www.ivifoundation.org [Accessed: 08-Jan-2013]

[4] Online: http://www.ni.com/mstudio/ [Accessed: 08-Jan-2013]

[5] Agilent Technologies, "Generic MDIF" Online: http://cp.literature.agilent.com/litweb/pdf/ads2004a/cktsim/ck0418.html [Accessed: 08-Jan-2012]

Appendix C – Publications

Interpolation and Extrapolation Capabilities of Non-Linear Behavioural Models

R. S. Saini[#1], J. J. Bell[#], T. Williams[*2], J. Lees[#], J. Benedikt[#] and P. J. Tasker[#]

[#]*Centre for High Frequency Engineering, Department of Engineering, Cardiff University, Queen's Buildings, The Parade, Cardiff, UK. CF24 3AA*

[*]*Mesuro Limited*

European Office, 8th Floor Eastgate House, 35-43 Newport Road, Cardiff, CF24 0AB United Kingdom

[1]sainiR4@cardiff.ac.uk

[2]tudorwilliams@mesuro.com

***Abstract* — This paper demonstrates how the Poly Harmonic Distortion (PHD) modelling framework is effective in its ability to interpolate or extrapolate non-linear measured data and thereby improve the quality and speed of measurement systems. Fundamental interpolation was verified and demonstrated using a 7-coefficient model extracted from a sparse set of fundamental impedances (19 points). It was shown that a relatively low order polynomial was required to capture the second harmonic space. Interpolation accuracy was however increased by including more coefficients. Second harmonic extrapolation was carried out on measured data and shown to be accurate to an average confidence of 99% when 6 model coefficients were extracted on a 0.7 reflection coefficient circle and then used to predict data on a 1.0 reflection coefficient circle. Measurements were carried out using an open loop active load-pull system operating at a fundamental frequency of 9GHz, on a 0.5W 10x75um GaAs PHEMT device.**

***Index Terms* — HEMTs, Modeling, MMICs, Nonlinear systems, scattering parameters.**

I. Introduction

Load pull is the direct measurement of key non-linear performance parameters such as output power, gain, efficiency and linearity as a function of load impedances, input drive, frequency, bias and many other factors. With the rise in demand for system requirements, PA designers have to seek high efficiency modes of operation e.g. Continuous Class-F, Class-F [1-2] etc. Measurement conditions required for these modes include presenting specific impedance terminations at the fundamental and harmonic tones and thereby monitoring the device performance. This often leads to time-consuming characterization measurements due to the number of variables that have to be tuned. A fast and efficient non-linear measurement system i.e. source- and load-pull system is therefore critical for the PA design lifecycle.

In recent times, source- and load-pull systems can be categorized into passive, active and hybrid systems. In passive load-pull systems, computer controlled stepper-motor-driven mechanical systems which incorporate multiple stub tuners for fundamental and harmonics are used to achieve the desired terminal impedances [3]. Due to the losses in passive mechanical systems, coverage of the impedance plane is however limited and practically achieving high impedance terminations at harmonic frequencies require hybrid techniques [4] which incorporate an active load-pull loop. Active load-pull systems [5] can therefore overcome these losses by amplifying the injected wave, $A_{2,h}$ hence allowing unrestricted coverage of the impedance plane.

Non-linear measurement data has been exploited in various ways to create behavioural models for high frequency transistors. These include frequency-domain descriptive behavioural models, including Poly Harmonic Distortion (PHD) Models [6], S-functions [7] and X-parameters [8]. Formulations of these models have been developed in the travelling wave domain with a desire to represent nonlinear behaviour of high frequency transistors.

Previous work [9-10] based on PHD models has shown that by considering higher order mixing terms in the PHD formulation, a model can be developed which does not require the simulator to interpolate between datasets for different fundamental and harmonic source and load pull impedance measurements.

We can also utilize such a model to improve the quality and speed of measurements as well as the ability to overcome limitations of measurement systems discussed above. By carrying out interpolation and extrapolation on measurement data, the system can take advantage of the intelligence of behavioural modelling. Interpolation carried out on measurement data can reduce the density of impedance grids hence reducing utilization time. Measurement systems that cannot achieve a high enough impedance termination at higher harmonics can take advantage of harmonic extrapolation to achieve these values.

In this paper, the benefits of the PHD modelling framework will be demonstrated in various ways:
i) Interpolation accuracy of a fundamental load-pull grid.
ii) Interpolation and extrapolation accuracy of the second harmonic load-pull grid.

Open loop active harmonic load-pull measurements for these investigations were carried out on a 0.5W 10x75 um GaAs PHEMT device, operating at 9GHz biased in Class-B conditions. The device was measured at the P-2dB compression point for the entire analysis. The X-Band

978-1-4673-0282-1/11/$26.00 ©2011 IEEE

measurement system utilized was developed at Cardiff University [5] using three phase synchronized signal generators and a Tektronix DSA8200 oscilloscope as the primary receiver.

II. Behavioural Modelling Formulations

The frequency-domain model formulations described in the introduction all operate in the travelling-wave domain. The measured behaviour in this case can be described as a function of various inputs such as DC bias ($V_{1,0}$ and $V_{2,0}$) and input drive ($A_{1,1}$) as shown in (1), where the subscript h denotes the harmonic index and n denotes the port number.

$$B_{n,h} = P_1^h f(V_{1,0}, A_{1,1}, V_{2,0}, \frac{A_{2,1}}{P_1}) \quad (1)$$

$$P_1 = \angle A_{11}, Q_1 = \angle A_{21} \quad (2)$$

Previous work [9] has derived an equivalent Fourier series description of the behaviour (3), where the coefficients $K_{n,h,m}$ and the necessary mixing order, ω can be determined via a least-squares fit of measured data. Theoretically, the minimum number of measurements required for the least-squares algorithm to extract x coefficients is x measurements. In order allow for inaccuracies in the practical measurement scenario and allow for redundancies, $2x$ measurements can be considered as a recommended minimum set.

$$B_{n,h} = P_1^h \sum_{-(\omega-1)/2}^{+(\omega-1)/2} K_{n,h,m} \left(\frac{Q_1}{P_1}\right)^m \quad (3)$$

Where $K_{n,h,m} = g(V_{1,0}, |A_{1,1}|, V_{2,0}, |A_{2,1}|)$

m: phase index

A further reduction in the complexity of (3) can be achieved (4) by including the variation of the coefficients $K_{n,h,m}$ as a function of the measured fundamental impedance $|\Gamma_{2,1}|$. Fundamental load interpolation can be achieved by this simplified equation, due to its ability to interpolate in both polar co-ordinates (magnitude, $|\Gamma_{2,1}|$ and phase Q_1/P_1).

$$B_{n,h} = P_1^h \sum_{p=|m|}^{p=|m|+2q} M_{n,h,m,p} |\Gamma_{2,1}|^p \quad (4)$$

p: magnitude index

III. Fundamental Load Interpolation

In order to investigate the quality of interpolation for the fundamental grid, various sets of impedances were measured, all centred on the measured device optimum for power. All higher harmonics were held constant at 50 ohms. Through out the analysis, the fundamental frequency, bias and drive were held constant. These impedance points were grouped by, and contained within, the measured output power contours, in 0.5dB steps up to 3.5 dBm from the measured optimum for power (at 27.6 dBm). Behavioural models of increasing order, defined by changing ω in (3) were then used to capture the non-linear behaviour for each of these impedance subsets. Results from this analysis are shown in Figure 1, comparing the error in re-generating B_{21} with varying model complexity.

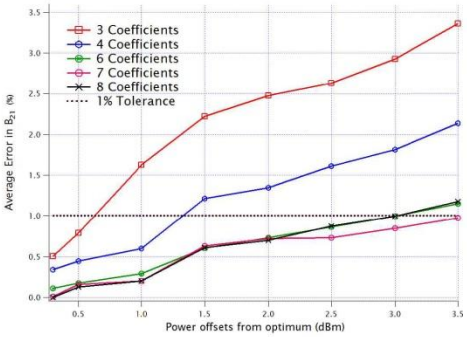

Figure 1: Error in B_{21} with increasing model complexity

From the figure above, it can be seen that the model complexity required to accurately capture impedances local to the optimum (within 0.5dB) requires a polynomial with only 3 model coefficients. However, in order to accurately capture the design space defined by the entire fundamental grid (0.5-3.5dB) a higher-order polynomial is required (6-8 coefficients).

Applying the above findings, interpolation was demonstrated practically via two sets of measured fundamental load pull grids. The first set contained a "sparse" distribution and second with a "fine" distribution of impedances. In the first case, an impedance grid of 15 points (sparse grid) was measured around the optimum of the device. In the second case, a grid of 100 points (fine grid) was measured in the same region. In both conditions, the fundamental frequency, bias conditions and drive level was held constant. Data collected from measurements on the sparse grid was then used to extract a behavioural model containing 7 model coefficients as shown in (5) and the interpolation was verified against data collected from measurements on the fine grid.

$$\frac{B_{2,h}}{P_1} = M_{2,h,-2,2}\left(\Gamma_{2,1}^{\ *}\right)^2 + M_{2,h,-1,1}\left(\Gamma_{2,1}^{\ *}\right) + M_{2,h,0,0} +$$
$$+ M_{2,h,0,2}\left(|\Gamma_{2,1}|\right)^2 + M_{2,h,1,1}\left(\Gamma_{2,1}\right) + M_{2,h,2,2}\left(\Gamma_{2,1}\right)^2 + M_{2,h,3,3}\left(\Gamma_{2,1}\right)^3$$

(5)

978-1-4673-0282-1/11/$26.00 ©2011 IEEE

Figure 2, an error contour plot, illustrates predictions of the model when compared to measured data on the fine grid. The average error in predicting the B_{21} for this analysis was 0.6% and the worst-case error was 4.2%. It can also be seen that in a comparison of the same impedance point, the measured output voltage and current time-domain waveforms (red) show excellent agreement to the modelled versions (blue).

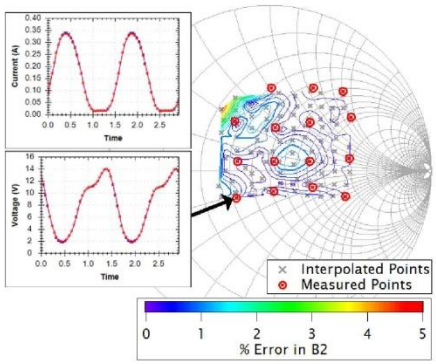

Figure 2: Fundamental Interpolation on a sparse grid using a 5th order behavioural model

The extracted model coefficients were then used to refit data onto an "ideal grid" for use in the simulator, using (5). Results of the interpolation technique described above show a significant reduction in the total number of measurements required for fundamental behavioural model generation, compared to traditional lookup-table approaches. It also highlights that the measurement system no longer needs to place impedances on a "fixed-grid", hence significantly increasing its utilization efficiency.

IV. Second Harmonic Interpolation and Extrapolation

With the presence of an active load pull system capable of harmonic tuning, the impedance plane had capability to achieve high reflection coefficients ($|\Gamma_{22}|>1$). Varying Γ_{22} in magnitude and phase allowed measurement of a dense second harmonic impedance grid thus providing a platform for investigation of harmonic- interpolation and extrapolation. For this analysis, the fundamental was kept at the optimum efficiency impedance-point and all higher harmonics, except the second (2F0), terminated into 50 ohms. Input drive, frequency and bias were held constant. The dataset utilized for this analysis included measured 2F0 reflection coefficients ranging from $|\Gamma_{22}|$=0.0 to $|\Gamma_{22}|$=1 with impedance targets placed on concentric circles, providing for maximum coverage of the Smith chart.

A. Second Harmonic Interpolation

Data subsets of measured 2F0 impedances were filtered and grouped by varying magnitudes of the 2F0 reflection coefficients $|\Gamma_{22}|$. Models of increasing order, defined by changing ω in (3) were used to capture the behaviour for each of these subsets. Results from this analysis are shown in Figure 3, comparing the error in re-generating B_{22} with increasing model complexity.

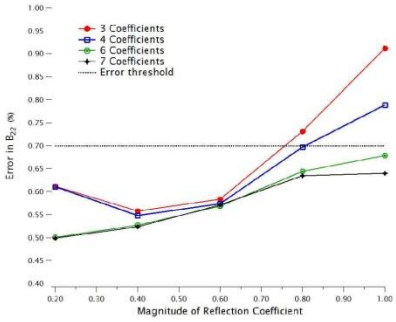

Figure 3: Average errors in B_{22} with model complexity

From the above result, it was shown that a relatively low model complexity is required to capture an accurate second harmonic model. Accuracy is however improved when the number of coefficients is increased; especially if the measurement data includes high impedance terminations ($|\Gamma_{22}|>0.7$).

B. Second Harmonic Extrapolation

Results from model interpolation in (A) above indicate the minimum appropriate model for the entire 2F0 impedance space contained 6 model coefficients shown in (6).

$$\frac{B_{2,h}}{P_1} = M_{2,h,-2,2}\left(A_{2,2}^{\ *}\right)^2 + M_{2,h,-1,1}\left(A_{2,2}^{\ *}\right) + M_{2,h,0,0} + \\ + M_{2,h,0,2}\left(\left|A_{2,2}\right|\right)^2 + M_{2,h,1,1}\left(A_{2,2}\right) + M_{2,h,2,2}\left(A_{2,2}\right)^2 \quad (6)$$

In order to test the extrapolation capability, these 6 coefficients were extracted under two conditions. i) For 2F0 impedances with $|\Gamma_{22}|$ <= 0.2. ii) For 2F0 impedances with $|\Gamma_{22}|$ <= 0.7. The generated models were used to extrapolate data that included points at edges of the smith chart i.e. $|\Gamma_{22}|$ <= 1.0. Figure 4 shows modelled results from these extrapolations, compared to measured data.

978-1-4673-0282-1/11/$26.00 ©2011 IEEE

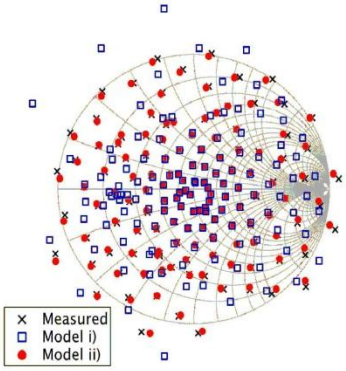

Figure 4: Second harmonic extrapolation results

Table 1 shows the average and peak errors in B_{22} as a result of extrapolating in both cases.

Model	Peak Error (%)	Average Error (%)
i) $\|\Gamma_{22}\|$ <= 0.2	88	4
ii) $\|\Gamma_{22}\|$ <= 0.7	4.64	1.17

Table 1: Summary of Error in Extrapolation

The above results demonstrate that measured second harmonic impedances can be utilized to extract a behavioural model capable of extrapolation to higher harmonic terminations. It has to be noted that the dynamic range of the measurement system can however constrain the minimum value of $|\Gamma_{22}|$ in order to extract accurate enough coefficients.

IV. Conclusion

Fundamental interpolation was demonstrated in this paper by including higher order terms to the PHD modelling framework. It was shown that a 7-coefficient model can accurately capture a fundamental impedance space containing 15 impedance points and predict accurate waveforms as well as refit data to an ideal grid; this result was verified against measured data covering the same impedance region with 100 points. It therefore showed a significant reduction in the number of measurements required for fundamental load-pull.

A comparison of the interpolation and extrapolation accuracy of the second harmonic was also investigated. It was shown that the model required to capture second harmonic behaviour is of a relatively low order. However, the quality of interpolation can be improved by including higher order terms in the extraction. Extrapolation behaviour of the second harmonic was found to be accurate when higher harmonic terminations were included in the extraction, i.e. $|\Gamma_{22}|$ <= 0.7. This result however depended on the dynamic range of the measurement system. It was shown reflection coefficients $|\Gamma_{22}|$ <= 1.0 could be obtained to an average confidence of 99%.

978-1-4673-0282-1/11/$26.00 ©2011 IEEE

Acknowledgements

The authors wish to acknowledge the assistance and support of Mr. Simon Woodington of Alcatel Lucent (UK).

References

[1] V. Carrubba et al., *"The continuous class-F mode power amplifier,"* in Proc. 40th European Microwave Conf., Paris, France, Sept.26–Oct. 1, 2010, pp. 1674–1677.

[2] P. Wright, A. Sheikh, C. Roff, P. J. Tasker, and J. Benedikt, *"Highly efficient operation modes in GaN power transistors delivering upwards of 81% efficiency and 12W output power,"* in IEEE MTT-S Int. Microwave Symp. Dig.,

[3] [Online]. Available: http://www.maurymw.com [Accessed: 21-June-2011]

[4] G. Simpson, "Hybrid active tuning load pull", Proc. 77th Microwave Measurements Conf. (ARFTG), June 2011.

[5] D. J. Williams and P.J. Tasker *"An automated active source and load pull measurement system,"* in Proc. 6th IEEE High Frequency Postgraduate Student Colloquium, Sept 9-10, 2001.

[6] J. Verspecht and D. E. Root, *"Polyharmonic distortion modeling,"* IEEE Microwave Mag., vol. 7, no. 3, pp. 44–57

[7] M. Myslinski, F. Verbeyst, M. V. Bossche, and D. Schreurs, *"Sfunctions behavioral model order reduction based on narrowband modulated large-signal network analyzer measurements,"* in Proc. 75th Microwave Measurements Conf. (ARFTG), May 2010, pp. 1–6.

[8] D. E. Root, J. Horn, L. Betts, C. Gillease, and J. Verspecht, *"Xparameters: The new paradigm for measurement, modeling, and design of nonlinear RF and microwave components,"* Microwave Eng. Europe, pp. 16–21, Dec. 2008..

[9] S. Woodington et al., *"Behavioral model analysis of active harmonic load-pull measurements,"* in Proc. IEEE MTT-S Int. Microwave Symp. Dig., pp. 1688–1691, May 2010.

[10] J. J. Bell et al., *"Behavioral Model Analysis using Simultaneous Active Fundamental Load-pull and Harmonic Source-pull Measurements at XBand"*, Spring 2011 IEEE IMS Symposium, 5-10 June 2011.

High Speed Non-linear Device Characterization and Uniformity Investigations at X-Band Frequencies exploiting Behavioral Models

R. S. Saini, J. W. Bell, T. A. J. Canning, S. P. Woodington, D. FitzPatrick, J. Lees, J. Benedikt and P. J. Tasker

School of Engineering, Cardiff University, Cardiff, UK, CF24 3TF Tel +44 2920 876347
SainiR4@Cardiff.ac.uk

***Abstract* — This paper outlines a non-linear measurement approach suitable for wafer mapping and technology screening applications. It is shown how rapid characterization and uniformity investigations of non-linear devices is possible through the development of an intelligence driven, open-loop active harmonic load pull measurement system, where localized behavioral models are exploited to dramatically improve measurement system speed and to improve utilization efficiency. The load pull measurement results obtained were then used to extract 5th order behavioral models for robust CAD integration. Device variations can now be included within the CAD tool. Technique demonstration involved the measurements of 10x75 µm GaAs pHEMT devices, operating at 9 GHz, biased in Class-AB on four different wafers. An example CAD investigation comparing the variation of the measured and modeled current and voltage waveforms is discussed.**

***Index Terms* — HEMTs, Modeling, MMICs, Nonlinear systems, scattering parameters,**

I. Introduction

At the present time, significant interest and effort has been devoted to the realization of Monolithic Microwave Integrated Circuits (MMICs) for high power and high efficiency applications such as mobile telecommunications, radar and satellite communications. These very demanding applications require a thorough optimization of the transistor technology along with the availability of accurate Computer Aided Design CAD device models.

The ideal CAD device model is one that describes transistor behavior across the entire range of external terminal parameters such as DC bias, input drive and input/output VSWR. As a consequence, analytical approaches are generally employed in foundry Process Design Kits (PDKs). Traditional PDK analytical models, when used in large signal simulations, rely on the extrapolations of the DC and small signal measurements. While such extrapolations can be successful in some regions of large signal operation, they can fail in others. Experimental verification under large signal conditions is therefore ideally required to validate the PDK analytical model's predictions in the application appropriate non-linear regions of operation.

In order to carry out this experimental validation, there has been considerable advancement in large signal RF measurement technologies such as active [1] and passive load pull [2]. Load pull is the direct measurement of key non-linear performance parameters such as output power, gain, efficiency and linearity as a function of primarily load impedances but also input drive, bias, temperature and many other factors. The constraint on measurement time is critical in non-linear device characterization and therefore, parameters measured during the load pull process are often focused towards a quantification of high power amplifier performance i.e. saturated power, efficiency and gain. This is in contrast to the more detailed device characterization involving the extraction of relevant non-linear parameters, which are required for process optimization and CAD model development. Therefore, in addition to the evolution of measurement hardware new techniques for system control and analysis/modeling of measured large signal parameters are required if these measurement systems are to be utilized more efficiently.

Measurement data from load pull systems has been, in recent times, exploited to develop various CAD compatible behavioral modeling approaches [3]. These can be categorized into Look-up table based [4], descriptive functional approaches using a modeling framework [5] or a combination of the two; X-Parameters [6] and S-Functions [7].

In order to rapidly test transistor structures, assess yield across a range of devices and wafers of the same technology and support CAD design, in the large signal domain, in a time efficient manner a new measurement strategy is required.

In this paper it will be shown that an intelligent active load pull system aided by localized poly-harmonic distortion models (PHD models) the parameterized behavioral modeling framework based on non-linear mixing can achieve this objective, providing for fast non-linear characterization and comparison of devices and wafers of the same technology. Load pull measurements were used to create a 5th order behavioral model which was used to summarize measurement variations and in addition, allowed a comparison to a reference PDK analytical model for the same transistor technology.

II. Active Load pull Measurements

Measurements presented in this work were carried out using an open loop active load pull system, developed in Cardiff University, and described in [1]. Integral to the accuracy and speed of the system is the use of phase coherent signal

978-1-61284-961-4/11/$26.00 ©2011 IEEE

generators and a 4-Channel Digital Sampling Oscilloscope (Tektronix DSA 8200) as the primary receiver. Alternatives to this setup can be realised by replacing the oscilloscope with a 5 channel non-linear network analyzer (e.g. Agilent PNA-X) or a large signal network analyzer as a receiver (e.g. VTD-SWAP X-402).

Figure 1 shows the active load pull loops in this measurement setup. Load emulation is achieved in this system by solving (1) for $A_{2,h}$ with h indicating the harmonic index.

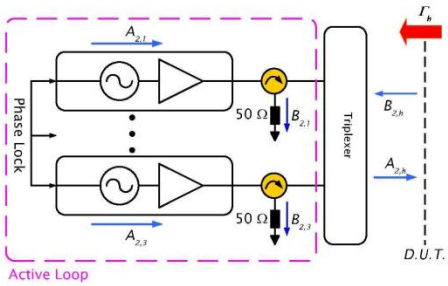

Figure 1: Schematic of the Active load pull loop

$$A_{2,h} - \Gamma_h . B_{2,h}(A_{2,1}, A_{2,2}, .., A_{2,h}) = 0 \qquad (1)$$

The work presented in [6-7] describes the use of localized poly-harmonic distortion models to predict the values of $B_{2,h}$ and hence solving for (1). This intelligence driven approach greatly improves the efficiency of the load pull system, minimizing the need for an iterative solution and carrying forward intelligence in a "batched" processing mode. Applying the technique described in [7], the flow graph in Figure 2 summarizes the measurement procedure utilized to carry out load pull on a "batch" of preset load impedances.

Two perturbation measurements are required to compute the local PHD model. These measurements can be regarded as "redundant" since they are aiding the measurement system to achieve an emulation target. The utilization efficiency of the measurement system (η_{meas}) can therefore be quantified by (2); the ratio of useful measurements (M_{useful}) to the total measurements. An ideal measurement system, with η_{meas} = 100% would therefore require only one measurement per load point.

$$\eta_{meas} = \frac{M_{useful}}{M_{useful} + M_{redundant}} * 100 \qquad (2)$$

In order to maximize this efficiency, throughout the load pull measurement process, each generated local model is saved in a database and can be re-used. This is particularly beneficial during a wafer mapping process as when moving from device to device or wafer to wafer, the load pull system is required to measure device performance under the same excitations conditions. It can be assumed that in this scenario, different devices would exhibit similar responses.

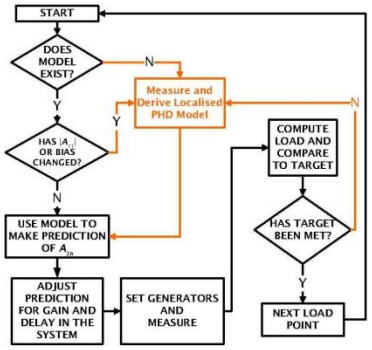

Figure 2: Flow graph of load pull measurement procedure

III. Measurement Strategy

High efficiency power amplifier modes of operation are governed by maximizing DC-to-RF conversion. The DUT is therefore required to be driven hard enough to generate spectral components at relevant harmonic frequencies. A deduction from the detailed consideration of the time varying voltage $V(t)$ and current $I(t)$ waveforms shows us that by presenting favorable impedances at the fundamental and harmonic frequencies, designers can synthesize these waveforms for high efficiency modes of operation [8-9] e.g. Class-B, Class-F, Class-F^{-1}.

The load-pull space required for the comparison and later-on model generation was therefore focused around the relevant optimum impedance emulation points, such as the optimum loads for power and efficiency. Measurements were carried out on a series of 10x75µm GaAs PHEMT devices all operating in Class-AB bias conditions at 9 GHz. According to the above discussion and considering the fundamental signal, it was first necessary to find the output fundamental impedance point which corresponded to the load for optimum power, Γ_{OPT}.

The approximate value of the Γ_{OPT} can be predicted by using an estimation of the measured transfer characteristic of the DUT [8]. Alternatively, if a PDK analytical device model is available in CAD, the predicted load pull contours can give

us an estimated value for Γ_{OPT} provided that it was stimulated using the same excitation parameters such as bias, frequency and drive level.

Using the latter approach, Figure 3 shows results from load pull simulations of the device's analytical model in CAD with the predicted power contours at the P-1dB compression point, highlighting the area of interest for the non-linear comparison analysis and model generation.

The next step was to cover the impedance space predicted by the above result on the actual DUT. A spiral grid of points, centered near the predicted optimum impedance (32.9+j21.7Ω), was therefore chosen to maximize the interpolation capability of the measurements around the area of interest.

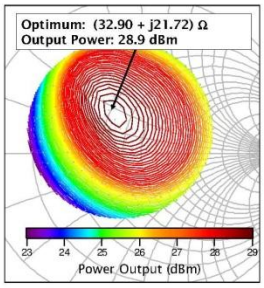

Figure 3: Predicted power contours achieved by carrying out load pull of the analytical model in CAD

Applying the measurement concept introduced in Section II, locally computed PHD models were used to aid the measurement of this impedance space for the first device, D1. Figure 4 shows the output of this measurement sequence, highlighting the load pull points that required the computation of a local PHD model and the resulting measured power contours. The measurement system utilization efficiency (η_{meas}) for this 56-point load pull grid was 70%; requiring 12 local models to complete the entire grid.

In order to further improve this utilization efficiency and taking note of the fact that all the DUTs to be compared are of the same device technology and geometry (10x75µm GaAs PHEMTs), the measurement stimulus (A_{11}, A_{21}, I_{ds}, V_{ds} and fundamental frequency) used to characterize "D1", having been stored, can now be recalled for all the subsequent device to device and wafer to wafer, measurements. As a consequence, neither further iterations nor local model generation was necessary in the comparison process, thus improving the measurement system utilization efficiency to 100% for all subsequent load pull measurement sequences i.e. the next three sets of measurements in this simple example study. This validates this approach as a fast and efficient technology screening and wafer mapping process.

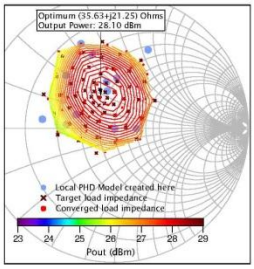

Figure 4: Measured power contours on device "D1"

In order to carry out the complete load-pull characterization on "D1", the total measurement time taken was 30 minutes. It required approximately 7 minutes (23% of the original time taken) to characterize all the other devices and achieve the same set of preset load emulation points.

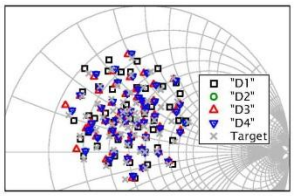

Figure 5: Results from measuring all 4 DUTs with the same stimuli as "D1"

Figure 5 illustrates the impedances measured by applying these stimuli on all the other DUTs (D2, D3, D4). A consequence of this approach is device to device variation will cause a small scatter in the measurement impedance locations. Once we have identified both device-to-device and wafer-to-wafer variations, it would be advantageous to include these variations within the CAD models. In a simple data-based look-up model, this is difficult to quantify. Also, these models need to be defined on a standard grid. However, in our approach, measured data is transformed into an equivalent behavioral model. This removes the need for a fixed grid and also i) multiple models based on random lookup can account for device-to-device variations and ii) the model can incorporate these variations in the extracted coefficient space.

Table I is a summary of these measurements, showing the variation in the output power and Γ_{OPT}. It can be seen from the results that devices D1-D4 show very similar characteristics in the position of Γ_{OPT} (Real: 35.1±0.5Ω, Imag: 21.5±0.50Ω) and

output power (28.0±0.2dBm). There is however a 0.8dB difference between the measurement results and the predictions from the PDK analytical model.

TABLE I
SUMMARY OF MEASUREMENTS

Device	Power (dBm)	Γ_{OPT} (Ω)	Γ_{IN} (Ω)
PDK	28.90	32.90+ j21.72	4.66 - j9.00
D1	28.10	35.63 + j21.25	4.37 - j13.22
D2	28.10	35.15 + j22.00	4.21 - j12.23
D3	28.01	35.00 + j21.60	4.55 - j9.67
D4	27.80	35.32 + j21.80	4.24 - j13.00

IV. Device Comparison Under Large Signal Conditions Using Behavioral Modeling

In order to carry out a parameterized extraction and comparison analysis of the measured devices, a 5th order behavioral model, extracted via a Polynomial Least-Means Squares (LMS) function, was determined for each. Each of these parameterized models can be utilized with the CAD tool during circuit design, optimization and now yield analysis. In addition, an averaged-set of extracted coefficients can also be computed and thus used as an averaged "reference" parameterized data look-up CAD model.

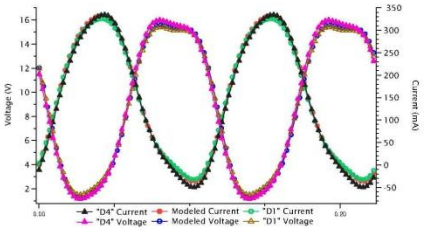

Figure 6: Voltage and Current waveforms, Compared to the best case and worst case measured results

Figure 6 is a simple example of the use of this new capability. Computed time domain waveforms between the best case (D1), worst case (D4) are compared with those predicted by the measurement based "reference" model (using the average set of coefficients), all generated for the load point corresponding to their respective Γ_{OPT}. For device D1, the average difference between current waveforms was 0.5%, compared to device D4 whose average difference in current waveforms was 3.92%.

VII. Conclusion

A non-linear measurement approach, based on the active open-loop load-pull architecture, suitable for wafer mapping and technology screening has been demonstrated. The necessary improvement in measurement speed is achieved by improving its utilization in two ways. Initially, locally computed poly-harmonic distortion models guide the active load pull system, thus minimizing the load setting iterations. During this initial device load-pull measurement sequence the required open – loop load-pull settings are stored. These can then be recalled, eliminating load-setting iterations, for all subsequent device load-pull measurements reducing measurement time significantly. For exploitation within CAD tools these load-pull measurements were used to create 5th order parameterized behavioural model. These models can then be used within the CAD tool to study device variations and undertake circuit yield analysis. In addition, an averaged "reference" parameterized data look-up model based on many measurements can now be computed.

Acknowledgement

The authors wish to acknowledge the assistance and support provided by the EMRS DTC, Agilent Technologies and Mr. Mervin Haynes (Selex Galileo UK).

References

[1] D.J. Williams, P.J. Tasker, "*An Automated Active Source and Load Pull Measurement System*", *Proceedings of 6th IEEE High Frequency Postgraduate Colloquium, Cardiff, UK*, pp. 7-12, September 9th-10th 2001.

[2] J. Sevic, "*Introduction to Tuner-Based Measurement and Characterization*," Maury Microwave Corporation, Application Note 5C-054, 31st August 2004.

[3] Hao Qi, Johannes Benedikt, Paul Tasker, "*A Novel Approach for Effective Import of Nonlinear Device Characteristics into CAD for Large Signal Power Amplifier Design*", IEEE MTT-S International, Page(s) 2019-2022, 3-8 June 2007.

[4] Hao Qi, Johannes Benedikt, Paul Tasker, "*A Novel Approach for Effective Import of Nonlinear Device Characteristics into CAD for Large Signal Power Amplifier Design*", IEEE MTT-S International, Page(s) 2019-2022, 3-8 June 2007.

[5] S. Woodington et al. "*Behavioural Model Analysis of Active Harmonic Load-Pull Measurements*," IEEE IMS Page(s) 1688-1691, 2010

[6] R. E. Leoni; S. A. Harris; D. G. Ries, "*Active simultaneous harmonic source and load pull assisted by local polyharmonic distortion models*," Microwave Symposium Digest (MTT), 2010 IEEE MTT-S International

[7] R. S. Saini; S. Woodington.; J. Lees; J. Benedikt; P.J. Tasker, "*An intelligence driven active loadpull system*," Microwave Measurements Conference (ARFTG), 75th ARFTG 2010

[8] S. C. Cripps, "*RF Power Amplifiers for Wireless Communications*," Norwood, MA: Artech House, 1999.

[9] Wright, P.; Lees, J.; Tasker, P.J.; Benedikt, J.; Cripps, S.C.; , "*An efficient, linear, broadband class-J-mode PA realised using RF*

An Intelligence Driven Active Loadpull System

R. S. Saini, S. Woodington, J. Lees, J. Benedikt and P. J. Tasker

School of Engineering, Cardiff University, Cardiff, UK, CF24 3TF
Tel +44 2920 876347 email: SainiR4@Cardiff.ac.uk

***Abstract* — This paper describes how the application of the PHD model can add intelligence to an open loop active loadpull system. This intelligence driven approach by providing for an improved prediction of the operating conditions required to emulate a specified load speeds up the load emulation convergence process by minimizing the number of iterations to predict the injected signal, therefore making more efficient use of a measurement system.**

The results were validated by carrying out loadpull measurements on the fundamental tone of a 10x75um GaAs HEMT, operating at 3 GHz.

***Index Terms* — active loadpull, X-parameters, device non-linear models.**

I. Introduction

Load and Source-pull measurements are widely used in the design of power amplifiers to deduce optimum efficiency, gain, linearity and power, providing a clear understanding of the various modes of amplifier operation. This paper is based around measurements carried out using the Open Loop Active Loadpull system, developed in Cardiff University and described in [1] and [2], with phase coherent Signal Generators. The architecture of the single-tone (continuous wave) setup is illustrated in Fig 1 and is based on the Tektronix DSA 8200 four-channel oscilloscope as a receiver [3].

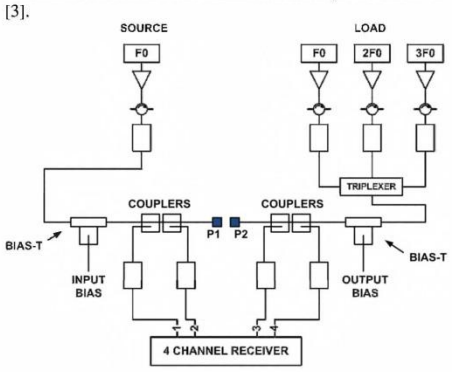

Fig 1 Schematic of measurement system

Such a setup reduces losses faced by most passive tuning systems by actively injecting the desired signals to realize the required reflection coefficient. The system is also less prone to RF oscillations noticed in closed loop systems [4].

Load emulation is achieved in this system by solving (1) for A_{2h}, with h indicating the harmonic index.

$$A_{2h} - \Gamma_h . B_{2,h}\left(A_{2,1}, A_{2,2}, \ldots, A_{2,h}\right) = 0 \qquad (1)$$

Therefore, if we have no prior knowledge of the function $B_{2,h}(.)$, the solution to (1) is found using a numerical technique. This process is iterative and can take up to 5-10 iterations to converge to a solution for the fundamental harmonic tone. If harmonic loadpull is required, the iterations are further increased due to a change in the fundamental tone causing distortion in higher harmonics. This problem is further compounded by the fact that the numerical techniques utilized present their own disadvantages such as multiple roots and numerical oscillations [5].

Recent advancements in device behavioral modeling have seen the introduction of the Poly Harmonic Distortion Modeling (PHD) framework [6]-[8]. As well as containing magnitude and phase relating to the spectral components of the input signal, this framework introduces harmonic cross product information. These products give us the relationships between harmonic frequencies for a given drive level and frequency and could therefore be beneficial in an Open Loop Active Loadpull measurement scenario, since a locally derived model can be used to assist in calculating the required injection signals to simultaneously perform both fundamental and harmonic loadpull emulation [9] when solving (1).

The motivation of this paper is to demonstrate how the behavioral modeling framework, based on non linear mixing terms can be used to aid prediction of the desired injection signals necessary in an Open Loop Active Harmonic Loadpull system to provide a desired load impedance.

II. Theory and Design of a Model Based Algorithm

The technique explained in [6] (see (2) with h indicating the harmonic index) provides a mathematical framework for describing the response, $B_{2,h}$ of a non-linear system as a function of the respective injection signals. Combining this with (1) thus allows for the formulation of a new open loop loadpull algorithm with improved load emulation capability.

978-1-4244-6366-4/10/$26.00 ©2010 IEEE

This algorithm therefore provides us with a singular approximation to the solution of (1), which is valid in the region that it is determined.

$$B_{2h} = S_{21}(|A_{11}|)|A_{11}| + \sum_h S_{22}(|A_{11}|)A_{2h} + \sum_h T_{22,h}(|A_{11}|)(A_{2h}^*) \quad (2)$$

This formulation can be modified as illustrated in [8] by describing P and Q as input and output a-wave harmonic phase operators, as shown in (3)-(4). This expression, a third order model, can be generalized to give the formulation shown in (5)-(6).

$$B_{2h} = S_{21}.|A_{11}|\left(\frac{Q}{P}\right)^0.P + \sum_h S_{22}.|A_{2h}|\left(\frac{Q}{P}\right)^1.P + \sum_h T_{22}.|A_{2h}|\left(\frac{Q}{P}\right)^{-1}.P \quad (3)$$

$$P = \frac{A_{11}}{|A_{11}|} \qquad Q = \frac{A_{21}}{|A_{21}|} \quad (4)$$

$$B_{2,h} = P\sum_{n=-1}^{n=1}\left\{R_{2,h,n}\cdot\left(\frac{Q}{P}\right)^n\right\} \quad (5)$$

$$R_{2,h,n} = G_{h,n}(|A_{1,1}|,|A_{2,1}|,\ldots) \quad (6)$$

Adapting this generalized formulation and assuming that the magnitude of the input signal ($|A_{11}|$) during this process is held constant; we can simplify it to (7) by considering only the linear third order mixing terms. This is analogous to "X-parameter" formulation described in [7].

$$B_{2h} = \underline{G_{2,0,h}} + \underline{G_{2,1,h}.|A_{2h}|.\left(\frac{Q}{P}\right)} + \underline{G_{2,-1,h}.|A_{2h}|.\left(\frac{P}{Q}\right)} \quad (7)$$

In a measurement scenario, $G_{2,0}$ can be deduced from the output response of $|A_{11}|$ at the harmonic being load-pulled. Parameters $G_{2,1}$ and $G_{2,-1}$ are extracted by applying a perturbation signal to the incident A_{21} wave, first of all with a zero degree phase and then followed by the same signal with a 90 degree shift, keeping $|A_{11}|$ constant in both cases [6]. By utilizing the measured values of A_{2h} and B_{2h} at the center and the offset points (indicated by subscripts 0, 1 and 2), we can then calculate the G parameters using the equation set (8)-(11).

$$\Delta_1 = A_{2h,1} - A_{2h,0} \qquad \Delta_2 = A_{2h,2} - A_{2h,0} \quad (8)$$

$$G_{2,1,h} = \frac{(\Delta_2^*)(B_{2h,1} - B_{2h,0}) - (\Delta_1^*)(B_{2h,2} - B_{2h,0})}{(\Delta_1)(\Delta_2^*) - (\Delta_1^*)(\Delta_2)} \quad (9)$$

$$G_{2,-1} = \frac{B_{2h,1} - B_{2h,0} - G_{2,1,h}(\Delta_1)}{(\Delta_1^*)} \quad (10)$$

$$G_{2,0,h} = B_{2h,0} - G_{2,1,h}(A_{2h,0}) - G_{2,-1,h}(A_{2h,0}^*) \quad (11)$$

If we consider Γ_h as the target reflection coefficient in (1), the computed value of A_{2h}; the desired injection signal to achieve the desired load emulation can now be analytically computed. If the resulting load accuracy is not sufficient, the process can be repeated.

III. Implementation of the Algorithm

In order to implement the algorithm for the measurement system described in the introduction, we have to include the following practical considerations.

Firstly, the predicted signal computed using (1) does not take into account the non-ideal behaviors of the Open Loop loadpull realization. This is best described by the error model shown in Fig. 2; whereby $T_{s,h}$ accounts for the insertion gain/loss of the loadpull amplifiers and couplers, etc., while $\Gamma_{L,h}$ accounts for the load match of the measurement system, both of which can be dependent on $A_{2set,h}$. It is therefore imperative to re-adjust the calculated signal ($A_{2,h}$) to the compensated value ($A_{2set,h}$) to account for the physical state of the system. To achieve this, the characterized system impedance at the harmonic being load-pulled ($\Gamma_{L,h}$) and amplifier gain ($T_{x,h}$) is incorporated into (1), as shown in Fig. 2 and (12).

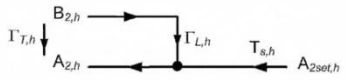

Fig 2 Flow graph showing the losses in the system and amplifier gain

$$A_{2set,h} = \frac{B_{2,h}(\Gamma_{T,h} - \Gamma_{L,h})}{T_{s,h}} \quad (12)$$

As two distinct measurements are required to compute the local model, an optimization is necessary to maximize the use of an existing set of G parameters, provided the input drive ($|A_{11}|$) or biasing conditions have remained unchanged. If the new load position is found to be within the acceptable tolerance of the target load, the existing model would have converged without requiring an update; this is beneficial during load pull of an impedance grid. The efficiency of this

algorithm can therefore be calculated by comparing the number of useful to redundant measurements.

Finally, as described in the introduction, any adjustments in the fundamental injection signal (A_{21}) distorts higher harmonic components, thereby requiring additional iterations, if they were of interest. This effect can be compensated-for by utilizing harmonic cross-product information from the local model generated by the fundamental tone. For example, during loadpull of the fundamental, the second harmonic may be required to stay at constant impedance.

In this case, the measured output response of the second harmonic (B_{22}) can be used to calculate the adjustments required in the injection signal (A_{22}) to achieve a constant impedance using the process described above and the equation set (8)-(11).

The flow chart in Fig. 3 summarizes the implementation of the algorithm, including the optimization and adjustment steps.

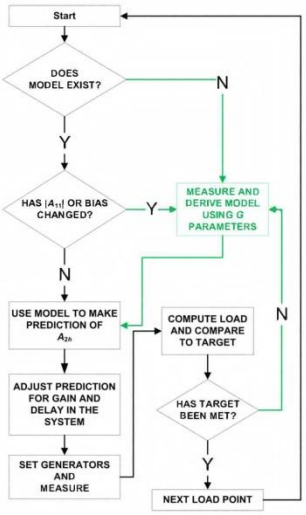

Fig 3 Flow chart of the implementation

IV. Testing and Validation

In order to illustrate how the target load is attained, a single target was considered. This was followed by carrying out measurements to attain multiple targets using two types of grid. The measurements were carried out on a 10x75µm GaAs HEMT, operating at 3 GHz with Class-B biasing conditions. Figure 4 illustrates the path taken by the algorithm to achieve the target impedance.

At the starting point (-0.2 + 0i), two perturbations are made to the $A_{2,\ 1}$ injection signal; thereby creating the two offset points (indicated by green square-shaped markers) which allow the calculation of a local model. The local model is then used to compute a value of $A_{2set,\ h}$ which moves the load to a new position (-0.08+0.65i), which in this case is not within the tolerance range (set at 5%) of the algorithm. The algorithm therefore requires the model to update itself at this stage, hence the additional set of offset points. The position of the load now obtained (-0.003+0.61i) is within 1% of the target (0+0.6i); implying the algorithm has now converged to a solution.

Fig. 5 shows the convergence results on a 5x5 square grid of target impedances. In Fig. 6, a 25 point impedance-shaped grid is utilized. In both cases, the points at which the algorithm required the model to be updated are highlighted.

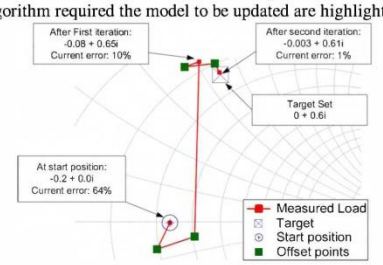

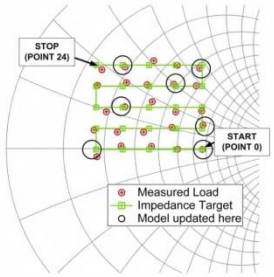

Fig 7-8 show the cumulative number of measurements required in the convergence of each load point in both cases and percentage error between the target and attained values of load. In both cases, the points at which the algorithm required the model to be updated are highlighted.

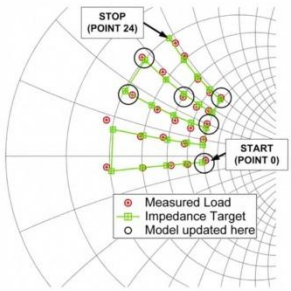

Fig 6 25 point impedance-shaped grid of targets

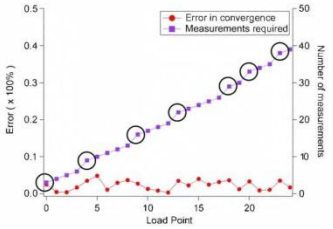

Fig 7 Cumulative measurements and convergence error from the square grid

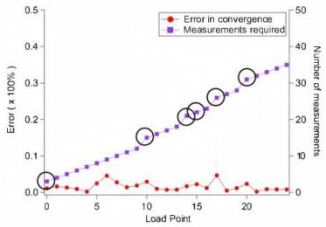

Fig 8 Cumulative measurements and convergence error from the impedance-shaped grid

The performance of the algorithm can be quantified in terms of its efficient use of the measurement system. An ideal system 100% efficient would require only one measurement per load point. The efficiency of the algorithm to converge to a solution is 44% for the square-shaped grid (averaging 2.26 measurements per point) and 62% for the impedance-shaped grid (averaging 1.56 measurements per point), compared to a typical value previously of only 5% to 10%. The average error in convergence for both grids is less than 3% of the target value required.

VII. Conclusion

The PHD model has shown to be capable of adding intelligence to an open loop active loadpull system. This approach enabled a significant improvement in the system's ability to provide the desired load emulation. The algorithm was also optimized to maximize use of locally generated parameters. Hence the measurement system utilization efficiency for realization of the desired load conditions, with less than 3% error in the achieved load-impedances on a multi-point load grid was significantly improved since PHD model generation was not necessary for each load point.

Acknowledgement

The authors would like to acknowledge the support provided by Agilent Technologies, Mimix Broadband and the EMRS DTC.

References

[1] D.J. Williams, P.J. Tasker, "An Automated Active Source and Load Pull Measurement System", *Proceedings of 6th IEEE High Frequency Postgraduate Colloquium, Cardiff, UK*, pp. 7-12, September 9th-10th 2001.

[2] Tasker, P.J, "Practical Waveform Engineering", *Microwave Magazine, IEEE, Volume 10, Issue 7*, pp 65-76, December 2009

[3] D. Williams, P. Hale, K. A. Remley, "The sampling oscilloscope as a microwave instrument," *IEEE Microwave Mag., vol. 8, no. 4*, pp.59–68, Aug. 2007

[4] T. Williams, J. Benedikt and P. J. Tasker, "Experimental Evaluation of an Active Envelope Load-Pull Architecture for High Speed Device Characterization", *IEEE MTT-S International Microwave Symposium 2005*

[5] Chapra, Steven C., "Numerical methods for Engineers", pp 73-75, 5-ed, 2002

[6] Jan Verspecht, David E. Root, "Poly-harmonic Distortion Modeling", *IEEE microwave magazine 1527-3342/06,* June 2006

[7] Jason Horn, Daniel Gunyan, Loren Betts, Chad Gillease, Jan Verspect, David E. Root, "Measurement-Based Large-Signal Simulation of Active Components from Automated Nonlinear Vector Network Analyzer Data via X-Parameters", *COMCAS 2008,*13-14 May 2008 Page(s):1 - 6, IEEE

[8] S. Woodington, T. Williams, H. Qi and P.J. Tasker, "A novel measurement based method enabling rapid extraction of a RF Waveform Look-Up table based behavioral model", *Microwave Symposium Digest, 2008 IEEE MTT-S 2008,* June 2008 Page(s): 1453 – 145

[9] J. Horn, S. Woodington, R. Saini, J. Benedikt, P.J. Tasker, D.E. Root, "Harmonic Load Tuning Predictions from X-parameters", *Fall 2009 IEEE Power Amplifier Symposium*, September 2008.